

REGULARITY UNDERLYING COMPLEXITY: A REDSHIFT-INDEPENDENT DESCRIPTION OF THE CONTINUOUS VARIATION OF GALAXY-SCALE MOLECULAR GAS PROPERTIES IN THE MASS-STAR FORMATION RATE PLANE

M. T. SARGENT^{1,*}, E. DADDI¹, M. BÉTHERMIN¹, H. AUSSEL¹, G. MAGDIS², H. S. HWANG³, S. JUNEAU¹, D. ELBAZ¹, E. DA CUNHA⁴

Submitted to the Astrophysical Journal

ABSTRACT

Star-forming galaxies display a continuous distribution of specific star formation rates (sSFR) which, in the simplest approximation, can be reproduced by the superposition of two log-normal distributions. The first of these encompasses the main sequence of star-forming galaxies, the second one a rarer population of starbursting systems. We show that the sSFR-distribution of starbursts can be regarded as the result of a physical process (plausibly major mergers) that takes the mathematical form of a log-normal boosting kernel and that enhances star formation activity. In this article we explore the utility of splitting the star-forming population into main-sequence and starburst galaxies – an approach we term ‘2-Star Formation Mode’ (2-SFM) framework – for understanding their molecular gas properties. We show that variations of star formation efficiency (SFE) and gas fractions among star-forming galaxies take a very simple, redshift-independent form, once these quantities are normalized to the characteristic value of an average, massive main-sequence galaxy. The change in SFE for galaxies undergoing a starburst event scales supra-linearly with the SFR-increase, as expected for merging events. This implies a continuous distribution of galaxies in the Schmidt-Kennicutt plane that separates more clearly into loci for starbursts and normal galaxies than observed in a plot of (s)SFR vs. M_* . Starbursts with the largest deviations (>10 -fold) from the main sequence, like many local ULIRGs, are not average starbursts, but even rarer events with progenitors having larger gas fractions than typical main-sequence galaxies. We statistically infer that the gas fractions of typical starbursts are reduced by a factor of two to three with respect to their direct main-sequence progenitors, as expected to occur in short-term SFR-booster during which internal gas reservoirs are drained more quickly than gas is accreted from the cosmic web. We predict variations of the CO-to-H₂ conversion factor α_{CO} in the SFR- M_* plane and provide strong evidence that the higher sSFR of distant galaxies is a direct consequence of the higher gas fraction of these systems.

Subject headings: cosmology: observations – galaxies: evolution – galaxies: spiral – galaxies: ISM – surveys

1. INTRODUCTION

Studies over the last decade of star-forming galaxies (SFGs) have revealed a positive and tight correlation between their current star formation rate (SFR) and stellar mass M_* , which is intimately linked to the integral of the preceding star formation (SF) activity. Initially observed at low redshift (e.g. Brinchmann et al. 2004, Salim et al. 2007, Wyder et al. 2007), this ‘star-forming main sequence’ was soon shown to be present out to $z \sim 2$ (Noeske et al. 2007, Elbaz et al. 2007, Daddi et al. 2007b). Subsequent work on the relation between SFR and M_* in SFGs charted its evolution to $z \sim 2.5$ using different SFR tracers and selection criteria (e.g. Damen et al. 2009, Dunne et al. 2009, Pannella et al. 2009, Santini et al. 2009, Kajisawa et al. 2010, Oliver et al. 2010, Elbaz et al. 2011, Lee et al. 2011, Rodighiero et al. 2011, Wuyts et al. 2011,

Whitaker et al. 2012), has explored factors affecting the exact shape and dispersion of the main sequence (e.g. Karim et al. 2011, Salmi et al. 2012; T. Bschorr et al., in prep.) and has traced it out to even higher redshifts $z \sim 3-4$ (e.g. Daddi et al. 2009, Magdis et al. 2010). The existence of a scaling relation between SFR and M_* throughout much of cosmic time implies that the (mass-dependent) assembly history of SFGs is characterized by a high degree of homogeneity and simplicity (e.g. Noeske et al. 2007, Bouché et al. 2010, Peng et al. 2010, Leitner 2012, Behroozi et al. 2012) and that the strong decline of the cosmic star formation rate density (e.g. Reddy & Steidel 2009, Rodighiero et al. 2010, Karim et al. 2011, Magnelli et al. 2011, Cucciati et al. 2012; and references therein) since $z \sim 2$ reflects the uniform SFR-evolution of the majority of the SFG population rather than a decreased frequency of episodic starburst events. Nevertheless, the study of starbursts remains central to understanding the nature of interacting galaxies and the physics of merging events which may produce the most luminous sources at all redshifts (Sargent et al. 2012).

Star formation activity at a rate which locally occurs only in strong starbursts is common in massive main-sequence galaxies in the distance universe. Hence

* E-mail: mark.sargent@cea.fr

¹ CEA Saclay, DSM/Irfu/Sérvise d’Astrophysique, Orme des Merisiers, F-91191 Gif-sur-Yvette Cedex, France

² Department of Physics, University of Oxford, Keble Road, Oxford OX1 3RH, UK

³ Smithsonian Astrophysical Observatory, 60 Garden Street, Cambridge, MA 02138, USA

⁴ Max-Planck-Institut für Astronomie, Königstuhl 17, D-69117 Heidelberg, Germany

alternative strategies to pure luminosity-selection are required for obtaining a census of bursty SF activity at high redshift, e.g. based on their position in the SFR vs M_* plane (e.g. Rodighiero et al. 2011, Whitaker et al. 2012) or based on their morphology (e.g. Kartaltepe et al. 2012, Kaviraj et al. 2013). The latter approach relies on the assumption that starbursts are generally triggered by interactions between galaxies, as observed in the local universe (e.g. Sanders et al. 1988, Barton et al. 2000), while main-sequence galaxies would represent a ‘normal’, secular channel of stellar mass growth in galaxies that is fueled by the steady accretion of cold, primordial gas (e.g. Bouché et al. 2010).

A series of studies on the star-forming population have improved our understanding of normal (MS) galaxies and starbursts and are in qualitative agreement with this picture. Starbursting sources are more compact on average (e.g. Elbaz et al. 2011, Rujopakarn et al. 2011) than main-sequence galaxies which have a stellar structure that is well described by exponential disks (e.g. Wuyts et al. 2011, Salmi et al. 2012). They display deficits in the intensity of infrared (IR) spectral features (e.g. PAH bands or in the far-IR [CII]-line; Elbaz et al. 2011, Graciá-Carpio et al. 2011), and have warmer IR spectral energy distributions (SEDs; e.g. Heisler & Vader 1994, Sanders & Mirabel 1996, Chapman et al. 2003, Elbaz et al. 2011, Magdis et al. 2011, Béthermin et al. 2012; and references therein). These are telltale features of intense and spatially concentrated star formation as is expected to occur in interacting or merging galaxies where gravitational torques funnel gas to their centers (e.g. Mihos & Hernquist 1996, Hopkins et al. 2006).

The efficiency with which gas is converted into stars in such settings may be up to an order of magnitude higher than in the extended gas reservoirs which fuel star formation activity in normal galaxies out to $z \sim 2$ (e.g. Daddi et al. 2010b, Genzel et al. 2010, Tacconi et al. 2013). This strong contrast in star formation efficiency ($\text{SFE} \equiv \text{SFR}/M_{\text{gas}}$) is often taken as one of the most clear-cut manifestations for the existence of two distinct star formation laws – a secular mode in main-sequence galaxies and a starburst mode characterized by short depletion timescales ($\lesssim 100$ Myr, e.g. Solomon & Vanden Bout 2005; and references therein). Whether or not such a bimodality represents the physical reality has been questioned (e.g. Narayanan et al. 2012) on the grounds of discrete ‘concordance’ values being assumed for the CO-to- H_2 conversion factor α_{CO} and, secondly, due to the expectation that star formation laws at a basic level should be expressed in terms of volumetric quantities rather than observationally more easily accessible surface densities of SFR and gas (e.g. Krumholz et al. 2012). The lack of known sources with SFEs between those measured for normal disk galaxies and strong starbursts could also be a selection effect: initial CO follow-up observations of high-redshift galaxies targeted only highly luminous sources experiencing ‘bursty’ star formation (sub-millimeter galaxies and QSOs; e.g. Omont et al. 1996, Frayer et al. 1998, Walter et al. 2003, Greve et al. 2005, Maiolino et al. 2007, Tacconi et al. 2008) and following improvements in the sensitivity of millimeter receivers (Chenu et al. 2007, Perley et al. 2011), dedicated studies of typical main-sequence galaxies were undertaken (e.g. Daddi et al.

2008, 2010a, Tacconi et al. 2010, Geach et al. 2011, Tacconi et al. 2013). If, as discussed in Renaud et al. (2012), the gas density distribution function – which reflects the turbulence-driven structure of the interstellar medium (ISM) – is a crucial factor in determining the shape of star formation laws, then intermediate SFEs should indeed occur in, e.g., minor mergers or in certain stages of galaxy interactions when the gas density distribution is not modified from the steady state as strongly as during final coalescence. However, a dichotomy in the distribution of SFEs could still occur if the timescales for such variations were short (e.g. Teyssier et al. 2010, Bournaud et al. 2011a).

In this paper we consider a large sample of local and high-redshift SFGs which we use to extend the ‘2 Star-Formation Mode framework’ (2-SFM) introduced in Sargent et al. (2012; henceforth abbreviated as ‘S12’) to the molecular gas component of SFGs. The 2-SFM framework relies on basic observables (e.g. the evolution of sSFR in main-sequence galaxies or their stellar mass distribution) and correlations between observables (e.g. the star-forming main sequence or the Schmidt-Kennicutt relation). Our goal is to describe how the star formation efficiency (SFE) and the molecular gas content of galaxies are related to their location with respect to the main sequence, i.e. to their specific star formation rate (sSFR), which is the main diagnostic of ‘starburstiness’ within the 2-SFM framework. We will postulate that there is a different law linking the SFE and sSFR for main-sequence galaxies and starbursts, and derive these laws from comparison with the observations. We will show that the population of massive SFGs that reside on the main sequence has similar molecular gas properties across a broad range of redshifts ($z \lesssim 3$) and we will use our detailed description of the starburst population and its SFR-‘boosting’ developed in Section 4.2 to demonstrate how in the 2-SFM framework a bimodal behavior in terms of SFE arises naturally even in the absence of discrete star formation laws for normal galaxies and starbursts. The description of SFE in the SFG-population developed in this paper forms the basis for the prediction of molecular gas mass functions and CO luminosity functions in a companion paper (Sargent et al. in prep.; Paper II, henceforth).

The outline of this manuscript is as follows. Section 2 introduces the observational dataset we use and how it was homogenized. We then employ this reference sample in Section 3 to calibrate galaxy-scale star formation laws – both in terms of observables (L_{IR} & L'_{CO}) or intrinsic quantities (SFR & M_{H_2}) – for galaxies at low and high redshift. These calibrations depend on the adopted CO-to- H_2 conversion factor α_{CO} , and the corresponding systematics will also be assessed in Section 3. The mathematical description of the starburst population in the 2-SFM framework, and its relation to main-sequence galaxies is the focus of Sect. 4 where we derive the distribution of the burst amplitudes – the ‘boost-function’ – that transforms a theoretical population of pure main-sequence star forming galaxies into the observed distribution of sSFR. We discuss what physical mechanisms could produce this boost-function and consider in particular the possible link between starbursts and galaxy mergers. In Section 5 we will combine the redshift-independent Schmidt-Kennicutt law derived in Section 3

with the evolution of the sSFR distribution from S12 to construct prescriptions for the relative variation of molecular gas properties of normal and starburst galaxies that are particularly simple (and self-similar) once they are referred to the properties of the average main-sequence galaxy. Our results are presented in three main blocks: the SFE and gas fractions of main-sequence galaxies and starbursts are the subject of Section 5.1 and 5.2, respectively; Section 5.3 focuses on the CO-to-H₂ conversion factor and its variation within the main sequence and among starbursting systems. We then discuss and summarize our findings in Sections 6 and 7.

Throughout this article we adopt the WMAP-7 cosmology ($\Omega_m = 0.273$, $\Omega_\Lambda + \Omega_m = 1$ and $H_0 = 70.4$ km s⁻¹ Mpc⁻¹; Larson et al. 2011). Star formation rates and stellar masses are given for a Chabrier (2003) initial mass function⁶ (IMF). All literature values have been adapted accordingly. Metallicities are given on the Kewley & Dopita (2002; henceforth ‘KD02’) scale⁷ and (molecular) gas mass estimates include a 36% correction for helium.

2. DATA

We discuss two different kinds of data sets in this section. To begin with (Sect. 2.1), we describe individual, CO-detected SFGs which we will utilize to establish the basic scaling relations (e.g. for SFE or gas fractions) that link the molecular gas content of massive ($M_\star > 10^{10} M_\odot$) SFGs to fundamental galaxy properties like (s)SFR or M_\star . In Section 2.2 we introduce statistical samples of SFGs at $z \sim 1$ and 2. These will subsequently be used (1) to visualize/simulate complete samples of galaxies that obey the aforementioned scaling relations, and (2) to extend the analysis to fainter galaxies where the validity of such scaling relations can be verified with image stacking.

2.1. The reference sample of individual star-forming galaxies

Our ‘reference sample’ of normal galaxies at redshifts $z \lesssim 3$ comprises 91 sources from the recent literature (see Sects. 2.1.1 & 2.1.2). We complement these with local and high-redshift starbursts with measured CO-to-H₂ conversion factors (see Sect. 2.1.3). These are essential for a further investigation of the notion that the ‘bimodality’ of star formation is particularly pronounced in terms of SFE (e.g. Daddi et al. 2010a, Genzel et al. 2010).

2.1.1. Normal galaxies: low redshift CO-detections

The HERACLES survey (Leroy et al. 2008, 2009, 2013) targeted the CO($J=2 \rightarrow 1$) transition in nearby ($D \lesssim 15$ Mpc) THINGS galaxies (Walter et al. 2008) with the IRAM 30 m single-dish telescope. Here we select 20 galaxies with spiral galaxy morphology and stellar mass $M_\star \geq 10^{10} M_\odot$ from the HERACLES sample. Stellar masses (converted to the Chabrier (2003)

scale) and morphological information are taken from the compilations of Skibba et al. (2011) or Leroy et al. (2008, 2009), or from the NASA/IPAC Extragalactic Database⁸ if not listed in either of the former. Metallicity estimates for most of the selected HERACLES spirals are provided in Moustakas et al. (2010). The IR (8-1000 μ m) luminosities attributed to the HERACLES galaxies are based on the photometry reported in Dale et al. (2007) and have been calculated following eq. 22 in Draine & Li (2007).

We augment the local main-sequence galaxies from the HERACLES data set with a subset of galaxies from the first release of the COLD GASS survey (Saintonge et al. 2011) for which an accurate IR luminosity could be calculated thanks to the presence of a counterpart in either the *IRAS* Faint Source Catalog (v2; Moshir et al. 1992) or the *AKARI*/Far-Infrared Surveyor (FIS; Kawada et al. 2007) all-sky survey Bright Source Catalog (v1.0; Yamamura et al. 2010). An additional cut in stellar mass (taken from Saintonge et al. 2011) at $M_\star = 10^{10} M_\odot$ excluded all less massive sources. Among the 222 sources in the first COLD GASS data release 32 fulfill these criteria; they lie in the redshift range $0.025 < z < 0.05$ and are all late-type galaxies with CO($J=1 \rightarrow 0$) fluxes measured by the IRAM 30 m telescope at $S/N > 4$. IR luminosities for these galaxies were computed using the spectral energy distribution (SED) library of Chary & Elbaz (2001) and allowing renormalization of the templates when fitting the reliable⁹ *IRAS* or *AKARI* photometry at $\lambda_{\text{rest}} \geq 30 \mu\text{m}$ (for details on the IR SED-fitting see Hwang et al. 2010).

2.1.2. Normal galaxies: high redshift CO-detections

CO-transitions in main-sequence galaxies at $z \gg 0$ have been targeted by Geach et al. (2009, 2011; CO($J=1 \rightarrow 0$) at $z \sim 0.4$), Daddi et al. (2010a,b; CO($J=2 \rightarrow 1$) at $z \sim 0.5$ & 1.5), Tacconi et al. (2010; CO($J=3 \rightarrow 2$) at $z \sim 1.2$ & 2.3), and Magdis et al. (2012a; CO($J=3 \rightarrow 2$) at $z \sim 3$) – all using the IRAM Plateau de Bure (PdBI) interferometer – leading to line flux measurements at $S/N \gtrsim 4$ toward 32 of 39 observed galaxies (for the remaining galaxies 3σ upper flux limits are available.) The stellar masses of these sources are in the range $5 \times 10^{10} < M_\star/M_\odot \lesssim 5 \times 10^{11}$, as determined by SED fitting of the near-UV to near-IR broad-band photometry.

The derivation of SFRs varies among the different aforementioned studies. Geach et al. (2009, 2011) estimate the IR-luminosity from the flux of the $7.7 \mu\text{m}$ emission, as constrained by the *Spitzer* IR spectrograph (IRS), while Daddi et al. (2010b) based the luminosity measurements for their $z \sim 0.5$ sources on *Spitzer*/MIPS $24 \mu\text{m}$ fluxes. SFR-estimates for $z \sim 1.5$ sBzK galaxies presented in Daddi et al. (2010a) are an average of dust corrected UV luminosities, mid-IR continuum luminosities from $24 \mu\text{m}$ imaging and VLA 1.4 GHz radio continuum fluxes, all of which were found to give consistent SFR-estimates. Magdis et al. (2012a) adopted a similar averaging approach but were able to add *Herschel*/PACS and SPIRE photometry to constrain the

⁶ Logarithmic masses and SFRs based on a Salpeter (1955), a Kroupa (2001) and a Baldry & Glazebrook (2003) IMF are converted to the Chabrier scale by adding -0.24 dex, 0 dex and 0.02 dex, respectively.

⁷ When necessary, metallicity information from the literature was converted to the KD02 calibration by means of the prescriptions in Kewley & Ellison (2008).

⁸ <http://ned.ipac.caltech.edu>

⁹ Flux quality flags are either ‘high’ or ‘moderate’ for *IRAS* sources and ‘high’ for *AKARI* sources.

dust-emission of their $z \sim 3$ LBGs. We adopted all these SFR (L_{IR}) measurements without further modifications but in the interest of maximal sample homogeneity chose to re-compute L_{IR} values for the $z \sim 1.2$ sources in Tacconi et al. (2010) as these authors report SFRs that are based on a combination of extinction-corrected optical emission lines, UV flux and mid-IR photometry. To derive new L_{IR} estimates we searched the Far Infrared Deep Extragalactic Legacy (FIDEL, PI: M. Dickinson, see also data description in Magnelli et al. 2009) coverage of the Extended Groth Strip for associated *Spitzer*/MIPS $24\mu\text{m}$ detections and converted these to IR luminosities with the main-sequence star-forming galaxy IR SED of Elbaz et al. (2011). Two of the ten sources with $z \sim 1.2$ from the Tacconi et al. (2010) sample had VLA 1.4 GHz detections from the AEGIS 20 catalog (Iverson et al. 2007), such that the $24\mu\text{m}$ - and radio-based SFR could be averaged. For sources at $z \sim 2.3$ in the sample of Tacconi et al. (2010), neither IR nor radio flux measurements were available; we hence used the original SFRs reported by Tacconi et al. (2010) which are based on extinction-corrected $H\alpha$ luminosities and which we converted to an IR-luminosity following Kennicutt (1998b).

To summarize, we have compiled a sample of 91 massive ($M_* \geq 10^{10} M_\odot$), main-sequence galaxies with CO-detections of which 57% are local ($z < 0.05$) systems and the remaining 43% redshifted to $0.35 < z < 3.2$.

2.1.3. Starbursting galaxies with measured α_{CO}

Starbursting galaxies with the same information as available for our reference sample of normal galaxies are listed in the recent study of Magdis et al. (2012b; starburst-like galaxies at $2.3 < z < 4$) and in Solomon et al. (1997; local starbursting *IRAS* ULIRGs). An accurate assessment of the behavior of SFE during starburst episodes – one of the main aims of this paper – requires an observational determination of the CO-to- H_2 conversion factor α_{CO} . In the case of the local ULIRGs, we thus restrict ourselves to nine objects – VII Zw 31, Arp 193, Arp 220, Mrk 273, 00057+4021, 02483+4302, 10565+2448, 17208-0014, 23365+3604 – with two independent measurements of α_{CO} : one based on dynamical constraints¹⁰ by Downes & Solomon (1998) and the other based on large velocity gradient (LVG) radiative transfer modeling by Papadopoulos et al. (2012). The flux of the CO($J=1 \rightarrow 0$) transition toward our subsample of nine $z < 0.07$ *IRAS*-detected ULIRGs was measured with the IRAM 30 m single-dish telescope by Solomon et al. (1997). We computed their IR luminosities (and thence SFRs) using spectroscopic redshifts from NED and all available *IRAS* photometry, following the standard recipes provided by Sanders & Mirabel (1996; their Table 1). Stellar masses – which are particularly important for the characterization of these systems in terms of sSFR, our prime indicator of “starburstiness” – have been published for some of the ULIRGs in our sample (e.g., Elbaz et al. 2007, da Cunha et al.

2010, Howell et al. 2010, U et al. 2012), but to our knowledge no single study has done this consistently for all sources of interest. We hence re-estimated stellar masses for the Downes & Solomon (1998) ULIRGs based on 2MASS K -band fluxes (Skrutskie et al. 2006) and prescriptions for mass-to-light ratios, M_*/L_K , as derived by Arnouts et al. (2007; their eq. 2) and Juneau et al. (2011; their eq. B2). The stellar masses we adopt in the following for the Downes & Solomon (1998) ULIRGs were obtained by averaging the estimates calculated according to these two prescriptions. They agree well with the available literature measurements (median offset 0.1 dex).

In addition to the nine low-redshift starbursts just described we also include the three high- z sub-millimeter galaxies GN20 ($z = 4.05$), SMMJ2135-0102 ($z = 2.325$) and HERMES J105751.1+573027 ($z = 2.957$) in our analysis. The recent determination of their conversion factor α_{CO} in Magdis et al. (2012b) by means of the $M_{\text{gas}}/M_{\text{dust}}$ -ratio technique (see also Leroy et al. 2011, Magdis et al. 2011) relied on: (i) a far-IR SED/dust emission that is accurately constrained by *Herschel* and millimetric continuum observations (see Magdis et al. 2012b for a detailed listing), and (ii) CO($J=1 \rightarrow 0$) line fluxes from the (J)VLA (for GN20; see Carilli et al. 2010, Hodge et al. 2012) and the Green Bank Telescope (for SMMJ2135-0102 and HERMES J105751.1+573027; see Swinbank et al. 2010 and Riechers et al. 2011, resp.). All three sources have sSFR-enhancements with respect to the main sequence of at least a factor three, as constrained by the optical to near-IR and IR SED-fitting of Magdis et al. (2012b). Furthermore their CO-to- H_2 conversion factors are systematically lower than that of the Milky Way, similar to the values typically measured in interacting local ULIRGs.

2.2. Statistical samples of star-forming galaxies in GOODS-South

With the purpose of demonstrating the applicability of our recipes for computing molecular gas properties for observed galaxy samples, based on individual measurements of stellar masses and SFRs, we use two samples of K -selected galaxies in the GOODS-S field, at $z \sim 1$ and 2 taken from the work of Daddi et al. (2007a) and Daddi et al. (2007b; see also Salmi et al. 2012 for more details on the $z \sim 1$ sample). The same samples were used in the recent papers by Magdis et al. (2012b) and Mullaney et al. (2012). We refer to the original papers for details of how stellar masses were derived, based on empirical recipes using colors and absolute luminosities. The SFRs of the galaxies at $z \sim 1$ and 2 are based on $24\mu\text{m}$ and UV observations, respectively, and are known to compare well on average with other tracers including *Herschel*-based SFR-measurements (Daddi et al. 2007a, Elbaz et al. 2010, Reddy et al. 2012).

3. GALAXY-SCALE STAR FORMATION LAWS: CORRELATIONS BETWEEN SFR AND GAS MASS AND THE ASSOCIATED OBSERVABLES

Recent reports (e.g. Daddi et al. 2010b, Genzel et al. 2010) of a systematic offset between the power law relation linking the overall surface density of SFR and gas mass (the Schmidt-Kennicutt (S-K) law $\Sigma_{\text{SFR}} \propto \Sigma_{\text{gas}}^n$;

¹⁰ In the following we adopt a mass-to-light ratio α_{CO} that is given by the ratio between gas mass and dynamical mass within a $\sim 1\text{--}3\text{ kpc}$ region encompassing both the inner, high-density nuclear disk/ring and an outer, lower-density disk (with volume filling factor ~ 0.1 for the gas) of the ULIRGs modeled in Downes & Solomon (1998; see their Tables 3 & 9).

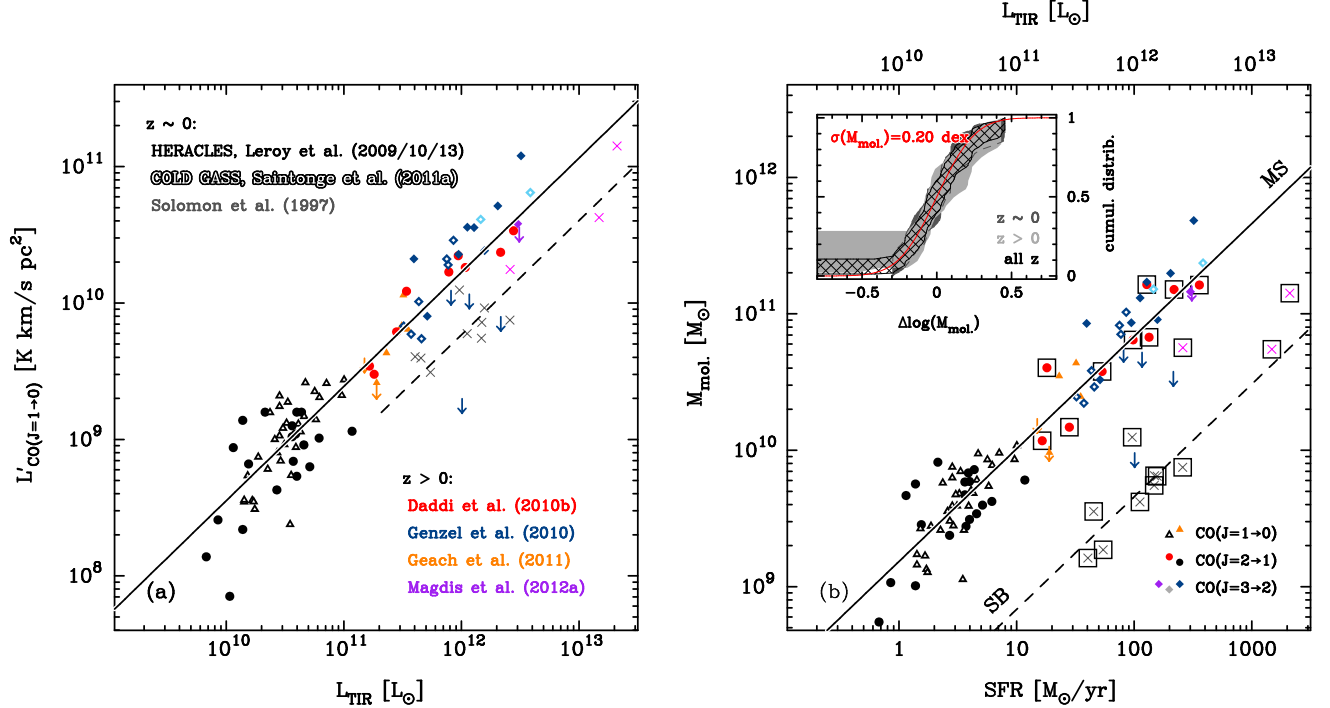


FIG. 1.—: Observed correlation between measures of star formation rate and molecular gas content for massive ($M_{\star} > 10^{10} M_{\odot}$) main-sequence galaxies and starbursts at low and high redshift. Low redshift sources (filled/open black symbols – normal galaxies; grey crosses – starbursting (U)LIRGs) are from the HERACLES, GOLD GASS and *IRAS* surveys. Redshifted galaxies from the literature (see legend) are plotted in color (orange – $z \sim 0.4$; red – $z \sim 0.55$ & $z \sim 1.5$; blue – $z \sim 1.2$ & $z \sim 2.3$; magenta – starbursts at $2.3 < z < 4$), with arrows indicating 3σ upper limits for CO non-detections. Open blue and cyan symbols indicate modified SFR estimates (see section 2.1.2 for details) based on radio or IR data for sources in Genzel et al. (2010) and Tacconi et al. (2010). The shape of the symbol indicates which CO transition was detected toward the individual sources (cf. legend in lower right corner of panel b).

(a): Correlation between infrared luminosity (L_{IR}) and CO-luminosity ($L'_{\text{CO}(J=1\rightarrow0)}$; standard excitation corrections – e.g. Dannerbauer et al. (2009), Leroy et al. (2009) – were applied to $J > 1$ transitions) with the best-fitting relation derived for the main-sequence galaxy sample plotted as a solid black line. The strong starbursts considered here (cross symbols) are on average offset to higher SFRs by a factor of three (dashed line).

(b): Inverse, integrated Schmidt-Kennicutt relation between SFR and molecular gas mass ($M_{\text{mol.}}$), the latter having been derived based on either (i) observational determinations of α_{CO} (available for sources with boxed symbols) or (ii) using a metallicity-dependent conversion factor (see text of Sect. 3.2). The dispersion about the best-fit linear trend (solid black line) for main-sequence galaxies is approximately Gaussian with a dispersion $\sigma(M_{\text{mol.}}) \sim 0.2$ dex (red curve in inset). Dashed line – offset locus with approx. 15-fold higher SFE for strong starburst galaxies.

Schmidt 1959, Kennicutt 1998a) of normal galaxies and starbursts were highly influential in shaping the notion of ‘bimodal’ star formation. These findings are subject to two systematic uncertainties. Firstly, the measured offset between normal and starburst galaxies depends on (potentially population-dependent) recipes for CO-to- H_2 conversion factors which are hard to estimate for a statistically significant number of SFGs, especially at $z \gg 0$. Secondly, the sampling of the S-K plane obtained as a result of targeted CO follow-up observations toward selected SFGs is patchy. Constructing a reliable and statistically representative sampling of the distribution of SFGs in the S-K plane is thus not only important to explore different modes of star formation. The observed S-K law is also often referred to as a benchmark for the performance/validity of recipes for ISM processes in simulations (e.g. Robertson & Kravtsov 2008, Monaco et al. 2012) and hence used to gauge our understanding of the underlying physics itself.

In this section we return to our literature compilation of low- and high-redshift main-sequence galaxies with CO-detections that we presented in Sects. 2.1.1 and 2.1.2. We re-measure the slope and dispersion of the galaxy-scale star formation law and in doing so for the first time are able to incorporate α_{CO} -measurements from the recent study of Magdis et al. (2012b) for a fraction of our reference sample of normal galaxies. Rather than using SFR and gas mass surface densities, we consider the simpler relations between integrated quantities, namely the total SFR and molecular gas mass or the corresponding observables, L_{IR} and $L'_{\text{CO}(J=1\rightarrow0)}$. For the rest of this article we will use ‘ L'_{CO} ’ as a shorthand for the line luminosity $L'_{\text{CO}(J=1\rightarrow0)}$ of the first rotational transition of ^{12}CO .

3.1. $L'_{\text{CO}(J=1\rightarrow0)}$ vs. L_{IR}

We begin with the relation between the observables, L_{IR} and L'_{CO} , that are the starting point for estimat-

ing SFRs and molecular gas content of SFGs. As described in Sect. 2.1 all galaxies considered in the following have stellar masses $M_\star \geq 10^{10} M_\odot$. Current observations of BzK-selected main-sequence galaxies (e.g. Dannerbauer et al. 2009, Aravena et al. 2010) suggest that typical excitation corrections for the first two higher order transitions $J=2 \rightarrow 1$ and $3 \rightarrow 2$ are $r_{21} = 0.8-0.9$ and $r_{31} \simeq 0.5$. Similarly, Leroy et al. (2009) find an average $J=2 \rightarrow 1/J=1 \rightarrow 0$ line ratio of 0.8 for HERACLES galaxies. In Fig. 1a we plot the accordingly corrected $\text{CO}(J=1 \rightarrow 0)$ luminosities of local (black and white symbols) and redshifted sources (colored symbols) against their IR luminosity. We then fitted the CO line luminosity as a function of IR luminosity. While performing a regression of L_{IR} on L'_{CO} would be more natural (as representing the relation between cause and effect, i.e. $M_{\text{mol.}}$ and SFR, resp.) our choice is motivated by the aim to provide recipes for the molecular gas content and associated tracer emission beginning with the currently observationally more easily accessible SFR-measurements. A Buckley & James (1979; ‘BJ’ hereafter) regression (implemented as described in Isobe et al. 1986), which allows for a statistically correct treatment of the 3σ upper detection limits for six galaxies from Tacconi et al. (2010) and Geach et al. (2011), gives

$$\log \left(\frac{L'_{\text{CO}(J=1 \rightarrow 0)}}{\text{K km/s pc}^2} \right) = \alpha_1 + \beta_1 \log \left(\frac{L_{\text{IR}}}{L_\odot} \right), \quad \text{with} \quad (1)$$

$$(\alpha_1; \beta_1) = (0.18 \pm 0.02; 0.84 \pm 0.03) \quad \text{for normal galaxies.}$$

The dispersion about this best-fit trend line in the y -direction is 0.21 dex. In performing the linear regression we have down-weighted sources detected in $\text{CO}(J=3 \rightarrow 2)$ by a factor of two due to the large excitation corrections r_{31} .

Under the assumption that starbursts follow a correlation with identical slope, we use our reference sample of starburst galaxies (see Sect. 2.1.3) to solve for the normalization of eq. 1 which best reproduces their average offset. We find

$$(\alpha_1; \beta_1) = (-0.28^{+0.15}_{-0.09}; 0.84),$$

i.e. an offset of 0.46 dex or approx. a factor 2.9 with respect to the locus of main-sequence galaxies. This similar systematic difference was already indicated by Solomon et al. (1997; see their Fig. 3) in their pioneering analysis of CO-emission in nearby ULIRGs. Local main-sequence galaxies with the IR luminosities of starbursting ULIRGs are, however, exceedingly rare (e.g. S12) such that this difference could also have been explained by a double power-law nature of the star formation law or a single, steeper relation ($L_{\text{IR}} \propto L'_{\text{CO}}{}^{1.3}$) owing to different probability gas density distributions in mergers and normal galaxies (Narayanan et al. 2008, Juneau et al. 2009). The advent of CO line flux measurements for high- z normal galaxies with ULIRG-luminosities has since added another piece of evidence in support of a systematic offset (e.g. Genzel et al. 2010)

3.2. $M_{\text{mol.}}$ vs. SFR

The integrated S-K law linking the molecular gas mass ($M_{\text{mol.}}$) and SFR is expected to have a different slope or curvature than the correlation between logarithmic

luminosities L'_{CO} and L_{IR} unless the average CO-to- H_2 conversion factor

$$\alpha_{\text{CO}(J=1 \rightarrow 0)} = \frac{M_{\text{mol.}}}{L'_{\text{CO}(J=1 \rightarrow 0)}}$$

is a constant. Evidence to the contrary has been presented in numerous studies, the most recent of which are Leroy et al. (2011), Schruba et al. (2012) and Genzel et al. (2012) who show – albeit with large uncertainties – how α_{CO} decreases with metallicity among galaxies in the Local Group and in massive main-sequence galaxies at $z < 2.5$, respectively. Note that Sandstrom et al. (2013) find a similar trend for decreasing α_{CO} with increasing metallicity when considering spatially distinct regions within nearby galaxies. In the next paragraphs we discuss a scheme for assigning metallicity-dependent α_{CO} -values to the normal SFGs in our reference sample (Sect. 3.2.1) and then proceed to fit the resulting relation between SFR and $M_{\text{mol.}}$ in Sect. 3.2.2. We close this section with an assessment of the robustness of the galaxy-scale star formation law obtained in this way (Sect. 3.2.3).

3.2.1. Statistically inferred CO-conversion factors

For nine of the 91 main-sequence galaxies in our reference sample the CO-to- H_2 conversion factor has been measured and found to be broadly consistent with the (negative) power-law relation between α_{CO} and metallicity found for galaxy samples in the nearby Universe (Magdis et al. 2012b). For the remainder of the population we assume that their α_{CO} too follows a relation with metallicity Z that has the form

$$\log(\alpha_{\text{CO}}) = \nu + \xi \log(Z/Z_\odot), \quad (2)$$

and that metallicity can be deduced in a statistical sense from stellar mass and SFR as proposed by Mannucci et al. (2010) and Lara-López et al. (2010) who describe the interdependence of these three quantities as a 2D manifold in M_\star -SFR- Z space (see Fig. 2a). In the following we use this ‘fundamental metallicity relation’ (FMR) as parametrized by Mannucci et al. (2010). Since starbursts constitute a small fraction of the star-forming population, the FMR primarily reflects the dependence of metallicity on SFR and M_\star for main-sequence galaxies. As the stellar mass and SFR of the CO-detections in our reference sample are known (within observational errors) we can use the FMR to statistically infer metallicities $Z(\text{SFR}, M_\star)$, and thence CO-conversion factors α_{CO} for each of the galaxies in our reference sample¹¹. This enables us to calibrate the $M_{\text{mol.}}$ vs. SFR relation independently from the correlation between L'_{CO} and L_{IR} derived in Sect. 3.1. Note that more general expectations for α_{CO} -variations in the M_\star vs. SFR plane that account

¹¹ Mannucci et al. (2010) originally were only able to study the FMR at $z \gg 0$ for massive ($M_\star/M_\odot \geq 10^{10}$) field galaxies. New work has since extended the relation to lower stellar masses (Cresci et al. 2012) and separately verified its validity in the cluster environment at $z \sim 1.4$ (Magrini et al. 2012). The FMR is generally assumed to hold over the range $0 < z < 2.5$, i.e. should apply to almost all galaxies in our reference sample. Beyond $z \sim 2.5$ conflicting evidence for constancy (e.g. Dessauges-Zavadsky et al. 2011, Richard et al. 2011, Lara-López et al. 2012, Belli et al. 2013) and evolution (e.g. Laskar et al. 2011, Sommariva et al. 2012) of the FMR has been presented.

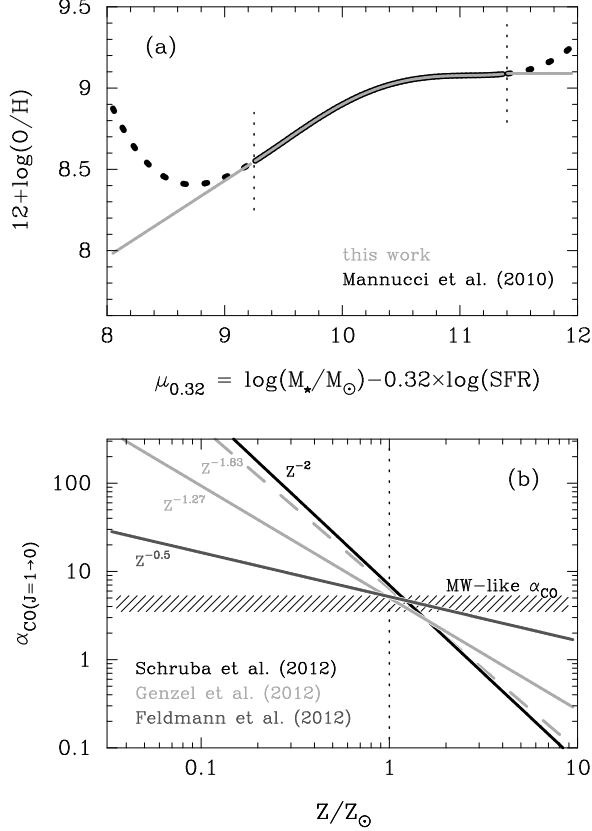


FIG. 2.— Overview of recipes used to assign CO-to-H₂ conversion factors, α_{CO} , to observed and modeled galaxies based on their SFR and stellar mass.

(a): Fundamental metallicity relation (FMR) as determined by Mannucci et al. (2010; *thick line section*) and continuation of the FMR assumed in our analytic-empirical modelling to regions of parameter space where the mathematical description of the plane proposed in Mannucci et al. (2010) diverges due to the absence of data. Note that the extension beyond $\mu_{0.32} \in [9.25, 11.4]$ affects only a minority of the galaxies modeled in the present work.

(b): Recently proposed relations between metallicity (expressed in multiples of the solar metallicity Z_{\odot} in the system of Kewley & Dopita 2002) and α_{CO} based on simulations (Feldmann et al. 2012) or observations (Schruba et al. 2012, Genzel et al. 2012; for the latter study the fit derived for both low- and high- z SFGs (*light grey, dashed*) and that for a sample restricted to $z \geq 1$ SFGs (*light grey, solid*) is shown). All recipes predict a Milky Way-like α_{CO} at approx. solar metallicity but diverge significantly at lower/higher enrichment due to the different measured slopes (see annotations beside trend lines).

for (1) changes of the conversion factor within both the normal and starbursting galaxy population, and (2) the relative importance of these to classes of SFGs depending on the location in the plane, are the topic of 5.3.2. Existing literature consistently reports the normalization ν of the α_{CO} vs. metallicity relation in eq. 2 to be such that Milky Way-like conversion factors $\alpha_{\text{CO}} = 4.4 M_{\odot}/(\text{K km/s pc}^2)$ are reached around solar

metallicity. Measurements and expectations for the slope ξ span a larger range which we illustrate in Fig. 2b. In view of these poor constraints we took a different approach to estimating slope and normalization of the relation between α_{CO} and metallicity. The details of this calculation (and the underlying assumptions) are described in Paper II where we use the 2-SFM framework to infer the redshift-evolution of the molecular gas mass function and CO luminosity function (LF) starting from the stellar mass function of SFGs. The 2-SFM prediction for the $z \sim 0$ CO LF can be directly compared to the local CO LF measured by Keres et al. (2003). In particular, the Schechter function parameters of the observed local CO LF are sensitive to the choice of ν and ξ in eq. 2. The best-fit slope and normalization we obtain in this way are $\xi \simeq -0.9$ and $\nu \simeq 0.7$ (or $\alpha_{\text{CO}} \simeq 5$ at solar metallicity Z_{\odot}) and we subsequently adopt these values to assign conversion factors to all galaxies in our reference sample that lack an observational determination of α_{CO} . It should be clear that our strategy for constraining the shape of the α_{CO} vs. metallicity relation is subject to certain systematics (e.g., the assumed scatter of the correlation between α_{CO} and metallicity) which we discuss in Paper II and which are the reason why we do not provide error estimates on ν and ξ . However, our main goal here is to determine the integrated S-K relation for massive main-sequence galaxies and we will show in Sect 3.2.3 that it is quite insensitive to the slope and normalization of eq. 2 due to the almost flat mass-metallicity relation in this stellar mass range (e.g. Tremonti et al. 2004). Moreover, it is interesting that with slope $\xi \simeq -0.9$ and normalization $\nu \simeq 0.7$ the scatter of the S-K relation is smaller than with any other of the recipes for α_{CO} shown in Fig. 2b.

3.2.2. Integrated Schmidt-Kennicutt laws

Multiplication of the excitation-corrected CO-luminosities of Fig. 1a with (i) observed CO-to-H₂ conversion factors if available or (ii) the statistical CO-conversion factors discussed in the previous section provides a measure of the molecular gas mass for each of the main-sequence galaxies in our reference sample. These measurements are plotted against their SFR in Fig. 1b. At the stellar masses considered here, the IR-excess $L_{\text{IR}}/L_{\text{UV}}$ of main-sequence galaxies is in general ~ 10 or larger (e.g. Whitaker et al. 2012; M. Pannella et al., in prep.), leading to a nearly 1:1 correspondence between L_{IR} and SFR, as indicated by the lower and upper scale for the x -axis of Fig. 1b. We convert IR luminosities to SFRs following the prescription of Kennicutt (1998b).

BJ-regression, applied to the data in Fig. 1b, returns a very similar logarithmic slope as for the correlation between L'_{CO} and L_{IR} due to the relatively narrow range of metallicities spanned by our low- and high- z data:

$$\log\left(\frac{M_{\text{mol.}}}{M_{\odot}}\right) = \alpha_{2, \text{SFR}} + \beta_2 \log\left(\frac{\text{SFR}}{M_{\odot}/\text{yr}}\right), \quad \text{with} \quad (3)$$

$$(\alpha_{2, \text{SFR}}; \beta_2) = \begin{cases} (9.18 \pm 0.02; 0.83 \pm 0.03) & \text{for normal galaxies} \\ (8.00^{+0.29}_{-0.10}; 0.83) & \text{for strong starbursts.} \end{cases}$$

Here the line parameters for the starbursts in our reference sample were derived by solving for the normalization under the assumption of an identical, slightly sub-linear

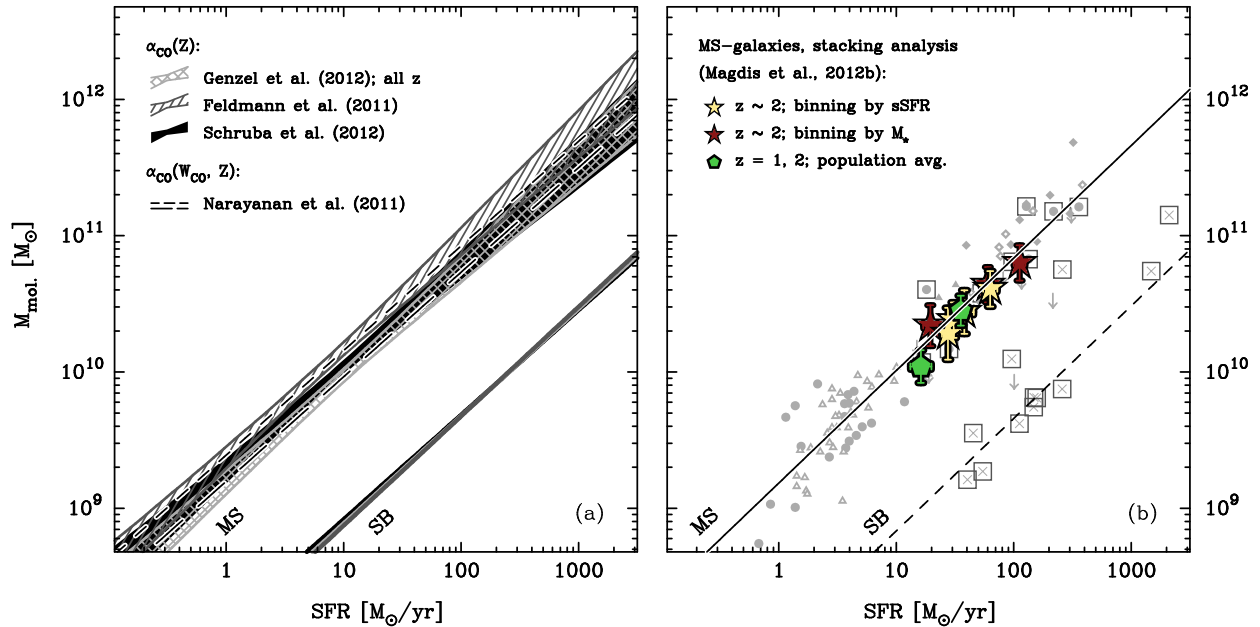


FIG. 3.— Robustness assessment of the integrated inverse S-K relation calibrated in Fig. 1 (see also eq. 3). (a) Changes in the best-fit S-K relation, depending on the metallicity-dependence, Z^β , of the conversion factor, α_{CO} , reported by recent observational (Genzel et al. 2012, Schrubba et al. 2012) and numerical (Narayanan et al. 2011, Feldmann et al. 2012) work. (Filled/hatched areas encompass the 95% confidence region of the corresponding best-fit relations.) The additional dependence on the CO surface brightness, W_{CO} , proposed by Narayanan et al. (2011) introduces an implicit dependence on galaxy size (long dashes – CO-flux averaged over optical half-light radius; short dashes – CO-flux averaged over two optical half-light radii).

(b) Extension of high- z S-K relations to the highest SFRs ($\sim 20 M_\odot/\text{yr}$) reached by the $z \sim 0$ main-sequence galaxies in our calibration sample. (Grey symbols in background reproduce data plotted in Fig. 1b). After inclusion of the stacked samples of $z \sim 2$ main-sequence galaxies from Magdis et al. (2012b; colored symbols), the $z \sim 2$ S-K relation is sampled over two orders of magnitude in SFR. The stacked samples bridge the gap between local and $z > 0$ calibration sources and are aligned with the best-fit S-K relation determined using these, thereby providing evidence of a universal S-K relation for massive main-sequence galaxies.

slope of the star-formation law for main-sequence and starbursting galaxies. Alternatively, in units of L_{IR} ,

$$\log\left(\frac{M_{\text{mol.}}}{M_\odot}\right) = \alpha_{2,\text{IR}} + \beta_2 \log\left(\frac{L_{\text{IR}}}{L_\odot}\right), \quad \text{with} \quad (4)$$

$$(\alpha_{2,\text{IR}}; \beta_2) = \begin{cases} (0.90 \pm 0.02; 0.83 \pm 0.03) & \text{for normal galaxies} \\ (-0.28^{+0.29}_{-0.10}; 0.83) & \text{for strong starbursts.} \end{cases}$$

The dispersion of the correlation is 0.20 dex and almost equal for the low- and high- z subsamples as shown in the inset panel of Fig. 1b where we plot the Kaplan & Meier (1958) estimator for the cumulative distribution functions of the offsets $\Delta(M_{\text{mol.}})$ of the individual measurements from the best-fitting trend line in eq. 3. The average offset of the reference starbursts with respect to the locus for normal galaxies is $1.18^{+0.10}_{-0.29}$ dex or roughly a factor 15 in terms of SFE¹². It should be emphasized, that this bimodality is arbitrary and merely reflects the properties of our small and incomplete selection of strong starbursts. In Sect 5.1.2 we propose an empirical description of the starburst population that allows for a contin-

uous enhancement of SFE, depending on the importance of burst-induced star formation activity.

3.2.3. Robustness of calibrated $M_{\text{mol.}}$ vs. SFR relation

The integrated S-K law for main-sequence galaxies which we calibrated in the previous section (eq. 3) constitutes a key ingredient for the description of the gaseous component of SFGs in the 2-SFM framework. It is thus essential to ascertain that the shape of our best-fit S-K law is not strongly dependent on assumptions made during the calculation of, e.g., gas masses.

A first potential cause of systematic uncertainty is our choice of the exponent of the relation between α_{CO} and metallicity discussed in Sect. 3.2.1. In calibrating the integrated S-K law, we adopted a dependence $\alpha_{\text{CO}} \propto Z^{-0.9}$ which is intermediate between the observed trends that range from Z^0 (e.g. Bolatto et al. 2008) to $Z^{-2.7}$ (e.g. Israel 1997). As representative examples of these different measurements¹³ we show in Fig.

¹² In this section we have used the dynamical constraints from Downes & Solomon (1998) to convert L'_{CO} to $M_{\text{mol.}}$ for the local starburst ULIRGs. As discussed in Sect. 5.3.1, the average offset from the integrated S-K law does not change for this sample when we use the α_{CO} -values given by Papadopoulos et al. (2012).

¹³ Observational studies generally parametrize α_{CO} -variations as a function of an absolute value of oxygen abundance rather than relative to the solar metallicity. The inferred oxygen abundances may vary significantly depending on the metallicity calibration and abundance diagnostic used (e.g. Kewley & Ellison 2008). In addition to these systematic uncertainties concerning the normalization of the metallicity scale, transformations between metallicity systems following, e.g., the recipes in Kewley & Ellison (2008) also

3a the star formation laws that we obtain when applying the simulation-based recipe of Feldmann et al. (2012; $\alpha_{\text{CO}} \propto Z^{-0.5}$), and those observationally determined by Genzel et al. (2012; $\alpha_{\text{CO}} \propto Z^{-1.27}$) and Schruba et al. (2012; $\alpha_{\text{CO}} \propto Z^{-2}$), to the normal galaxies in our reference sample (where we again have assigned metallicities using the FMR). We find that the slope of the different S-K laws are very similar and that their normalization only varies by 0.2 dex, such that they are all consistent within uncertainties among each other and also with our best-fit star formation law as given by eq. 3. We also tested the prescription Narayanan et al. (2011) developed based on their simulations of disks and mergers. These authors parametrize α_{CO} as a function of metallicity and CO surface brightness, W_{CO} , which introduces an implicit dependence on galaxy size. Using optical size measurements from the literature¹⁴ and the CO-fluxes of our reference galaxies we calculated CO-to- H_2 conversion factors and thence molecular gas masses following Narayanan et al. (2011). Our subsequent fit to the data showed that – for reasonable assumptions about the relative spatial distribution of optical and CO emission, see Fig. 3a – the Narayanan et al. (2011) prescription also leads to a star-formation law that is fully consistent with our preferred integrated S-K relation (eq. 3). The good general agreement between all these different recipes is due to the flatness of the mass-metallicity relation at $M_* > 10^{10} M_\odot$.

A second source of systematic uncertainty is our assumption that massive galaxies at all redshifts align along a single S-K law. By combining high-redshift galaxies from the PHIBBS survey with COLD GASS data Tacconi et al. (2013) recently presented an alternative scenario of parallel and linear S-K laws which are characterized by an SFE that increases with redshift. Tacconi et al. (2013) based their gas surface mass densities on CO($J=3 \rightarrow 2$) fluxes for $z > 1$ SFGs and uniformly applied a Milky Way-like conversion factor to all sources in their sample, regardless of mass, SFR and redshift. Both the strong excitation corrections applied to the high- z SFGs which dominate the high- Σ_{gas} regime of the S-K relation and the universal α_{CO} are in principle uncertain enough to bring about seemingly systematic shifts between the high- and low-redshift galaxy population in the S-K plane. Given the fact that there is little overlap in L_{IR} between our own subsamples of low- and

high-redshift galaxies plotted in Fig. 1b, we cannot rule out a series of offset and conceivably also curved star formation laws. By including average SFE-constraints from the stacking analysis of Magdis et al. (2012b), however, it is possible to bridge the luminosity-gap between $z > 2$ and local SFGs, as shown in Fig. 3b. In combination with the BM/BX-selected galaxies of Tacconi et al. (2010), the $z \sim 2$ S-K relation thus spans one and a half orders of magnitude and is seen to extend continuously into the parameter space of intermediate-redshift ($0.4 < z < 0.6$) and local disks without evidence for a discontinuity. When considering individual detections, the $z \sim 0.4$ galaxies of Geach et al. (2009, 2011) are aligned with the $z \sim 1.2$ and 1.5 sample of Tacconi et al. (2010) and Daddi et al. (2010a). Moreover, the skew and scatter around our universal S-K law are very similar for the subsets of $z \sim 0$ and $z \gg 0$ galaxies in our reference sample (see inset of Fig. 1b). Based on these observations, we conclude that the assumption of a single, slightly sub-linear relation between SFR and M_{mol} is presently a valid working hypothesis.

4. THE INNER WORKINGS OF THE 2-SFM FRAMEWORK: MAIN-SEQUENCE GALAXIES AND BOOSTED, STAR-BURSTING SOURCES

While the S-K relation we found in Sect. 3 for main-sequence galaxies is very well defined, it is much less obvious which concrete form of the star formation law should be used to describe the sparse and scattered starburst data. Our approach to interpreting the incomplete information on these sources will be to statistically link them to a synthetic and complete starburst population where we are able to relate the starburst properties to the pre-starburst (main-sequence) state. We describe in the following the ‘2 Star-Formation Mode framework’ (2-SFM) which is the basis for establishing this link.

4.1. Basic ingredients and successes of the 2-SFM framework

2-SFM is a simple and self-consistent scheme for the prediction of basic properties of the SFG-population that relies on basic observables (e.g. the evolution of sSFR in main-sequence galaxies or their stellar mass distribution) and uses their mathematical description (e.g. the Schechter function parametrization of the stellar mass distribution or slope and normalization of the main sequence) to produce an analytico-empirical description of the statistical properties of SFGs. It can be both predictive (see, e.g., the indirect measurement of the evolution of molecular gas mass functions in Paper II) or help to (re-)interpret existing measurements (e.g. IR luminosity functions or source counts; see Sargent et al. 2012, Béthermin et al. 2012, Gruppioni et al. 2013).

We introduced the 2-SFM framework in S12 where we demonstrated that the observational constraints on the $z \lesssim 2.5$ IR luminosity functions can be reproduced based on only three observables: (i) the redshift evolution of the stellar mass function for SFGs, (ii) the evolution of the specific star formation rate (sSFR) of main-sequence galaxies, and (iii) a double log-normal decomposition of the sSFR-distribution at fixed stellar mass into contributions (assumed redshift- and mass-invariant) from main-sequence and starburst ac-

change the curvature of the α_{CO} vs. metallicity relation. As an example, a log-linear relation between α_{CO} and metallicity derived using the R_{23} indicator (e.g. Pilyugin 2001, Kewley & Dopita 2002) may become a convex or concave function of metallicity when converted directly to a system based on the N2 diagnostic (e.g. Denicoló et al. 2002, Pettini & Pagel 2004). In view of these complications we chose to renormalize all literature determinations of the α_{CO} vs. metallicity relation considered here to solar metallicity (see Fig. 2b). In terms of oxygen abundance, solar enrichment generally corresponds to a value of $\log(\text{O}/\text{H}) + 12 \approx 8.7$, but this may change somewhat depending on the metallicity calibration (e.g. $\log(Z_\odot) + 12 = 8.9$ in the scale of Kewley & Dopita 2002).

¹⁴ Optical half-light radii for main-sequence galaxies in our reference sample were derived using the following literature sources: Leroy et al. (2008, 2009) for HERACLES galaxies; Förster Schreiber et al. (2009, 2011) and Genzel et al. (2010) for SINS galaxies; Daddi et al. (2010a) for CO-detected sBzK galaxies. No size information was available for the $z \sim 0.4\text{--}0.6$ galaxies from Geach et al. (2011) and Daddi et al. (2010b), nor for galaxies in the COLD GASS sample (Saintonge et al. 2011).

tivity. The split into (overlapping but offset) (s)SFR-distributions associated with main-sequence and starburst activity is based on the distributions of sSFR published for massive ($M_*/M_\odot > 10^{10}$) SFGs at $z \sim 2$ published by Rodighiero et al. (2011). The assumption that this double log-normal decomposition of the (s)SFR-distribution is invariant with stellar mass and redshift leads to a good agreement with IR-observables (a mild decrease of the importance of the starburst-component by $< 50\%$ between $z < 1$ and 0 leads to additional small improvements; see discussion in S12 and Béthermin et al. 2012).

The distinction between “normal” SFGs (implicitly assumed to be growing their stellar mass in a secular mode on the star-forming main sequence) and starbursting galaxies is central to the 2-SFM framework and of particular interest since it yields observationally verifiable predictions of the notion that star-formation is a bi-modal process at low and high redshift. In this vein Béthermin et al. (2012) assigned a characteristic (albeit redshift-dependent; see Magdis et al. 2012b) IR spectral energy distribution to main-sequence and starburst galaxies and showed that this simple approach is capable of reproducing the IR/radio source counts (incl. new *Herschel* counts) at 24 to $1100 \mu\text{m}$ and 1.4 GHz. Given the sensitivity of the source counts, this observation evidences that the 2-SFM framework provides a valid description of the dust emission from SFGs out to at least $z \sim 4$, (i.e. over 84% of the age of the Universe). The 2-SFM description of the IR-properties of SFGs has also provided testable predictions which were verified in recent work, e.g. the redshift distribution of SCUBA-2 $450 \mu\text{m}$ sources (Geach et al. 2012) and the redshift distribution of lensed 1.4 mm sources detected with the South Pole Telescope (see Weiss et al. 2013; Fig. 9). The good agreement of the predictions with the latter measurement suggests that the basic ingredients of the 2-SFM framework (e.g. the minor role of starbursts) remain applicable out to $z \sim 6$.

4.2. Boosting of main-sequence galaxies: mathematical description

Encouraged by the successful reproduction of the IR properties of the SFG-population we now further develop the 2-SFM framework with the primary aim of using it for a predictive analysis of the molecular gas properties of SFGs at high redshift. In preparation for this we revisit the key ingredient of the 2-SFM framework – the double log-normal decomposition of the (s)SFR-distribution at fixed stellar mass. Analogously to S12 we write this (s)SFR-distribution as the sum of two log-normal distribution functions \mathcal{G} describing main-sequence (MS) and starburst (SB) galaxies, respectively:

$$p(\text{sSFR})|_{M_*} = \mathcal{G}_{\text{MS}}(\text{sSFR}) + \mathcal{G}_{\text{SB}}(\text{sSFR}). \quad (5)$$

Note that with this parametrization “starburstiness” is not an all-or-nothing property, but that this *Ansatz* naturally leads to a continuous spectrum of burst-bearing sources ranging from those with strongly boosted star formation activity to others with only a mild enhancement.

4.2.1. The boost-function: basic properties

Both the burst-bearing and the normal galaxy population are described by an amplitude A_X with units of $[\text{Mpc}^{-3} \text{ dex}(\text{sSFR})^{-1}]$, a dispersion σ_X (units: $[\text{dex}(\text{sSFR})]$) and a mode $\langle \text{sSFR} \rangle_X$ ($X \in \{\text{MS}, \text{SB}\}$). In particular, the MS-distribution has the functional form

$$\begin{aligned} \mathcal{G}_{\text{MS}}(\text{sSFR}) = & \\ & A_{\text{MS}} \exp\left(-\frac{[\log(\text{sSFR}) - \log(\langle \text{sSFR} \rangle_{\text{MS}})]^2}{2\sigma_{\text{MS}}^2}\right), \quad \text{or} \\ & A_{\text{MS}} \exp\left(-\frac{x^2}{2\sigma_{\text{MS}}^2}\right) \end{aligned} \quad (6)$$

if, for the sake of brevity, we introduce a specific star formation rate $x \equiv \log(\text{sSFR}/\langle \text{sSFR} \rangle_{\text{MS}})$ that is normalized to the stellar mass- and redshift-dependent average sSFR of main-sequence galaxies, $\langle \text{sSFR} \rangle_{\text{MS}}$. Similarly, for starbursting sources, we write

$$\begin{aligned} \mathcal{G}_{\text{SB}}(\text{sSFR}) = & \\ & A_{\text{SB}} \exp\left(-\frac{[\log(\text{sSFR}) - \log(\langle \text{sSFR} \rangle_{\text{SB}})]^2}{2\sigma_{\text{SB}}^2}\right) \\ & A_{\text{SB}} \exp\left(-\frac{[\log(\text{sSFR}) - \{\log(\langle \text{sSFR} \rangle_{\text{MS}}) + B_{\text{SB}}\}]^2}{2\sigma_{\text{SB}}^2}\right) \\ & A_{\text{SB}} \exp\left(-\frac{[x - B_{\text{SB}}]^2}{2\sigma_{\text{SB}}^2}\right). \end{aligned} \quad (7)$$

Here B_{SB} is the offset between the peak position of the main sequence and starburst component of the sSFR-distribution. In our interpretation it represents the average sSFR-enhancement – or boost – brought about by the burst-inducing process. In the following we will assume that there is a process (to be discussed in Sect. 6.1) which boosts the star formation activity of an (s)SFR-dependent fraction of main-sequence galaxies with initial sSFR-distribution $\mathcal{G}_{\text{MS}}^0$. $\mathcal{G}_{\text{MS}}^0$ is identical with the log-normal distribution in eq. 6, except for a higher normalization $A_{\text{MS}} \rightarrow A_{\text{MS}}^0 = A_{\text{MS}} \times I(\mathcal{G}_{\text{MS}} + \mathcal{G}_{\text{SB}} : x) / I(\mathcal{G}_{\text{MS}} : x)$. (Here $I(f : x)$ stands for the integral of the function f over the range $x \in]-\infty, \infty[$.)

The “boost-function” describes the spectrum of perturbations that main-sequence galaxies suffer. It is effectively a convolution kernel which transfers galaxies from the main sequence to the starburst-distribution:

$$\begin{aligned} \mathcal{G}_{\text{SB}}(x) = & (\mathcal{G}_{\text{MS}}^0 * \mathcal{BK})(x) \\ = & \int_{-\infty}^{\infty} \mathcal{G}_{\text{MS}}^0(y) \mathcal{BK}(x - y) dy. \end{aligned} \quad (8)$$

The boost-function kernel (\mathcal{BK}) is obtained using the convolution theorem which links the Fourier transforms¹⁵

$$\widehat{\mathcal{G}}_{\text{SB}}(k) = \widehat{\mathcal{G}}_{\text{MS}}^0(k) \times \widehat{\mathcal{BK}}(k), \quad (9)$$

¹⁵ For the one-dimensional Fourier transform and its inverse we use the following convention

$$\begin{aligned} \widehat{f}(k) &= \int_{-\infty}^{\infty} f(x) e^{-ikx} dx \\ f(x) &= \frac{1}{2\pi} \int_{-\infty}^{\infty} \widehat{f}(k) e^{ikx} dk. \end{aligned}$$

With this definition the Fourier transforms of the log-normal distributions for starbursting sources and the unperturbed main se-

and by then applying the inverse Fourier transform:

$$\mathcal{BK}(x) = \frac{1}{2\pi} \int_{-\infty}^{\infty} \frac{\hat{\mathcal{G}}_{\text{SB}}(k)}{\hat{\mathcal{G}}_{\text{MS}}^0(k)} e^{ikx} dk. \quad (10)$$

Eqs. 9 and 10 will not always have an analytical solution. In the present case however, since both parent and resultant distribution – $\mathcal{G}_{\text{MS}}^0$ and \mathcal{G}_{SB} , resp. – are log-normal, the boost-function kernel also has this functional form:

$$\mathcal{BK}(x) \equiv \mathcal{G}_{\text{BK}}(x) = C_{\text{BK}} \exp\left(-\frac{[x - \langle x \rangle_{\text{BK}}]^2}{2\sigma_{\text{BK}}^2}\right). \quad (11)$$

By explicitly solving eq. 8, the three free parameters of the boost-function in eq. 11 are found to be:

$$\begin{aligned} C_{\text{BK}} &= \frac{A_{\text{SB}}\sigma_{\text{SB}}}{A_{\text{MS}}^0\sigma_{\text{MS}}\sqrt{2\pi}\sigma_{\text{BK}}}, \quad \text{with} \\ \sigma_{\text{BK}} &= \sqrt{\sigma_{\text{SB}}^2 - \sigma_{\text{MS}}^2}, \quad \text{and} \\ \langle x \rangle_{\text{BK}} &= B_{\text{SB}}. \end{aligned} \quad (12)$$

The shape of the boost-function with free parameters given by expressions 12 is shown as a solid red line in Fig. 4 and compared to distributions of SFR-enhancements reported for simulated and observed interacting galaxies.

It is natural to expect that the process which statistically/physically links starbursting and normal galaxies is galaxy interactions and merging. In Sect. 6.1 we discuss in detail whether theory or observations can provide supporting evidence for such a straightforward connection. To summarize, some properties of the 2-SFM boost-function are suggestively reminiscent of SFR-enhancements in observations and simulations. Other aspects do not conform to the expectations of what a realistic boost distribution should look like if it accounts for, e.g. minor interactions, interactions including passive galaxies and the fact that an observational snapshot of the starburst population will catch different objects in different phases of the burst. This difference, however, could be entirely due to the impossibility of statistically distinguishing between normal and only weakly starbursting galaxies in a direct fit to the sSFR-distribution; the conventional view that starbursts are often tied to galaxy interactions hence remains a viable scenario and we now consider a modification to the boost-function that we expect to apply for the idealized case that all starburst events are triggered by merging.

4.2.2. Statistical correction for paired, ante-merger galaxies

In our presentation of the 2-SFM boost-function we have so far skipped issues that would complicate an immediate interpretation that is based purely on the mathematical description of the problem. A first and strong simplifying assumption is that the boost-function

quence become

$$\begin{aligned} \hat{\mathcal{G}}_{\text{SB}}(k) &= e^{ikB_{\text{SB}}} A_{\text{SB}} \sqrt{2\pi}\sigma_{\text{SB}} e^{-\left(\frac{\sigma_{\text{SB}}k}{\sqrt{2}}\right)^2}, \quad \text{and} \\ \hat{\mathcal{G}}_{\text{MS}}^0(k) &= A_{\text{MS}}^0 \sqrt{2\pi}\sigma_{\text{MS}} e^{-\left(\frac{\sigma_{\text{MS}}k}{\sqrt{2}}\right)^2}. \end{aligned}$$

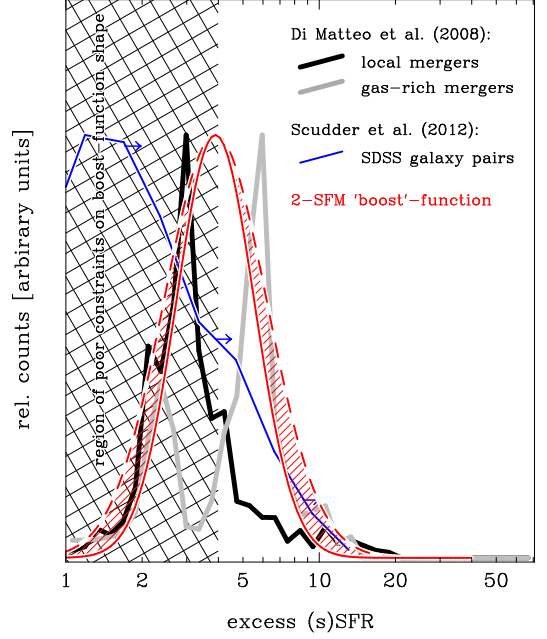


FIG. 4.— Comparison of the 2-SFM boost-function (i.e. the spectrum of (s)SFR-perturbations that move normal galaxies off the main sequence and into a starburst-state) with measured and simulated distributions of SFR-enhancements induced by galaxy interactions. Red (solid) – ‘direct’ boost-function; red (dashes) – boost-function including explicit correction for merger statistics (see Sect. 4.2.2). In the cross-hatched area the shape of the 2-SFM boost-function is not known accurately (see discussion in Sect. 6.1). The distribution of SFR-enhancements in massive ($M_{\star} > 10^{10} M_{\odot}$) members of $z \in [0.02, 0.15]$ SDSS galaxy pairs measured by Scudder et al. (2012; blue line) does not include mergers that have already undergone final coalescence and hence represents a lower observational limit to the total local SFR-excess distribution caused by interactions. Black and light grey lines – average of peak boosts (relative to isolated galaxies) measured in SPH and grid-based N-body simulations (cf. Di Matteo et al. 2008) of local mergers and gas-rich mergers with gas fraction similar to those of $z \sim 2$ main-sequence galaxies.

is mass- and redshift-independent. However, as discussed in S12 and Béthermin et al. (2012), current observations so far are consistent with this hypothesis. The sSFR-distributions of main-sequence galaxies and starbursting sources are snapshots that provide no direct information on the time scale over which star-formation in main-sequence galaxies is boosted (and over which they, possibly having undergone a merger, later fall back onto the relation or drop below it). The relative redshift-independence of the boost-function that is suggested by observations implies that the flux of galaxies into and out of the starburst-component of the double log-normal distribution also should not evolve strongly with redshift. If the SFR-enhancements were always the result of galaxy merging, then this would motivate a modification to the boost-function. We regard each pair of merging galaxies as a single system that is composed of two main-sequence galaxies. Because the parent sSFR-

distribution $\mathcal{G}_{\text{MS}}(\text{sSFR})$ is by assumption independent of mass and symmetric, both galaxies involved are drawn from the same distribution and their average SFR will follow a log-normal function that is centered on the same sSFR as the original distribution $\mathcal{G}_{\text{MS}}(\text{sSFR})$ but narrowed by a factor $\sqrt{2}$. For the boost-function this implies a broader distribution of SFR-enhancements while the peak location of the boost-spectrum remains identical (see also distribution plotted with a dashed red line in Fig. 4):

$$\begin{aligned} \sigma_{\text{BK}} &= \sqrt{\sigma_{\text{SB}}^2 - (\sigma_{\text{MS}}/\sqrt{2})^2}, \quad \text{and} \\ \langle x \rangle_{\text{BK}} &= B_{\text{SB}}, \quad \text{such that} \\ C_{\text{BK}} &= \frac{A_{\text{SB}}\sigma_{\text{SB}}}{A_{\text{MS}}^0\sigma_{\text{MS}}} \frac{1}{\sqrt{2\pi}\sigma_{\text{BK}}}. \end{aligned} \quad (13)$$

In the following we will refer to this version of the boost-function as “boost-function including an explicit correction for mergers” (as opposed to the boost-function described by eqs. 12 and henceforth called: “direct boost-function”). The principle findings of this paper are valid irrespective of the choice of boost-function, but for the sake of legibility we will only show results obtained with the direct boost-function where plotting both alternatives would reduce rather than improve clarity.

4.2.3. The continuously varying boost-distribution

As previously mentioned, the “typical” sSFR increase B_{SB} of starbursting sources is approx. a factor of four, but the average boost varies as a function of (s)SFR, as does the (relative) number of sources undergoing burst-like activity. For example, a source with measured sSFR twice as large as the (redshift- and stellar mass-dependent) main-sequence average could either display this excess simply due to a larger than average gas fraction and without having suffered any triggering, it could have experienced a modest boost, or – with a lesser probability – it could initially have been a gas-poor, low-(s)SFR outlier to the main sequence which has been strongly boosted. In the following we quantify these variations that are a consequence of the convolution in eq. 8.

To find the “typical” boost of burst-bearing sources at a given sSFR_0 (or $\log(\text{sSFR}_0/\langle \text{sSFR} \rangle_{\text{MS}}) = x_0$) we consider the integrand in eq. 8,

$$\mathcal{G}_{\text{MS}}^0(x) \mathcal{G}_{\text{BK}}(x_0 - x) = \mathcal{G}_{\text{MS}}^0(x_0 - b_{\text{sSFR}}) \mathcal{G}_{\text{BK}}(b_{\text{sSFR}}). \quad (14)$$

Here we introduced a variable for the logarithmic boost, $b_{\text{sSFR}} = x_0 - x \equiv \log(\text{sSFR}_0/\text{sSFR})$, in order to be able to directly locate the peak of the boost distribution, $b_{\text{sSFR}}^{\text{max}}$, by solving the minimization problem:

$$\frac{\partial}{\partial b_{\text{sSFR}}} \left\{ \mathcal{G}_{\text{MS}}^0(x_0 - b_{\text{sSFR}}) \mathcal{G}_{\text{BK}}(b_{\text{sSFR}}) \right\} \doteq 0. \quad (15)$$

Given the properties of the exponential function this is equivalent to requiring

$$\begin{aligned} \frac{\partial}{\partial b_{\text{sSFR}}} \left\{ \frac{-(x_0 - b_{\text{sSFR}})^2}{2\sigma_{\text{MS}}^2} \right\} + \dots \\ \dots + \frac{\partial}{\partial b_{\text{sSFR}}} \left\{ \frac{-(b_{\text{sSFR}} - B_{\text{SB}})^2}{2\sigma_{\text{BK}}^2} \right\} \doteq 0, \end{aligned} \quad (16)$$

an equation which has the solution

$$b_{\text{sSFR}}^{\text{max}} = \frac{B_{\text{SB}} + x_0 (\sigma_{\text{BK}}/\sigma_{\text{MS}})^2}{1 + (\sigma_{\text{BK}}/\sigma_{\text{MS}})^2}. \quad (17)$$

To determine the shape of the boost-spectrum which peaks at $b_{\text{sSFR}}^{\text{max}}$ we consider the product of the two Gaussians in eq. 14

$$\begin{aligned} \mathcal{G}_{\text{MS}}^0(x_0 - b_{\text{sSFR}}) \mathcal{G}_{\text{BK}}(b_{\text{sSFR}}) = \\ A_{\text{MS}}^0 C_{\text{BK}} \exp \left(- \left\{ \frac{[x_0 - b_{\text{sSFR}}]^2}{2\sigma_{\text{MS}}^2} + \frac{[b_{\text{sSFR}} - B_{\text{SB}}]^2}{2\sigma_{\text{BK}}^2} \right\} \right) \end{aligned} \quad (18)$$

and examine the exponent

$$\frac{[x_0 - b_{\text{sSFR}}]^2}{2\sigma_{\text{MS}}^2} + \frac{[b_{\text{sSFR}} - B_{\text{SB}}]^2}{2\sigma_{\text{BK}}^2}$$

which can be re-written as

$$\begin{aligned} \frac{1}{2 \frac{(\sigma_{\text{MS}}\sigma_{\text{BK}})^2}{\sigma_{\text{MS}}^2 + \sigma_{\text{BK}}^2}} \left\{ b_{\text{sSFR}}^2 - 2 \frac{x_0\sigma_{\text{BK}}^2 + B_{\text{SB}}\sigma_{\text{MS}}^2}{\sigma_{\text{MS}}^2 + \sigma_{\text{BK}}^2} b_{\text{sSFR}} + \dots \right. \\ \left. \dots + \frac{x_0^2\sigma_{\text{BK}}^2 + B_{\text{SB}}^2\sigma_{\text{MS}}^2}{\sigma_{\text{MS}}^2 + \sigma_{\text{BK}}^2} \right\}. \end{aligned} \quad (19)$$

This is again a quadratic form, implying that the boosts at fixed normalized specific star formation rate x_0 are distributed log-normally with a width $\sigma_b = \sqrt{\frac{(\sigma_{\text{MS}}\sigma_{\text{BK}})^2}{\sigma_{\text{MS}}^2 + \sigma_{\text{BK}}^2}}$ that is independent of sSFR.

On the left-hand side of Fig. 5 we visualize with different colors the changes in the boost-distribution for sSFRs ranging from ~ 0.1 to two hundred times the characteristic main-sequence value, $\langle \text{sSFR} \rangle_{\text{MS}}$. Note that the sSFR-variations take place within a given bin of stellar mass and that the integral over the boost-distributions at all sSFRs would give a total boost-distribution that is equal to the boost-function plotted with the red solid line in Fig. 4. This is not immediately obvious based on Fig. 5 where we have scaled all sSFR-dependent boost-distributions such that they give the fraction of sources with boost b_{sSFR} in a specific sSFR-bin. This representation highlights the evolution of the fraction f^{SB} of starbursting sources (given by the ratio of the two log-normal curves in eq. 5; see also Fig. 5, right) with sSFR while simultaneously compensating for the variation of the total number of sources across the width of the main sequence. The amplitude of the log-normal boost distributions thus grows until $\text{sSFR}/\langle \text{sSFR} \rangle_{\text{MS}} \simeq 8$ where the number of main-sequence galaxies becomes insignificant with respect to the number of starbursting sources (see also flattening of the evolution of f^{SB} in the right-hand panel of Fig. 5).

An alternative quantity which traces the increasing importance of starburst-activity at successively higher sSFRs is the typical fractional contribution, $\mathcal{C}^{\text{SB}} = (\text{SFR} - \text{SFR}_{\text{MS, init.}})/\text{SFR} = 1 - 10^{-b_{\text{sSFR}}}$, of the burst-induced activity to the total SFR of boosted sources. (Here $\text{SFR}_{\text{MS, init.}}$ is the SFR of the galaxy in the main-sequence state prior to boosting.) \mathcal{C}^{SB} is complementary to the starbursting fraction of the population, f^{SB} , in that it describes the impact of the boost on an individual galaxy, while f^{SB} provides the number of galaxies of

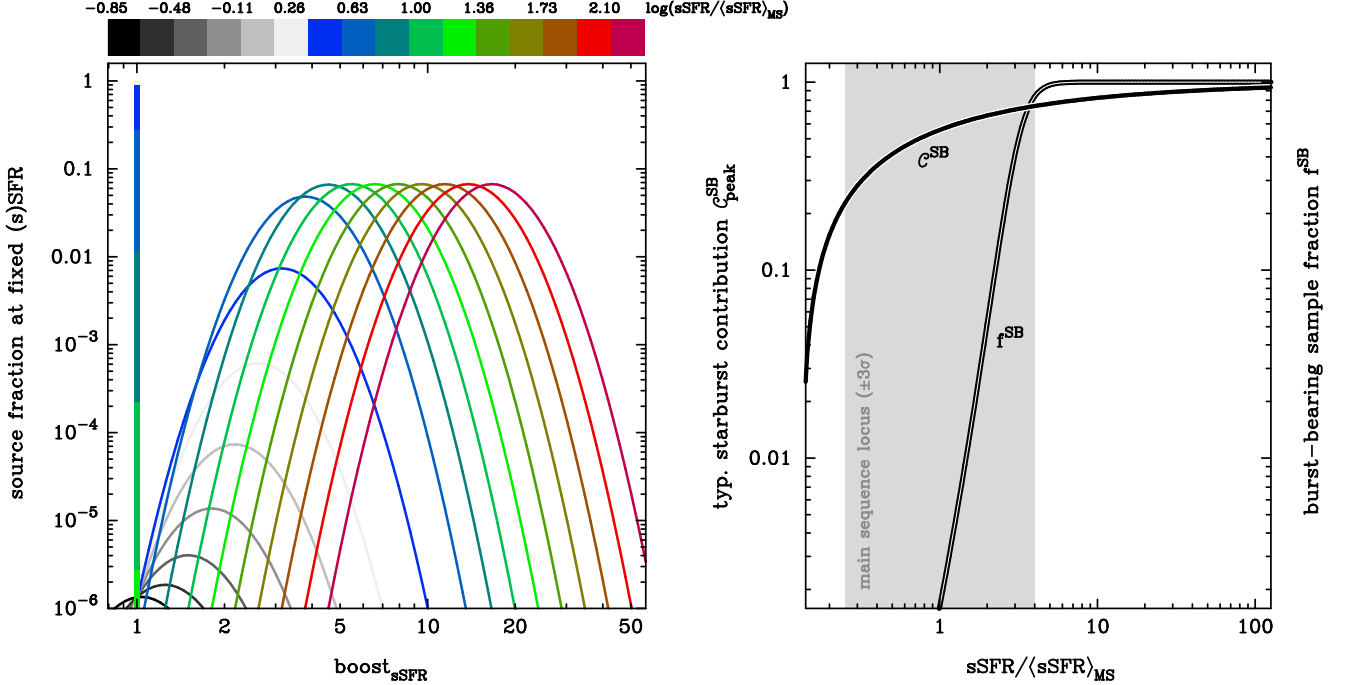


FIG. 5.— Illustration of the properties of the continuously varying, sSFR-dependent 2-SFM boost-distribution (i.e. the distribution of (s)SFR-enhancements of starbursting galaxies; see Sect. 4.2.2). Left – log-normal distribution of boosts (see eqs. 17 to 19) of SFGs with a specific sSFR. All distributions are normalized to the total number of sources at a given sSFR and colors vary according to the value of sSFR, where sSFR is referenced to the main-sequence average. For example, at $\text{sSFR}/\langle\text{sSFR}\rangle_{\text{MS}} = 10$ the median boost is approx. seven-fold and 95% of the starburst population have boosts in the range 2.5–17. Starbursts with $\text{sSFR}/\langle\text{sSFR}\rangle_{\text{MS}} = 1/2$, on the other hand, have on average experienced weak boosting by only approx. 30% and 95% of such systems have boosts that are smaller than a factor three. The relative number of secularly evolving galaxies (plotted at boost = 1 with a bar of appropriate height) and of boosted sources is given by the burst-bearing fraction f^{SB} . Right – variation of the starbursting fraction f^{SB} with normalized sSFR, compared to the evolution of the typical fractional contribution, C^{SB} , of the burst-induced activity to the total SFR of boosted sources at a given sSFR. (Here ‘typical fractional contribution’ is defined as the contribution of a source located at the sSFR-dependent peak of the boost-distribution.) Directly on the main-sequence locus ($\text{sSFR}/\langle\text{sSFR}\rangle_{\text{MS}} = 1$) starbursting sources are rare ($f^{\text{SB}} < 2\%$) but in those systems which have experienced boosting the contribution of the burst-activity to the total SFR is significant ($C^{\text{SB}} \sim 47\%$). At an sSFR-excess of $\text{sSFR}/\langle\text{sSFR}\rangle_{\text{MS}} \simeq 3$, above which starbursts are more numerous than normal galaxies ($f^{\text{SB}} \geq 0.5$), the starburst-contribution to the total SFR of boosted sources is already clearly dominant ($C^{\text{SB}} \sim 71\%$). These numbers are based on the ‘direct’ boost-function that uses the best-fit parameters of the double log-normal sSFR-decomposition in S12 (see also eq. 5 in this paper).

a given sSFR within the 2-SFM framework that are subject to such boosting. The relative variation of these two quantities is compared in the right-hand panel of Fig. 5. Burst-bearing sources at the lower envelope of the main sequence are rare and typically have small SFR-enhancements (e.g. by 15% at $-2\sigma_{\text{MS}}$). At an identical positive offset from the main-sequence locus ($+2\sigma_{\text{MS}}$) the star-formation activity of starbursting sources is on average tripled¹⁶ with respect to their main-sequence state prior to boosting. Note that the lower tail of the 2-SFM boost-function formally allows for “negative” boosts (i.e. suppression of star formation activity in interactions) but this only occurs for a negligibly small fraction of $<0.1\%$ and 2% of the SFG-population for the direct and merger-corrected boost-function, respec-

tively.

5. RESULTS

In the following we will show how a simpler understanding of the molecular gas properties of SFGs at all redshifts $z < 3$ emerges when variations of, e.g. SFE or gas fraction, about the typical value of main-sequence galaxies are considered. To be able to establish such normalized trends requires a reliable prescription for the evolution of slope and normalization of the star-forming main sequence with redshift. In Appendix A we parametrize the evolution of sSFR for main-sequence galaxies as a smoothly varying function of redshift and stellar mass (see eq. A1) which we fit to a compilation of sSFR-data from the literature. We find that on average a sSFR vs. M_* relation $\text{sSFR} \propto M_*^\nu$ with exponent $\nu \simeq -0.2$ reproduces the systematic shift between the sSFR-evolution of galaxies in different mass bins out to $z \sim 3$. The extrapolation of the sSFR-evolution to higher redshift (as briefly proposed for the discussion of gas fraction

¹⁶ These numbers are for the boost-function including the explicit correction for merger statistics. For the direct boost-function the typical boost $b_{\text{sSFR}}^{\text{max}}$ varies more slowly across the main sequence (see eq. 17 and Fig. 8).

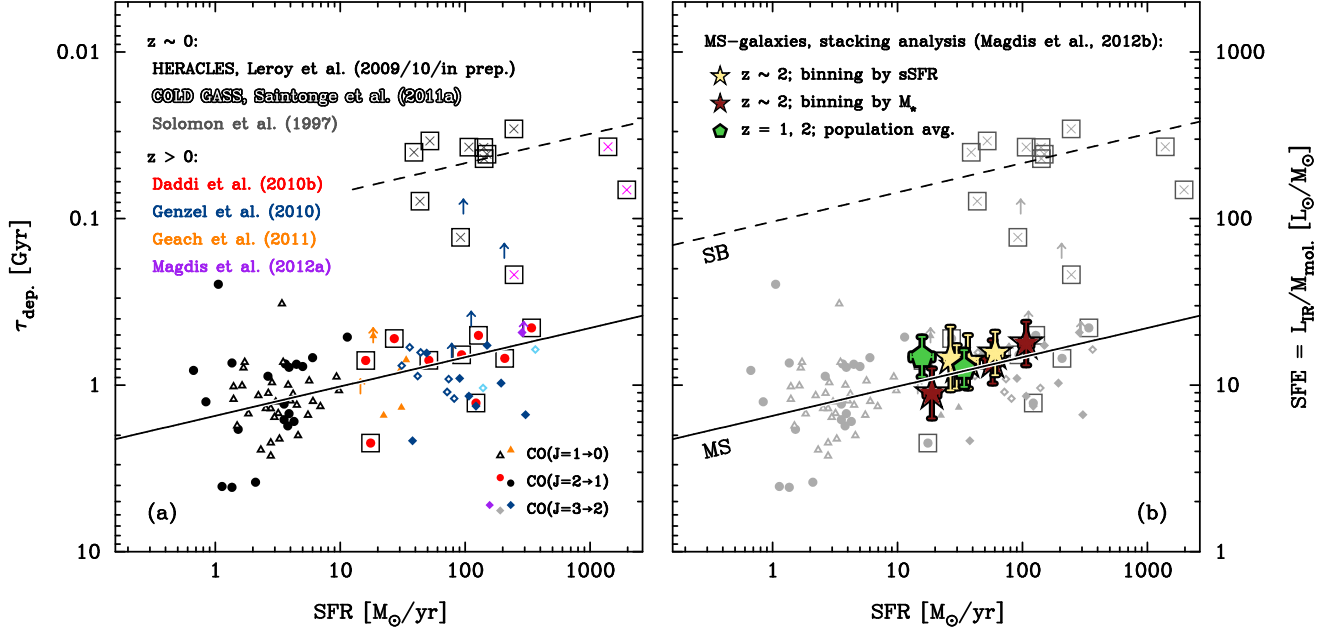


FIG. 6.—: Dependence of SFE (see scale on right) and gas depletion time $\tau_{\text{dep.}}$ (scale on left) on SFR for individual galaxies in our calibration sample (panel a) and for stacked galaxies from Magdis et al. (2012b; panel b). (All data and symbols as in Fig. 1.b and 3.b).

evolution in Sect. 5.2.2) is speculative, since constraints on the shape of the main sequence at $z > 3$ are much sparser.

We begin this section with our new description of SFE-variations between normal and starbursting galaxies (Sect. 5.1) and then discuss gas fractions variations and evolution plus empirical recipes for the CO-to-H₂ conversion factor (Sects. 5.2 and 5.3, resp.).

5.1. Simple recipes for star formation efficiency in massive star-forming galaxies

5.1.1. Star formation efficiency in normal and star-bursting galaxies: observations

The non-linearity of the integrated S-K law found in Sect. 3.2.2 implies a residual dependence of the gas depletion time, $\tau_{\text{dep.}} = M_{\text{mol.}}/\text{SFR}$, and its inverse, the SFE, on SFR. Using our fit for main-sequence galaxies from eq. 3 we obtain

$$\log\left(\frac{\tau_{\text{dep.}}}{\text{Gyr}}\right) = (\alpha_{2, \text{SFR}} - 9) + (\beta_2 - 1) \log\left(\frac{\text{SFR}}{M_{\odot}/\text{yr}}\right) \quad (20)$$

$$= 0.18(\pm 0.02) - 0.17(\pm 0.03) \times \log\left(\frac{\text{SFR}}{M_{\odot}/\text{yr}}\right)$$

and

$$\log\left(\frac{\text{SFE}}{\text{Gyr}^{-1}}\right) = (1 - \beta_2) \log\left(\frac{\text{SFR}}{M_{\odot}/\text{yr}}\right) - (\alpha_{2, \text{SFR}} - 9) \quad (21)$$

$$= 0.17(\pm 0.03) \times \log\left(\frac{\text{SFR}}{M_{\odot}/\text{yr}}\right) - 0.18(\pm 0.02).$$

The dispersion about this characteristic value is ~ 0.2 dex (see Sect. 3.2). Fig. 6 illustrates how the galaxies from our reference sample (see Sect. 2.1) and the stacked samples of Magdis et al. (2012b) scatter around this average trend which – due to the general redshift-

evolution of sSFR in SFGs – implies a roughly two-fold decrease of $\tau_{\text{dep.}}$ between $z \sim 0$ and $z \sim 2$ for galaxies of $M_{\star}/M_{\odot} = 4 \times 10^4$ which contribute most to the cosmic SFRD over this period (Cowie & Barger 2008, Gilbank et al. 2011, Karim et al. 2011). The variation between the depletion times of 1-2 Gyr in local spiral galaxies (e.g. Leroy et al. 2008, Bigiel et al. 2011) and the approx. 0.5-1 Gyr determined for BM/BX- and BzK-selected galaxies at $1.5 < z < 2.5$ (e.g. Daddi et al. 2010b, Tacconi et al. 2010) is much smaller than the difference between normal galaxies and strong starbursts (see offset, dashed locus in Fig. 6).

We attempt to correct for the implicit redshift-dependence of SFE by considering a re-normalized efficiency. For each galaxy in our reference sample the normalization constant, $\langle \text{SFE} \rangle_{\text{MS}}$, is the SFE that a galaxy of equal gas mass would have if it lay directly on the inverse S-K relation given by eq. 3. In Fig. 7 we then plot the normalized $\text{SFE}/\langle \text{SFE} \rangle_{\text{MS}}$ as a function of the normalized specific star formation rate $\text{sSFR}/\langle \text{sSFR} \rangle_{\text{MS}}$, which in the 2-SFM framework is a good measure of starburstiness. The stellar mass- and redshift-dependent main-sequence average $\langle \text{sSFR} \rangle_{\text{MS}}$ is calculated according to eq. A1.

With this choice for the representation of the data, main-sequence galaxies occupy the same region of parameter space regardless of their redshift. Our small reference sample of starburst galaxies, on the other hand, is clearly offset from the main-sequence population in the plane of normalized SFE and sSFR. Note that we assign statistically-estimated CO-to-H₂ conversion factors based on a M_{\star} - and SFR-dependent metallicity $Z(\text{SFR}, M_{\star})$ to the majority of the normal galaxies in our reference sample, but that α_{CO} has been directly measured for our sub-sample of starbursting galaxies. While the scatter of the normal galaxies about the main-

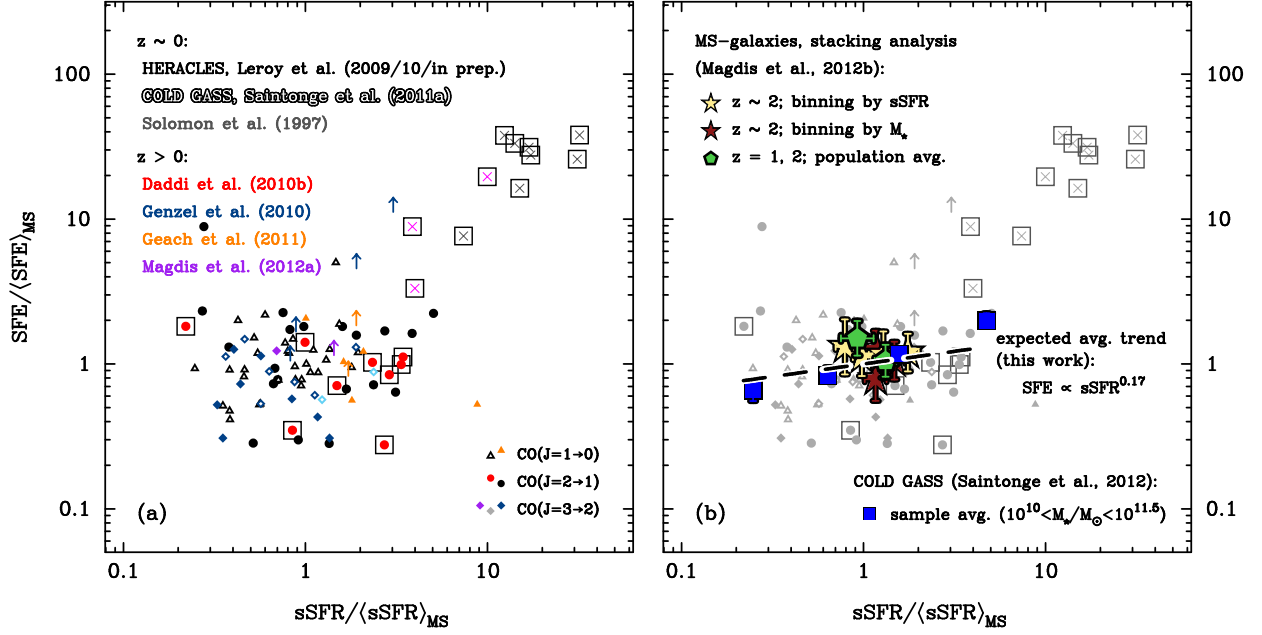


FIG. 7.—: Star-formation efficiency (SFE) vs. sSFR for selected main-sequence galaxies and starbursts at $z \lesssim 3$ (left) and for stacked galaxies from Magdis et al. (2012b; right). When normalized to the characteristic main-sequence value, $\langle \cdot \rangle_{\text{MS}}$, a homogeneous behaviour of main-sequence galaxies at all redshifts becomes visible: SFEs vary very little within the main sequence while starbursting sources display enhanced SFEs that lead to their excess (s)SFR. (All data and symbols as in Fig. 6. In panel (b) we also show sample SFR-averages for local COLD GASS galaxies binned by sSFR-excess.)

sequence average $\langle \text{SFE} \rangle_{\text{MS}}$ is thus model-dependent, the strong SFE-excess found for starbursts is thus not an artifact of, e.g., assuming Milky Way- and ULIRG-like conversion factors for main-sequence galaxies and starbursts, respectively. Fig. 7 shows that the sSFR- and SFE-excess of the strongest starbursts in the sample are of a similar order of magnitude. This suggests that there is some kind of link between the SFR-enhancement (or ‘boost’ in the terminology of Sect. 4) and the increased SFE that starbursts display. The empirical calibration of this relation is the topic of the next section.

5.1.2. Star formation efficiency in normal and star-bursting galaxies: the 2-SFM description

Stellar mass and star formation rate are fundamental parameters in the 2-SFM description of SFGs. The tight and apparently redshift-independent integrated Schmidt-Kennicutt law found in Sect. 3.2 links the SFR and gas mass of main-sequence galaxies and hence provides a straightforward recipe to extend the 2-SFM framework to their molecular gas properties. At fixed stellar mass, in which case $\text{SFR}/\langle \text{SFR} \rangle_{\text{MS}} \equiv \text{sSFR}/\langle \text{sSFR} \rangle_{\text{MS}}$ we can write

$$\log \left(\frac{\text{SFE}}{\langle \text{SFE} \rangle_{\text{MS}}} \right) = (1 - \beta_2) \times \log \left(\frac{\text{sSFR}}{\langle \text{sSFR} \rangle_{\text{MS}}} \right) \quad (22)$$

for the relation between normalized SFEs and sSFRs. This slow variation across the spread of the main sequence with $\text{SFE} \propto \text{sSFR}^{0.17 \pm 0.03}$ is superimposed on the data in Fig. 7b.

The 2-SFM framework distinguishes between main-sequence galaxies and starbursting systems which support an elevated level of star-formation activity compared to what is assumed to be an initial, pre-burst state

where such galaxies were indistinguishable from the large population of secularly-evolving, normal SFGs. Having derived a prescription which links the SFE of main-sequence galaxies to their offset from the main sequence in eq. 22 we now seek a similar relation for the starbursting fraction of the population. We adopt the following parametrization to describe the SFE of starbursts:

$$\log \left(\frac{\text{SFE}}{\text{SFE}_{\text{MS, init.}}} \right) = \gamma_{\text{SFE}} \times b_{\text{sSFR}} \quad (23)$$

where b_{sSFR} is the logarithmic boost introduced in eq. 14 and $\text{SFE}_{\text{MS, init.}}$ is the SFE in the main-sequence state, prior to the onset of the burst-activity. Since we refer the SFE to this initial state by definition no additional normalization constant is required in eq. 23. Observationally, the amount of boosting that the starburst galaxies in our reference sample have experienced is obviously unknown. We shall thus assume that their SFR-enhancements correspond to the median boost (i.e. the peak location of the boost-distribution, $b_{\text{sSFR}}^{\text{max}}$; see eq. 17) which is expected for sources with an sSFR-excess as determined for these starbursts. In Sect. 4.2.3 we derived the boost-spectrum at fixed sSFR-excess (or deficit), $\text{sSFR}/\langle \text{sSFR} \rangle_{\text{MS}}$, and calculated the shifting of its peak $b_{\text{sSFR}}^{\text{max}}$ with the normalized sSFR. We reproduce the average trends in Fig. 8a for both the direct boost-function and the boost-function including an explicit correction for mergers. Since the latter scenario assumes an sSFR-distribution of paired, ante-merger galaxies that is narrower (see explanations in Sect. 4.2.2), a larger boost is required on average to reach a given sSFR-excess. This fact is reflected in a steeper slope of the corresponding boost vs. $\text{sSFR}/\langle \text{sSFR} \rangle_{\text{MS}}$ relation in Fig. 8a. The

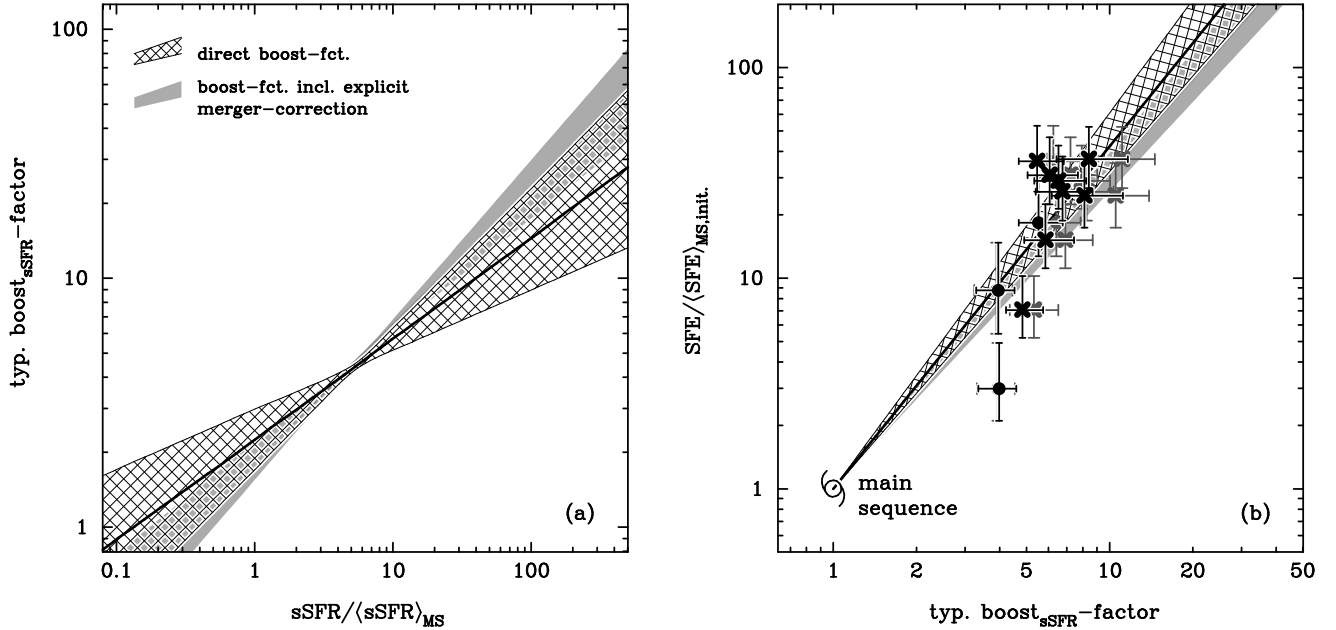


FIG. 8.— Illustration of the two steps needed to establish a link between the star formation efficiency SFE of starbursting galaxies (normalized to the average value of main-sequence galaxies with a given H_2 -mass, $\langle SFE \rangle_{MS}$) and their (s)SFR-boost within the 2-SFM framework. (a) Variation of the ‘typical boost’ (defined as the peak of the sSFR-dependent spectra of boosts shown in Fig. 5) of the burst-bearing fraction of SFGs with their sSFR (normalized to the M_* - and redshift-dependent value of main-sequence galaxies, $\langle sSFR \rangle_{MS}$). Two cases are considered: (1) boost-function including explicit correction for merger statistics (*grey shading*, cf. Sect. 4.2.2), and (2) ‘direct’ boost-function (*hatched area*). The shaded/hatched areas mark the 1σ -error on the typical boost, and were derived based on the uncertainties associated with the decomposition of the sSFR-distributions of massive $z \sim 2$ SFGs into two log-normal components (for main-sequence and starbursting galaxies, resp.; see S12 or the schematic representation in Fig. 9). Bold lines at the core of the highlighted confidence regions trace the best-fit variation of the typical boost values.

(b) Empirical calibration of the relation between SFE-enhancement and boost amplitude using a reference sample of selected starburst galaxies with measured α_{CO} (Solomon et al. 1997, Magdis et al. 2012b) and the relation between normalized sSFR and the typical boost of panel (a). The reference sample of starbursts is located with respect to the x -axis using the trend lines of panel (a) for the 2-SFM boost-function including explicit correction for merger statistics (*dark grey symbols*) and for the ‘direct’ 2-SFM boost-function (*black symbols*). (Crosses/dots are used for local/high- z starbursts from Solomon et al. (1997) and Magdis et al. (2012b), respectively; 1 sigma-error bars plotted account for observational uncertainty on SFR, M_* and $M_{mol.}$ but not systematic uncertainties, see discussion in Sect. 5.1.2.) The shaded/hatched areas span the 68% confidence region for a power-law relation between excess SFE and boost amplitude as parametrized in eq. 23 and passing through the main-sequence locus highlighted schematically.

shaded/hatched areas in this figure panel indicate the uncertainty on the average relation between boost and normalized sSFR, estimated with a full accounting of the errors on (and covariance between) the parameters of the 2-SFM double log-normal decomposition of the sSFR-distribution (see also Fig. 1 in S12).

In Fig. 8b we show the result of assigning representative boost values to the starbursts in our sample and then fitting eq. 23. In accordance with our assumption that they experienced the median burst expected for an object with their sSFR-excess, we equate $SFE/\langle SFE \rangle_{MS}$ – the SFE normalized to the average main-sequence value – and $SFE/SFE_{MS,init.}$ – the SFE-excess with respect to the pre-boost, main-sequence state of each individual galaxy – for these sources. The y -axis values of the starbursts in Fig. 8b are thus identical to those in Fig. 7. We emphasize that our small reference sample of starbursts does not provide sufficient statistics to justify the functional form of eq. 23. Here we simply use this data to derive the best fit given the preceding choice of a plau-

sible parametrization; in this context, the linear relation proposed in eq. 23 is the simplest possible form that can be envisaged. The best-fitting values of the slope are $\gamma_{SFE} = 1.63^{+0.16}_{-0.14}$ and $1.50^{+0.09}_{-0.10}$ for the direct and merger-corrected boost-function, respectively. The quoted 1σ errors reflect the observational uncertainty on SFR, M_* and $M_{mol.}$ (i.e. L'_{CO} & α_{CO}) – as plotted in Fig. 8b for our reference starbursts – but not the systematic uncertainties related to the calibration of the average sSFR and SFE of main-sequence galaxies, nor those related to the functional form of eq. 23. It is interesting to note that Di Matteo et al. (2007) find SFE-enhancements in merger simulations that exceed the boost in SFR. The behavior of the simulations thus qualitatively matches the supra-linear relation inferred here, according to which $SFE/SFE_{MS,init.} \propto (\text{boost})^{\gamma_{SFE}}$ with $\gamma_{SFE} > 1$.

A non-linearity of this kind is virtually inevitable in order to self-consistently match the SFEs of strong starbursts at the sSFR they display. If, instead, we were to describe

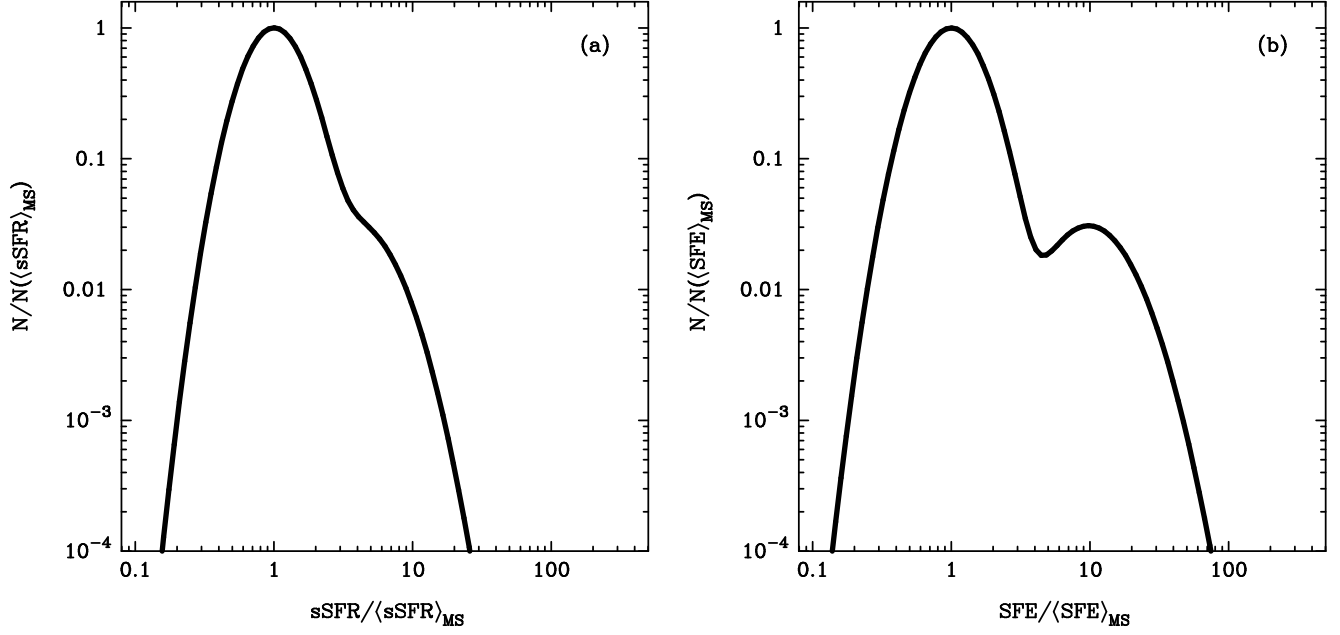


FIG. 9.—: Schematic comparison of the sSFR-distribution at fixed stellar mass (a) with the SFE-distribution at fixed molecular gas mass (b). The curves are representative examples, computed using the best-fit parameters of the double log-normal decomposition of the sSFR-distribution (eq. 5) and of the power-law relation fitted to the dependence of SFE on boost-amplitude for starbursting galaxies (eq. 23). Associated uncertainties are not shown.

the SFE of starbursts as a linear mixing of two distinct S-K laws (one for normal galaxies and one for starbursts) based on the starburst-contribution to the total SFR of boosted sources (\mathcal{C}^{SB} , see Fig. 5b), the high SFEs observed for, e.g., local ULIRGs could only be reproduced when assuming a ‘template’ S-K law for starbursts which is offset to higher SFE than observationally seen for even the most extreme sources.

An immediate consequence of the inferred supra-linear relation between SFE- and SFR-enhancements in starburst events is that the distributions of the SFG population with respect to (s)SFR and SFE are qualitatively different. (Here we consider the SFE-distribution at fixed gas mass.) We illustrate this in Fig. 9 for the case of the best-fitting double log-normal decomposition (eqs. 6 and 7) and SFE-boost relation for starbursts (eq. 23). While the sSFR-distributions of main-sequence galaxies and starbursts blend, the two sub-populations are more strongly separated in terms of SFE. In comparison with the distribution of galaxies in the $M_{\text{mol.}}$ vs. SFR plane in Fig. 1b, we see that the bimodality predicted by the 2-SFM framework is less pronounced. So far, CO follow-up observations of SFGs have generally explicitly targeted either strong starbursts (e.g. Solomon et al. 1997, Greve et al. 2005, Riechers et al. 2006, Ivison et al. 2011) or main-sequence galaxies (e.g. Leroy et al. 2008, Daddi et al. 2010a, Tacconi et al. 2010, Geach et al. 2011, Magdis et al. 2012a). It is thus very likely that this selective observing strategy has artificially deepened the expected trough between the main-sequence and starburst component in Fig. 9b into the genuine gap that is seen in Fig. 1b.

We now have all ingredients to provide an empirical prescription for the SFE of starbursting systems. In analogy to the expression for normal galaxies in eq. 22, we write

the recipe for starbursts in terms of a normalized SFE,

$$\begin{aligned} \log \left(\frac{\text{SFE}}{\langle \text{SFE} \rangle_{\text{MS}}} \right) &= \log \left(\frac{\text{SFE}}{\text{SFE}_{\text{MS, init.}}} \right) + \log \left(\frac{\text{SFE}_{\text{MS, init.}}}{\langle \text{SFE} \rangle_{\text{MS}}} \right) \\ &= \gamma_{\text{SFE}} \times b_{\text{sSFR}} + (1 - \beta_2) \times \log \left(\frac{\text{sSFR}_{\text{MS, init.}}}{\langle \text{sSFR} \rangle_{\text{MS}}} \right), \end{aligned} \quad (24)$$

which is a combination of the SFE of the initial, main-sequence state prior to boosting (second summand; see also eq. 22) and the burst-induced enhancement of this initial SFE (first summand; see also eq. 23). It is important to realize that eq. 24 stands for SFE-changes in individual starbursts rather than describing the sSFR-dependence of the average SFE-excess of the whole starbursting population. The latter trend will be discussed in the next paragraph.

By incorporating the prescriptions in eq. 22 and 24 we can predict the variation of SFE throughout the entire M_{\star} vs. SFR plane and for the entire SFG population (as opposed to individually for the sub-population of normal galaxies and starbursts). In doing so, we will again make the simplifying assumption that all recipes are independent of stellar mass, which reduces the problem to a calculation of the evolution of SFE with (s)SFR. The prediction involves several steps which we detail here in bulletized format for maximal clarity and in preparation of analogous procedures for the variation of gas fractions and α_{CO} in Sects. 5.2 and 5.3, respectively:

- The hypothetical population of SFGs is distributed in M_{\star} and SFR according to the double log-normal distribution in eq. 5.
- At each point in the M_{\star} vs. SFR plane an sSFR-dependent fraction f^{SB} of galaxies will fall into the

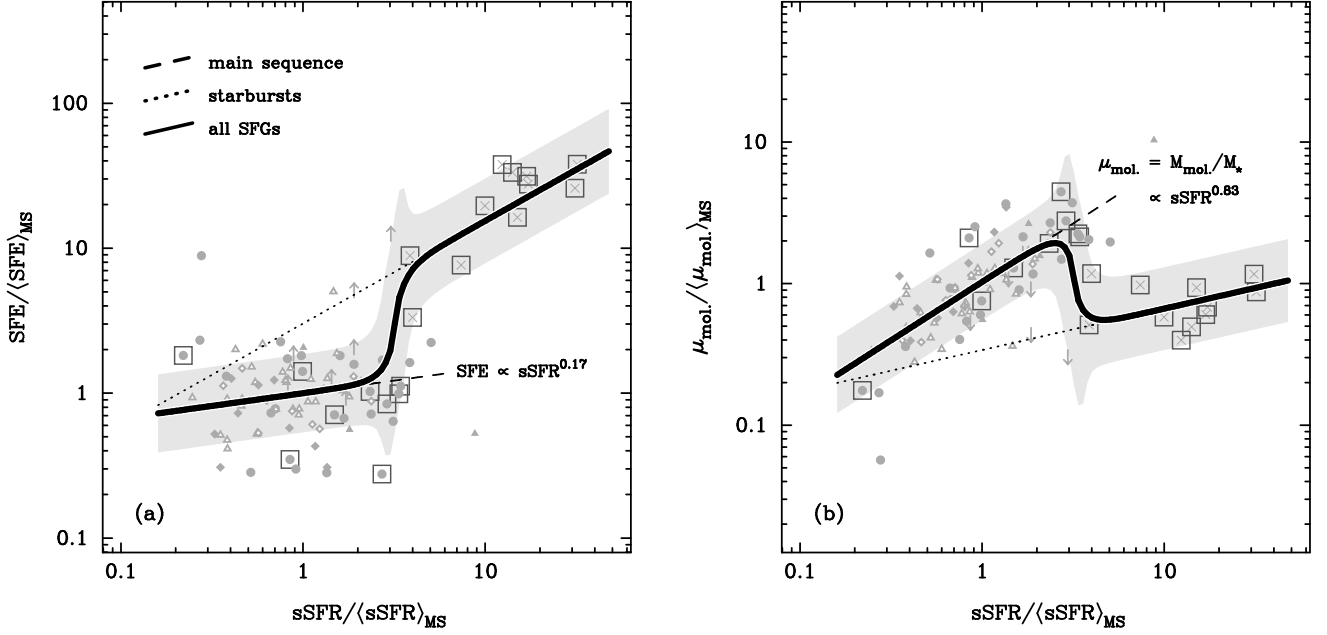


FIG. 10.—: Average variation of normalized SFE (*left*) and molecular gas mass fraction $\mu_{\text{mol.}} \equiv M_{\text{mol.}}/M_{\star}$ (*right*) with normalized sSFR, as predicted by the 2-SFM framework. Data points plotted in grey in the background are as in Figs. 7 and 11. Dashed line – expected average trend for main-sequence galaxies (sSFR-dependence as annotated adjacent to line); dotted line – expected average trend for the starbursting fraction of the star-forming population (‘direct’ boost-function assumed); solid line – average evolution for the total population of SFGs; light grey shading – expected 1σ scatter around average SFE-variation. The average evolution of the total population traces the variation of the median SFE ($\mu_{\text{mol.}}$) of the combined SFE-distribution ($\mu_{\text{mol.}}$ -distribution) of normal and starbursting galaxies. Its variation thus reflects the relative importance of main-sequence and starburst galaxies with offset from the main-sequence locus $\langle \text{sSFR} \rangle_{\text{MS}}$. When normalized to the typical main-sequence value, the predicted trends do not depend on redshift due to the simple power-law relations between SFR and molecular gas mass that are assumed in the 2-SFM framework (see Sects. 5.1.2 and 5.2.1 for details).

starburst-category (see Fig. 5, right) and hence require a different recipe for the computation of SFE than is applied to main-sequence sources.

- For main-sequence galaxies of a given sSFR, the SFE is computed with eq. 22.
- At each sSFR, relations 17 to 19 from Sect. 4.2.3 allow us to construct the spectrum of boosts b_{sSFR} and to infer the former pre-burst efficiencies, $\text{SFE}_{\text{MS, init.}}$, of the burst-bearing systems. Their SFEs then follow from eq. 24.
- A ‘typical’ SFE – here we use the median – is calculated for the joint population of normal and starbursting galaxies. It reflects the relative importance of the two sub-populations at a given location in the M_{\star} vs. SFR plane.

Fig. 10a shows how, beginning at the lower edge of the main-sequence locus, the median SFE of the total SFG population first traces the slow rise of SFE which characterizes normal galaxies. Meanwhile, the SFE of burst-bearing sources (dotted line) rises more quickly¹⁷ but such starbursts are exceedingly rare within most of the

main sequence. They become the dominant component of the SFG population at around $3 < \text{sSFR} / \langle \text{sSFR} \rangle_{\text{MS}} < 4$ where the global median abruptly jumps to join the trend of steadily rising SFE of starbursts, which reflects the increasing boost-amplitudes that are required to reach the highest sSFRs. Even though the 2-SFM framework assumes a full continuum of SFR- and SFE-enhancements, the changing population mix between normal and starbursting galaxies thus has led to a “bimodal” behaviour of the SFE. The exact shape of the jump depends not only on the parameters of the double log-normal decomposition but also on the SFE-dispersion of main-sequence galaxies. In plotting the average trend in Fig. 10a we have assumed a scatter of 0.2 dex, in accordance with the measurement made on Fig. 1. The scatter (indicated with light grey shading in Fig. 10) abruptly increases in the transition region with its mixture of main sequence and starburst galaxies and then at $\text{sSFR} / \langle \text{sSFR} \rangle_{\text{MS}} \gtrsim 4$ is predicted to settle to a constant value that is somewhat larger than the 0.2 dex of the main-sequence locus as it simultaneously reflects (a) the spectrum of initial main-sequence states that end up at a given sSFR-excess by virtue of their different SFR-boosts, and (b) of the dispersion in SFEs in the pre-burst main-sequence state. The depicted average trend also depends on the relation between SFE and boost. In Fig. 10a we show the prediction for the case of the ‘direct’ boost-function (the SFE-evolution for starbursting galaxies would steepen when

¹⁷ The average SFE of starbursting systems is predicted to have a slightly sub-linear dependence on sSFR. This is the consequence of convolving the supra-linear evolution of SFE with boost-amplitude (see eq. 23) with the shallow dependence of average boost amplitude on sSFR (see Fig. 8).

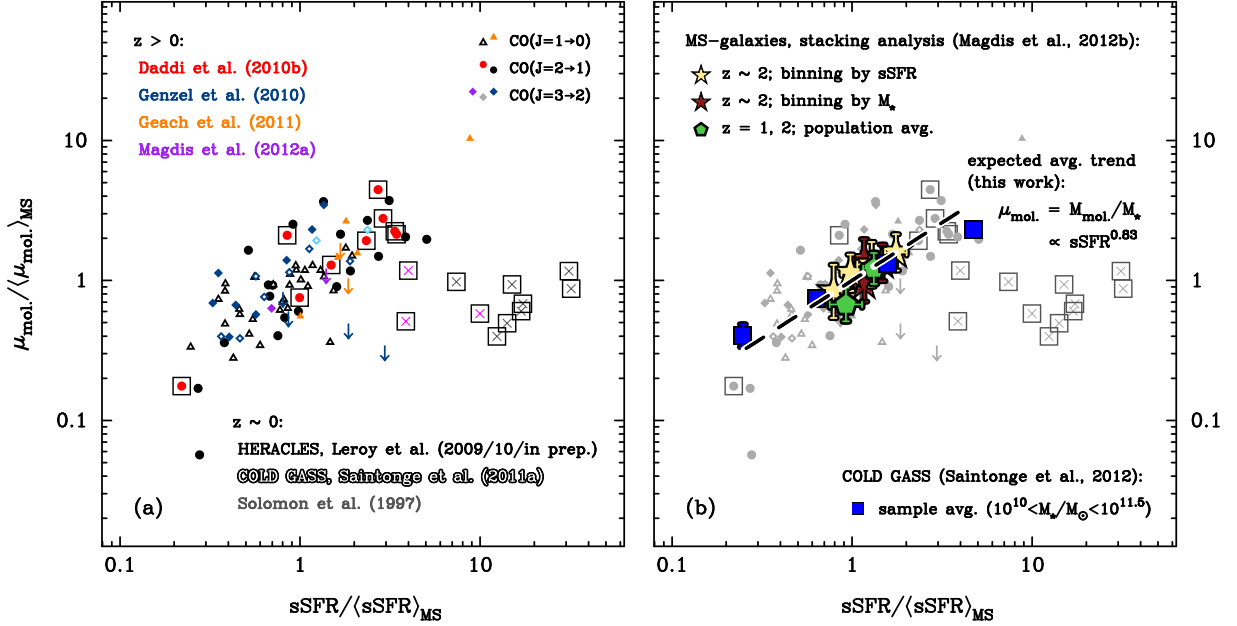


FIG. 11.—: Molecular gas mass fraction ($\mu_{\text{mol.}} \equiv M_{\text{mol.}}/M_*$) vs. sSFR for selected main-sequence galaxies and starbursts at $z \lesssim 3$ (left) and for stacked galaxies from Magdis et al. (2012b; right) (all measurements normalized to the M_* - and redshift-dependent average of the main-sequence and all symbols and data as in Fig. 6). The gas fractions of normal galaxies rise uniformly (independent of redshift) across the main sequence while starbursting sources have a gas content that is somewhat lower than the main-sequence average.

using the boost-function including an explicit correction for mergers) and do so only for the best-fit value of γ_{SFE} . We refrain from estimating formal errors for this average trend since the systematic uncertainties (for example those pertaining to the choice of a function relating SFE-excess and boost as in eq. 23) in any case strongly outweigh these.

Note that, by working with (s)SFRs that are normalized to the average main-sequence value rather than absolute quantities, we have removed all dependence on redshift. Our prediction for the variation of SFE can thus be summarized by a single track, as shown in Fig. 10a. It is generalizable to the full range of redshifts and stellar masses by (1) multiplying (s)SFRs by the normalization constant, $\langle\text{sSFR}\rangle_{\text{MS}}$, which is given by eq. A1, and by (2) using eq. 22 with $\text{SFR} = M_* \times \langle\text{sSFR}\rangle_{\text{MS}}$ to obtain the normalization, $\langle\text{SFE}\rangle_{\text{MS}}$, and thence the absolute value of SFE.

5.2. Molecular gas fractions in star-forming galaxies

5.2.1. Gas fractions in normal and star-bursting galaxies

The predictions of the previous section for the average variation of SFE in SFGs with offset from the main-sequence locus are equivalent to a variation of the molecular gas mass $M_{\text{mol.}} = \{M_* \times \text{sSFR}(M_*, z)\} / \text{SFE}$. By construction, the stellar mass M_* in this expression is known in the 2-SFM approach, implying that we can directly compute the molecular gas mass to stellar mass ratio, $\mu_{\text{mol.}} = M_{\text{mol.}}/M_*$, as a function of sSFR. To obtain predictions that are independent of redshift and stellar mass we again consider normalized quantities, $\text{sSFR}/\langle\text{sSFR}\rangle_{\text{MS}}$ and $\mu_{\text{mol.}}/\langle\mu_{\text{mol.}}\rangle$, in Fig. 10b. The bimodal behaviour of the average SFE-evolution leads to two distinct regimes: (1) a nearly linear increase of the

gas fraction across the main sequence, and (2) for strong starbursts, gas fractions that vary more slowly with sSFR and are somewhat lower than the gas fraction of the average main-sequence galaxy. (Note that as in Fig. 10a, gas fraction variations within the starbursting population are again shown for the direct boost-function; using the boost-function that includes the explicit correction for mergers would result in a shallower trend.) As in the case of SFE (see Fig. 10a), the transition between these two regimes is almost step-like and characterized by a large dispersion in $\mu_{\text{mol.}}$. We explore the link between gas fractions during a starburst episode and prior to the onset of burst-activity in more detail in section 6.3.

We compare these expectations of the 2-SFM framework with real data in Fig. 11. While our reference sample of starbursts is too small to quantitatively constrain any residual variation of gas fractions at high sSFRs, the predicted rise of gas fractions across the main sequence is well sampled by the reference sample of normal galaxies. As discussed in Sect. 5.2.2, the gas fractions inferred for 90% of the main-sequence galaxies involve an assumption about the metallicity-dependence of α_{CO} . Nevertheless, they show no systematically different behaviour than the eight sources (boxed symbols in Fig. 11) for which measurements of α_{CO} exist. A very similar slope ($\text{sSFR}^{0.9}$) was measured by Magdis et al. (2012b) for stacked samples of main-sequence galaxies divided in bins of sSFR-excess in which the gas mass was constrained via the far-IR dust emission. Stacking-based measurements of $\mu_{\text{mol.}}$ at $z = 1$, and 2 by Magdis et al. (2012b) are shown in Fig. 11b and found to coincide with the 2-SFM predictions and gas fractions determined on an individual basis for galaxies in our reference sample. Saintonge et al. (2012) were able to sample molecular gas mass fraction variations over a larger range in sSFR which extends

to significantly below the star forming main sequence and also slightly into the starburst-regime. In their local COLD GASS data set the average $\mu_{\text{mol.}}$ scales as approx. $\text{sSFR}^{0.7}$. A significant deviation from the 2-SFM predictions for normal galaxies is only seen in their highest sSFR-bin which lies in the transition region between main sequence and starbursting outliers and may hence be expected to reflect the transition to the lower gas fractions in starbursting galaxies (see also the indication of a SFE-increase in the COLD GASS data set at $\text{sSFR}/\langle\text{sSFR}\rangle_{\text{MS}} = 4.5$ shown in Fig. 7b).

5.2.2. Gas fraction evolution across cosmic time

The well-defined relations between M_* and SFR, and between SFR and H_2 -mass allow for a straightforward prediction of the redshift-evolution of the molecular gas fraction, $f_{\text{mol.}}$, in normal galaxies. Using eq. 3 we can write

$$f_{\text{mol.}} \equiv \frac{M_{\text{mol.}}}{M_{\text{mol.}} + M_*} = \frac{1}{1 + M_*/(\text{const.} \times \text{sSFR}^{\beta_2})} \\ = \frac{1}{1 + \frac{M_*^{1-\beta_2}}{\text{const.}} \times \text{sSFR}^{-\beta_2}}, \quad (25)$$

where $\text{const.} = 10^{\alpha_2, \text{sSFR}}$. If we insert the average $\text{sSFR}(M_*, z)$ of main-sequence galaxies (parametrized as in eq. A1) into this equation we obtain an evolutionary trend which we plot in the upper half of Fig. 12 for four different stellar masses in the range $5 \times 10^9 < M_*/M_\odot < 10^{11}$. The gas fractions of normal galaxies at $z \lesssim 3$ predicted in this manner are in excellent agreement with literature data, which suggests that the gas content of secularly-evolving SFGs is an important driver of the cosmic sSFR-evolution. Supporting evidence for this tight link between the evolution of sSFR and the gas fraction of main-sequence galaxies was recently provided by the analysis of more than 50 SFGs at $1 < z < 3$ with CO-flux measurements from the PHIBBS survey in Tacconi et al. (2013; dark blue stars in our Fig. 12). Combes et al. (2013), on the other hand, hold a joint redshift-evolution of both SFE and gas fractions by roughly similar amounts to be responsible for the cosmic evolution of star formation activity. This apparent discrepancy can be explained by the distinctly different behaviour of normal galaxies and starbursts with respect to SFE and $f_{\text{mol.}}$, which we illustrate in Fig. 10, and by the fact that the $0.2 < z < 1$ ULIRGs analyzed by Combes et al. (2011, 2013) have generally large sSFR-excesses (see Fig. 9 in Combes et al. 2013), while their local reference sample overlaps with the main-sequence population. These authors hence tend to compare fairly low-efficiency $z = 0$ systems with $z > 0.2$ starbursting galaxies (thereby overestimating the importance of SFE for sSFR-evolution) which on average have lower gas fractions than equally massive normal galaxies (leading to an underestimate of the gas fraction evolution). The link between sSFR and gas fraction also manifests itself at fixed redshift as a variation of sSFR across the main sequence (see Fig. 11). This is equivalent to stating that the dispersion of the main sequence can be at least partially ascribed to different gas fractions. In a recent morphological study of $z \sim 1$ disk galaxies Salmi et al. (2012) reported that systems with clumpy substructure are found to be systematically offset to higher val-

ues of sSFR than their smoother counterparts. Since clumps are a telltale signature of violent disk instabilities in gas-rich high-redshift galaxies (e.g. Agertz et al. 2009, Ceverino et al. 2010, Förster Schreiber et al. 2011, Swinbank et al. 2011, Wuyts et al. 2012) this observation thus provides independent evidence for increasing gas fractions within the main sequence.

Following the publication of simulation-based recipes for the calculation of α_{CO} by Narayanan et al. (2011), the same authors have recently questioned (Narayanan et al. 2012) the reliability of the high gas fractions reported in the literature. (Alternative predictions for α_{CO} that make use of the observed relations between L'_{CO} and L_{IR} and SFR and H_2 -mass are presented in Sect. 5.3.) Various additional predictions for gas fraction evolution based on numerical simulations (Davé et al. 2011, Duffy et al. 2012) or semi-analytical modeling (Fu et al. 2012) are shown in the lower half of Fig. 12. Although these predictions generally lie within the range of gas fractions expected in the 2-SFM framework for galaxies located on the main sequence, a tendency for shallower redshift evolution of $f_{\text{mol.}}$ in the simulations is ubiquitous. Rather than being the consequence of incompatible assumptions for the calculation of α_{CO} these differences compared to the 2-SFM predictions might reflect the well-known problem that both semi-analytical models (e.g. Fontanot et al. 2009) and cosmological hydrodynamical simulations (e.g. Weinmann et al. 2012) tend to produce too many stars too early in the history of the universe, especially in lower mass galaxies. The resulting accelerated exhaustion of gas reservoirs would then likely lead to lower gas fractions than we predict using the 2-SFM approach. Popping et al. (2012) used a similar, empirically motivated approach as the one proposed here to indirectly infer the gas content of both late- and early-type galaxies at $z < 2$. Here we show the redshift evolution of $f_{\text{mol.}}$ these authors derive for main-sequence galaxies with the stellar masses plotted in Fig. 12. Their expectations are in good agreement with ours at $z \lesssim 1$ but begin to differ from the 2-SFM predictions at higher redshift, probably due to incompleteness in their lower-mass ($M_*/M_\odot < 10^{11}$) galaxy samples.

We end this section by plotting explicitly in Fig. 13 the M_* -dependence of the molecular gas fraction which was already visible in Fig. 12 as a vertical offset between the evolutionary trends. Two panels with the 2-SFM predictions for $z \sim 1$ and 2 are shown. In both cases the range of expected gas fractions $f_{\text{mol.}} = M_{\text{mol.}}/(M_* + M_{\text{mol.}})$ at fixed stellar mass can be significant, e.g. for a stellar mass of $5 \times 10^{10} M_\odot$ a $\Delta f_{\text{mol.}}$ of approx. 0.5 is expected, depending on whether the source is located at a positive or negative offset of $2\sigma_{\text{MS}}$ with respect to the main sequence. We illustrate this considerable scatter with our two statistical samples of GOODS-S galaxies (see Sect. 2.2), to which we apply eq. 3 to indirectly infer gas masses. In spite of the large dispersion, a clear trend of decreasing gas fractions with increasing stellar mass is seen. Predictions from semi-analytical models show qualitatively similar, albeit somewhat shallower trends.

5.3. The CO-to- H_2 conversion factor α_{CO}

In Sect. 5.1.2 we showed how the sSFR-dependent starburst demographics of the 2-SFM approach led to a nearly step-like variation of the SFE even if star-

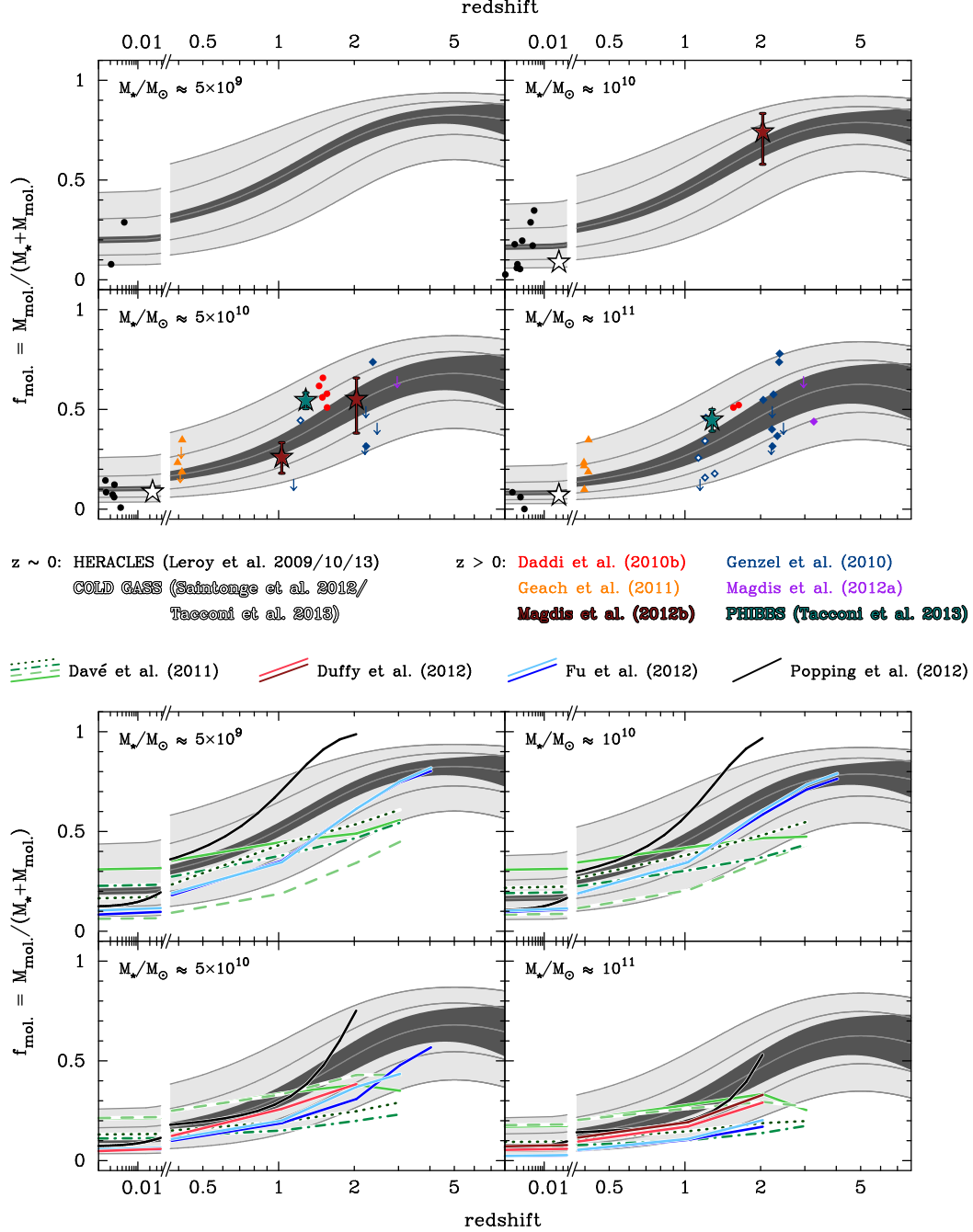


FIG. 12.—: Redshift-evolution of the molecular gas fraction, $f_{\text{mol.}}$, of main-sequence galaxies in four different stellar mass scales, as predicted by the 2-SFM framework based on the evolution of the sSFR and of the integrated S-K relation (see eq. 25). Upper half of figure – comparison with literature data (taken to have stellar masses within at most a factor two of the mass scale used for the analytical predictions); lower half – comparison with predictions from numerical simulations and semi-analytical modelling. The dark grey shading illustrates the uncertainty ($\pm 1\sigma$; reflects the uncertainty of the sSFR-evolution according to eq. A1 and of the integrated S-K law in eq. 3) on the evolution of $f_{\text{mol.}}$ for a typical main-sequence galaxy. Light grey areas illustrate the predicted dispersion of gas fractions. The evolution for galaxies offset by $+2/+1/0/-1/-2\sigma$ from the average main-sequence locus are additionally highlighted (uppermost to lowermost medium grey line). The good agreement between predictions and data in the upper half of the figure – i.e. the observation of a synchronous evolution of sSFR and $f_{\text{mol.}}$ – is consistent with the evolution of the gas reservoirs in normal galaxies being the primary driver of the cosmic sSFR evolution. Star-shaped symbols indicate gas fractions determined with stacking (Magdis et al. 2012b) or sample averaging (Saintonge et al. 2012, Tacconi et al. 2013). Colors/line styles used to represent different simulation predictions in the lower half of the figure are: dotted/dot-dashed/dashed/solid green lines for the vzw/cw/nw/sw (momentum-conserving/constant/no/slow wind) scenario in Davé et al. (2011); red/scarlet lines for the ‘L050N512’/‘L100N512’ realizations in Duffy et al. (2012); light/dark blue lines for ‘prescription 1’/‘prescription 2’ in Fu et al. (2012; H_2 fraction depending on local cold gas surface density and metallicity/ H_2 fraction depending on ISM pressure), and for the assumption of two different star-formation laws for regions where atomic and molecular gas dominates, resp. (see Bigiel et al. 2008).

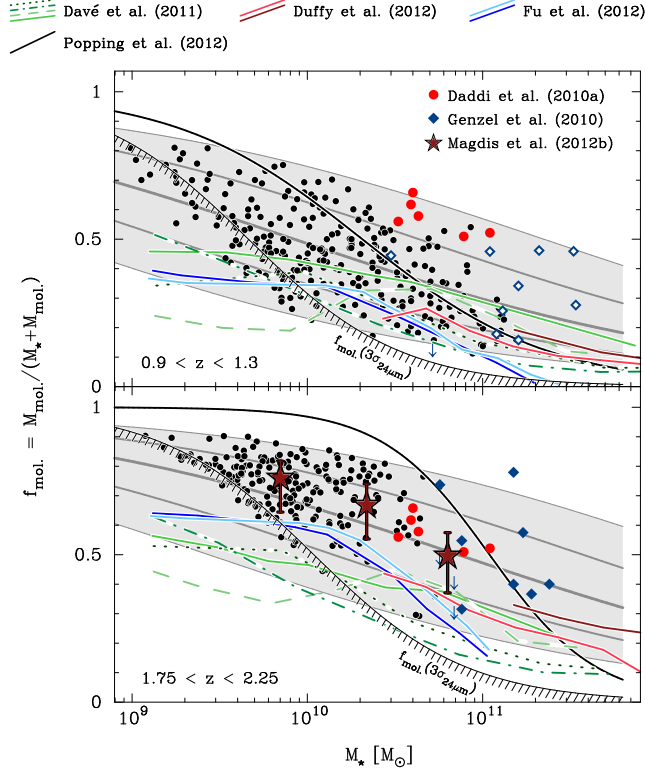


FIG. 13.—: Variation of the molecular gas fraction, $f_{\text{mol.}}$, of main-sequence galaxies with stellar mass in two different redshift bins ($z \sim 1$ – top; $z \sim 2$ – bottom). Selected main-sequence galaxies from Daddi et al. (2010a) and Tacconi et al. (2010), as well as average gas fractions determined in the stacking analysis of Magdis et al. (2012b) are plotted in color. Predictions from the 2-SFM framework and recent theoretical/numerical work in the literature are plotted with the identical symbols and color scheme as used in Fig. 12. Black dots – indirect measurements of $f_{\text{mol.}}$ for $24\mu\text{m}$ -selected GOODS-S galaxies based on the inverse S-K relation calibrated in Sect. 3.2. The hatched line indicates the completeness limit of the statistical GOODS-S sample, as determined by the depth of the $24\mu\text{m}$ imaging and the average redshift of the two bins displayed.

bursting galaxies are treated as a continuous extension of normal galaxies, with depletion times that decrease in proportion to the burst strength (referred to as ‘boost’ throughout this paper). The actual value of SFE is tightly linked to the CO-to- H_2 conversion factor, α_{CO} . In the past it has been common practice to adopt one of two discrete, ‘consensus’ values when estimating molecular gas masses for high-redshift galaxies: $\alpha_{\text{CO}} = 4.4 M_{\odot} (\text{K km/s pc}^2)^{-1}$ (the conversion factor which is found to apply to Giant Molecular Clouds in the Milky Way; e.g. Bolatto et al. 2008, Abdo et al. 2010) for normal galaxies and $0.8 M_{\odot} (\text{K km/s pc}^2)^{-1}$, a representative average for local starbursting ULIRGs (e.g. Downes & Solomon 1998). Although the collectively high luminosities of distant, CO-detected galaxies suggested that their α_{CO} -values should be ULIRG-like, the first actual estimates of α_{CO} for $z > 1$ disk galaxies (based on both dynamical arguments as in Daddi et al.

2010a or on the gas-to-dust ratio approach implemented in Magdis et al. 2011) were all broadly consistent with a Galactic α_{CO} . Going a step further, Genzel et al. (2012) subsequently were able to show that the conversion factor of high- z main-sequence galaxies scales with gas-phase metallicity in a similar manner as the negative power laws observed for local galaxies (e.g. Wilson 1995, Israel 1997, Boselli et al. 2002, Leroy et al. 2011, Schruba et al. 2012).

The physics of the multiphase ISM which ultimately determines the exact value of α_{CO} is complicated, regardless of whether the emission from individual star-forming regions (e.g. Glover & Mac Low 2011) or from larger scales even up to integrated emission are considered (e.g. Narayanan et al. 2011, Feldmann et al. 2012, Papadopoulos et al. 2012). A common feature of all these theoretical or numerical calculations is a dependence of α_{CO} on metallicity. Here we adopt a scaling $\alpha_{\text{CO}} \propto Z^{-0.9}$ for main-sequence galaxies, as motivated in Sect. 3.2. In the general spirit of the 2-SFM approach, the α_{CO} -recipe proposed here for starbursting sources does not attempt to capture the aforementioned complex ISM physics in its entirety, but rather treats it implicitly by letting the data dictate the functional form of the recipe. The fact that starbursts in the 2-SFM framework preserve a memory of their former main-sequence state means that our predicted starburst- α_{CO} values also depend on metallicity but in a more complicated way which is detailed in the following.

5.3.1. Conversion factors for starbursts: empirical calibration of boost-dependence

As for the SFE (see eq. 23) we assume that α_{CO} varies smoothly¹⁸ with the boost of a starburst,

$$\log \left(\frac{\alpha_{\text{CO}}}{\alpha_{\text{MS, init.}}} \right) = \gamma_{\alpha_{\text{CO}}} \times b_{\text{SFR}}, \quad (26)$$

and use our sample of reference-starbursts (cf. 2.1.3) to determine the most suitable value of $\gamma_{\alpha_{\text{CO}}}$, given this choice of parametrization. Boosts b_{SFR} are assigned as in Sect. 5.1.2 and α_{CO} -values are given in Downes & Solomon (1998) or Magdis et al. (2012b) for each starburst in the reference sample. $\alpha_{\text{MS, init.}}$ corresponds to the conversion factor of a main-sequence galaxy with the same SFR as a reference-starburst, but with L'_{CO} and M_{H_2} given by the inverse S-K relations in eq. 1 and 3, respectively. Since we refer the α_{CO} to this initial state by definition no constant term is required in eq. 26. Solving for $\gamma_{\alpha_{\text{CO}}}$ we obtain $\gamma_{\alpha_{\text{CO}}} = -0.78^{+0.07}_{-0.08}$ (1σ errors quoted) for the case of the direct boost-function and $\gamma_{\alpha_{\text{CO}}} = -0.72 \pm 0.05$ for the merger-corrected boost-function. The boost-dependence for the two scenarios is shown in Fig. 14a, together with the

¹⁸ The functional form of eq. 26 is not merely motivated by its symmetry with eq. 23, it also reflects the expectation that the state of the ISM evolves continuously, e.g. depending on the strength of the tidal forces which may enhance the amplitude of the turbulent motions during galaxy-galaxy interactions (e.g. Bournaud et al. 2011b). Larger velocity gradients and higher temperatures, which are generally characteristic of the turbulent and dense starbursting ISM, both lower α_{CO} while higher column densities increase the CO-to- H_2 conversion factor (see, e.g., eq. A4 in Papadopoulos et al. 2012).

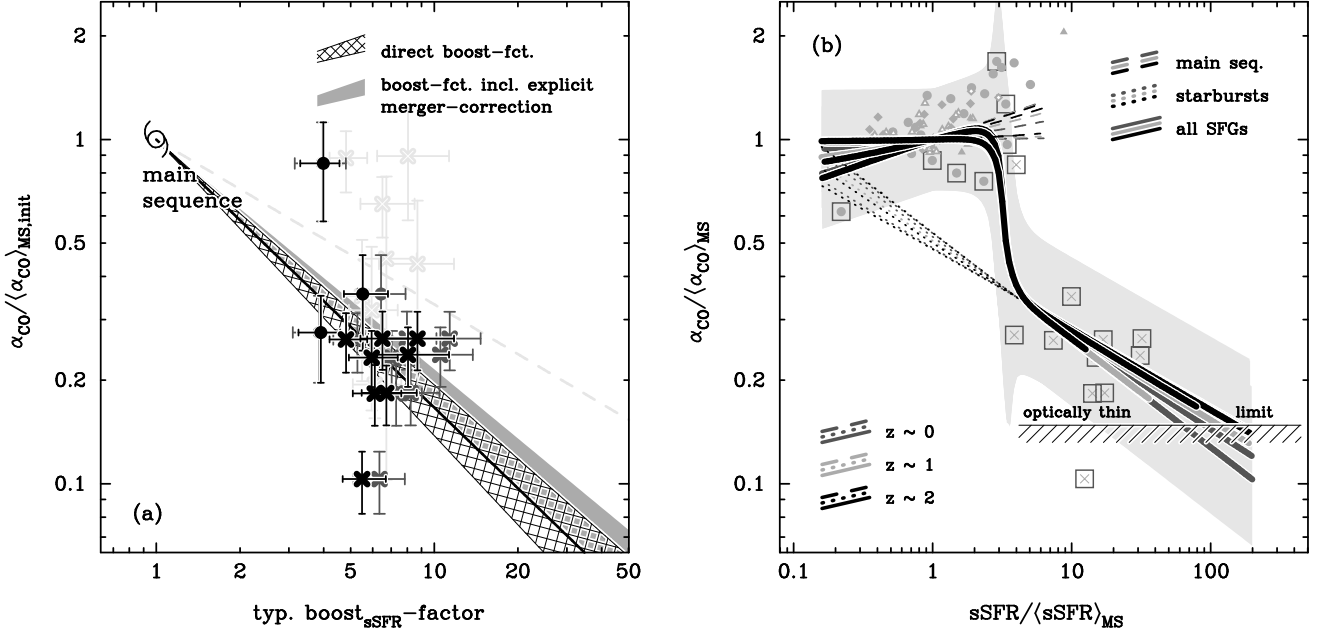


FIG. 14.—: (a) Empirical calibration of the decrement in α_{CO} with the amount of (s)SFR-boosting experienced by starbursts (all symbols and data as in Fig. 8b). The decrement is referred to the CO-to-H₂ conversion factor, $\langle \alpha_{\text{CO}} \rangle_{\text{MS, init.}}$, that would be expected for each starburst galaxy if it were a secularly-evolving, average, normal galaxy with the same molecular gas fraction (see Sect. 5.3.1 for details). Starburst α_{CO} -measurements plotted in black are from dynamical modelling in Downes & Solomon (1998), light grey symbols are for α_{CO} -values derived by Papadopoulos et al. (2012) using a two-phase LVG model. (Crosses/dots are used for local/high- z starbursts from Solomon et al. (1997) and Magdis et al. (2012b), respectively; 1 sigma-error bars plotted.) The shaded/hatched areas span the 68% confidence region for a power-law relation between starburst α_{CO} and boost amplitude as parametrized in eq. 26 and when fitting to α_{CO} -measurements from Downes & Solomon (1998). The light grey dashed line shows the best-fitting power-law relation inferred based on the α_{CO} -values from two-phase LVG modelling.

(b) Predicted variation of average, normalized α_{CO} with sSFR-excess for normal main-sequence galaxies (*dashed lines*), starbursts (*dotted lines*; ‘direct’ boost-function assumed) and the total population of SFGs (*solid lines*). Data points plotted in grey in the background are as in Fig. 10. Due to the non-linear dependence of the gas-phase metallicity on SFR and stellar mass (as parametrized by the FMR of Mannucci et al. 2010) the average α_{CO} -trends predicted by the 2-SFM framework are both stellar mass- and redshift dependent. In a given redshift bin (color-coded as shown in the upper right corner) the shallowest variation across the main sequence (i.e. in the range $1/6 < \text{sSFR} / \langle \text{sSFR} \rangle_{\text{MS}} < 6$) occurs for the most massive of the three stellar mass bins considered here ($M_*/M_\odot = 5 \times 10^9, 5 \times 10^{10}$ and 5×10^{11}), while the steepest variation occurs for the least massive bin. At high excesses of sSFR the α_{CO} -values are predicted to decrease the most steeply in the highest and most slowly in the lowest stellar mass bin plotted. Over the range $0 < z < 2$ shown here, the variation with stellar mass is expected to be more significant than with redshift. At the highest sSFR-excesses (boosts) the α_{CO} -values in starbursts plausibly asymptotically approach the lower limit set by optically thin CO line-emission.

starburst-data used for the fit. The relatively slow, sub-linear decline of α_{CO} with boost-amplitude (i.e. SFR-enhancement) according to $\alpha_{\text{CO}} \propto (\text{boost})^{\gamma_{\alpha_{\text{CO}}}}$ implies that to reach ULIRG-like values of the conversion factor, which are about $1/5$ of the typically assumed Milky Way-like $\alpha_{\text{CO}} = 4.4 M_\odot (\text{K km/s pc}^2)^{-1}$, a boost by a factor of eight to ten is expected according to the 2-SFM description.

Several of the α_{CO} -measurements for our reference starbursts deviate more strongly from the average trend between boost and conversion factor than was the case for the relation between SFE and boost we calibrated in Fig. 8b. As a consistency check we hence used the results of the LVG radiative transfer modelling by Papadopoulos et al. (2012) of all nine starbursting local ULIRGs in our reference sample to re-derive the logarithmic slope $\gamma_{\alpha_{\text{CO}}}$ in eq. 26. We find that

α_{CO} -values determined with one-phase radiative transfer models are on average consistent with the dynamical estimates of Downes & Solomon (1998), such that the resulting slope is almost identical to the previously measured one: $\gamma_{\alpha_{\text{CO}}} = -0.81^{+0.07}_{-0.09}$ (direct boost-function) and $\gamma_{\alpha_{\text{CO}}} = -0.75 \pm 0.06$ (boost-function corrected for merger-statistics). CO-to-H₂ conversion factors inferred with two-phase (for high- and low-excitation gas) ISM models are generally higher (see light grey crosses in Fig. 14a), leading to a shallower slope $\gamma_{\alpha_{\text{CO}}} = -0.48^{+0.09}_{-0.19}$ ($-0.44^{+0.08}_{-0.17}$) for the direct (merger-corrected) boost-function. Given the good agreement between the former two estimates of $\gamma_{\alpha_{\text{CO}}}$ we have adopted the dynamically-constrained CO-to-H₂ conversion factors reported in Downes & Solomon (1998) throughout this paper.

We can now write an expression that relates the conversion factor of a starburst in general to the main-sequence

average:

$$\begin{aligned} \log\left(\frac{\alpha_{\text{CO}}}{\langle\alpha_{\text{CO}}\rangle_{\text{MS}}}\right) &= \log\left(\frac{\alpha_{\text{CO}}}{\alpha_{\text{MS, init.}}}\right) + \log\left(\frac{\alpha_{\text{MS, init.}}}{\langle\alpha_{\text{CO}}\rangle_{\text{MS}}}\right) \\ &= \gamma_{\alpha_{\text{CO}}} \times b_{\text{sSFR}} + \dots \\ &\dots + \xi \times [f(\text{SFR}_{\text{MS, init.}}) - f(\langle\text{SFR}\rangle_{\text{MS}})] \quad (27) \end{aligned}$$

Here the first term – which describes the α_{CO} -deficit of starbursts with respect to the pre-boost, main-sequence state of each individual galaxy – corresponds to eq. 26. The second term relates the pre-boost, main-sequence state to the main-sequence average and depends on the slope ξ of the relation between α_{CO} and metallicity (eq. 2). Eq. 27 strongly resembles eq. 24 for the normalized SFE of starbursts but has the subtle difference that the term describing variations within the main sequence,

$$\begin{aligned} \log\left(\frac{\alpha_{\text{CO}}}{\langle\alpha_{\text{CO}}\rangle_{\text{MS}}}\right) &= \xi \times \log\left(\frac{Z}{\langle Z \rangle_{\text{MS}}}\right) \\ &= \xi \times [f(\mu_{0.32}) - f(\langle\mu_{0.32}\rangle_{\text{MS}})] \\ &\equiv \xi \times [f(\text{SFR}) - f(\langle\text{SFR}\rangle_{\text{MS}})] \quad (28) \end{aligned}$$

has higher order terms in $\log(\text{SFR})$ due to its dependence on the FMR parameter $\mu_{0.32} = \log(M_{\star}) - 0.32 \times \log(\text{SFR})$ defined in Mannucci et al. (2010). Since $f(\text{SFR}) = \mathcal{O}[\log(\text{SFR})^4]$ in general (see Sect. 3.2), the normalized logarithmic conversion factor for main-sequence galaxies, $\log(\alpha_{\text{CO}}/\langle\alpha_{\text{CO}}\rangle_{\text{MS}})$, can no longer be written as a function $f(\text{SFR}/\langle\text{SFR}\rangle_{\text{MS}})$ of normalized SFR (or, equivalently, sSFR when considering a fixed bin of stellar mass). This was possible, however, in the case of SFE and $f_{\text{mol.}}$ (see Sects. 5.1.2 and 5.2.1) and led to a redshift- and mass-independent recipe for the evolution of the population average of these quantities with $\text{sSFR}/\langle\text{sSFR}\rangle_{\text{MS}}$. In Fig. 14b we plot¹⁹ (fine dashes) the predicted variation of the median α_{CO} of main-sequence galaxies for three stellar mass bins ($M_{\star}/M_{\odot} = 5 \times 10^9$, 5×10^{10} and 5×10^{11}) and three different redshifts ($z = 0, 1, 2$). Due to the higher order (s)SFR-terms in eq. 28 these trends are no longer redshift- and mass-independent; while α_{CO} -values for SFGs vary little across the main sequence in our highest mass bin ($M_{\star}/M_{\odot} = 5 \times 10^{11}$), evolution by approx. a factor two is predicted between $\pm 4 \sigma_{\text{MS}}$ for stellar masses $M_{\star} \sim 5 \times 10^9 M_{\odot}$. For the mass and redshifts considered here, the mass-dependence of the average trends at fixed redshift is more pronounced than the redshift-dependence at fixed mass. Note that although we assume the relation between boost and α_{CO} -decrement for starbursts (see eq. 26) to be independent of redshift and stellar mass, the predicted average α_{CO} -trends for starbursting sources nevertheless vary with stellar mass and redshift. This is a consequence of the mass- and redshift-dependency found for the ‘parent’ main-sequence population. For example, the fact that at low masses conversion factors are predicted to rise across the main sequence implies that at fixed boost-dependent α_{CO} -decrement the α_{CO} of high-sSFR starbursts will be higher than for the highest mass bins where α_{CO} -values of normal galaxies on the main-sequence are expected to

be virtually constant. As a final comment on the description of α_{CO} -variations for starbursting sources we should point out that in practice the conversion factor cannot decrease indefinitely (as formally implied by eq. 27) but that optically thin CO line-emission sets a lower limit (see Fig. 14b). Assuming local thermal equilibrium and a gas temperature of 40-60 K for starburst sources, we estimated α_{CO} in the optically thin approximation using standard formulae (see, e.g., Appendix A1 in Bryant & Scoville 1996) and obtained values ranging between 0.45 and $0.75 M_{\odot} (\text{K km/s pc}^2)^{-1}$. Values at the lower (higher) end of this range are generally predicted for lower (higher) redshift sources due to the evolution of the temperature of the cosmic microwave background, and with an additional contribution from the likely quite mild evolution of the dust temperature in starbursts (e.g. Béthermin et al. 2012). In relative terms, at all redshifts $0 < z < 2.5$ this is about 10%-20% of the α_{CO} -values expected for massive main-sequence galaxies if their conversion factors also increase with redshift because of the general evolution of the population toward lower metallicity.

The median α_{CO} of the total population – computed in analogy to the bulletized procedure sketched in Sect. 5.1.2 – is plotted with thick, solid lines in Fig. 14b. The exact shape of the transition between main-sequence and starburst-regime depends both on the assumed scatter of the FMR and the dispersion of α_{CO} at fixed metallicity (see, e.g., Mannucci et al. 2010, Genzel et al. 2012, Schrubba et al. 2012). For the present case we assume these to be 0.05 dex and 0.1 dex, respectively, which leads to a step-like decrease by about a factor 2-3 at an sSFR-excess $\text{sSFR}/\langle\text{sSFR}\rangle_{\text{MS}} \sim 3-4$ with respect to the main-sequence average. Just as for the predicted slope of the normalized α_{CO} vs. sSFR relations for normal and starburst galaxies, this jump changes with redshift and stellar mass. In the next section we thus provide a more complete mapping of expected α_{CO} -variations for SFGs.

5.3.2. α_{CO} : predicted variations in the SFR- M_{\star} plane

To conclude this section on empirical recipes for the CO-to- H_2 conversion factor α_{CO} we map its predicted variation within the M_{\star} vs. SFR plane for three different redshift bins: $z = 0$ – Fig. 15; $z = 1$ – Fig. 16; $z = 2$ – Fig. 17. We do this explicitly because the mapping of metallicity into the M_{\star} vs. SFR plane following Mannucci et al. (2010) is such that the variation of the metallicity-dependent α_{CO} we adopt for 2-SFM framework is not self-similar (i.e. independent of stellar mass and redshift as was the case for SFE and $f_{\text{mol.}}$; see Fig. 10) and hence cannot be represented with a single, sSFR-dependent recipe.

The individual panels of Figs. 15 to 17 show the variation of α_{CO} in M_{\star} -SFR space for the total SFG population, for main-sequence galaxies and for starbursts (clockwise from lower left corner). We have superimposed contours of constant α_{CO} and in particular indicated the isolines for Milky Way-like and ULIRG-like conversion factors with a bold red and blue line, respectively. Due to the increasing normalization of the main sequence with redshift, metallicities at fixed stellar mass decrease with redshift (this reflects the well-established, measured evolution of the mass-metallicity relation, e.g. Kobulnicky & Kewley 2004, Erb et al. 2006, Liu et al.

¹⁹ All predictions shown in Fig. 14b and Figs. 15 to 17 assume the ‘direct’ boost-function and the corresponding best-fit value of $\gamma_{\alpha_{\text{CO}}}$.

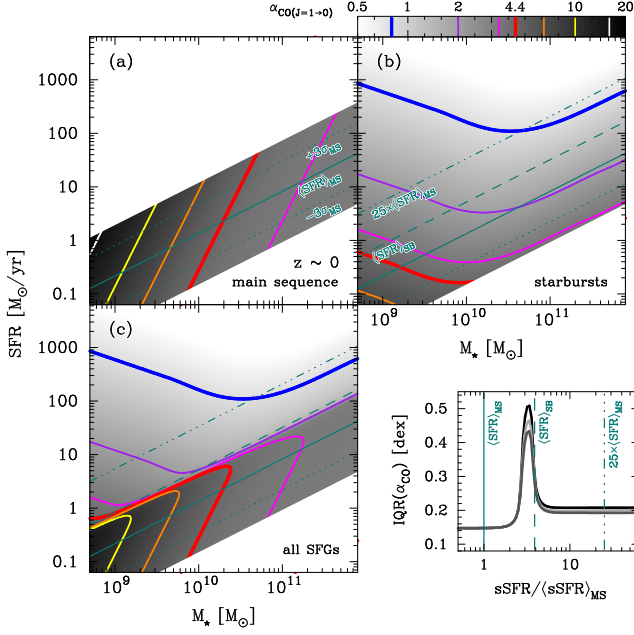


FIG. 15.—: Predicted variations of the CO-to-H₂ conversion factor, α_{CO} (for the $J = 1 \rightarrow 0$ transition and assuming the ‘direct’ boost-function), in the SFR- M_* plane for main-sequence galaxies (panel *a*), for starbursting galaxies (panel *b*) and for the combined population of normal SFGs and starbursts (panel *c*). α_{CO} -variations are mapped within ± 5 times the dispersion (σ_{MS}) of the main sequence for the normal galaxies (panel *a*) and between $-5 \sigma_{\text{MS}}$ and arbitrarily high sSFR-excesses for starburst galaxies and the total SFG population (panels *b* and *c*). Lines of constant $\alpha_{\text{CO}} = 0.8, 2, 3.5, 4.4, 6.5, 10$ and 16 are superimposed in blue, purple, magenta, red, orange, yellow and white (standard values of a ULIRG and Milky Way conversion factor – $\alpha_{\text{CO}} = 0.8$ & 4.4 – are highlighted with bold lines). Values plotted in panels (*a*) to (*c*) represent the median for the respective (sub-)population. Panel (*d*) shows the scatter of α_{CO} (visualized here by the interquartile range IQR of logarithmic α_{CO} -values) around the average trends for the total SFG population (cf. panel *c*) at stellar mass $M_*/M_\odot = 5 \times 10^9$ (black), 5×10^{10} (light grey) and 5×10^{11} (dark grey). Vertical green lines correspond to the lines of constant sSFR plotted in panels (*a*) to (*c*). The dispersion rises strongly over a fairly small range of sSFR where $f^{\text{SB}} \sim 50\%$ (see also Figs. 5 and 14b).

2008). While this evolution to lower enrichment is expected to be quite strong at the smallest stellar masses plotted in these figures ($M_* \sim 10^9 M_\odot$) the evolution is less strong for those galaxies of stellar mass $M_* \sim 3 \times 10^{10} M_\odot$ that contribute most to the cosmic SFR-density over the redshift range considered here (e.g. Karim et al. 2011). As a consequence, we expect that the conversion factor of such galaxies remains quite similar to the classic Milky Way-value of $4.4 M_\odot (\text{K km/s pc}^2)^{-1}$ over the range $0 < z < 2$. Specifically, for a galaxy of stellar mass $M_* \sim 3 \times 10^{10} M_\odot$ that is located directly on the average main-sequence locus, the recipes developed in Sect. 5.3.1 predict $\alpha_{\text{CO}} \simeq 4.1$ in the local universe and $\alpha_{\text{CO}} \simeq 5.3$ at $z \sim 2$. Note that this prediction is not the

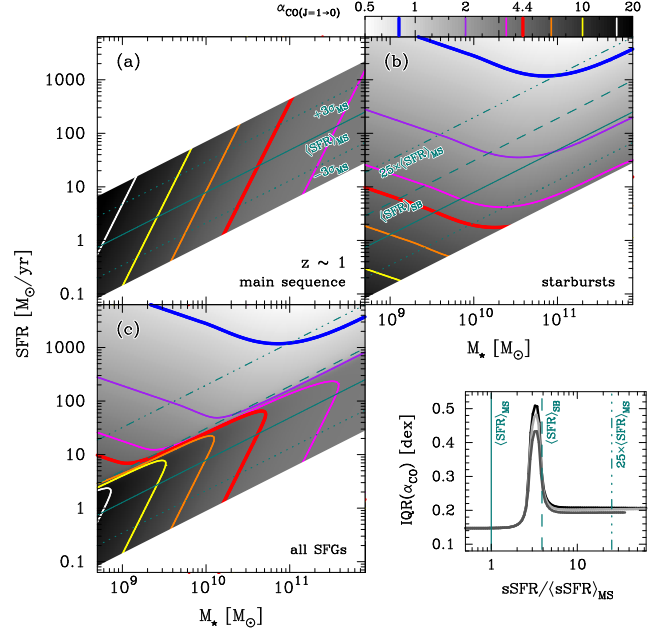


FIG. 16.—: As in Fig. 15, but for $z = 1$.

coincidental result of our choice of a specific slope and/or normalization of the relation between α_{CO} and metallicity in eq. 2. It would also hold for any of the other relations shown in Fig. 2 as these all attain quite similar, Milky Way-like conversion factors around solar metallicity.

For the variations of the conversion factor of starbursting sources in the M_* vs. SFR plane (upper right corner of Figs. 15 to 17) two different regimes exist. At high stellar masses, the α_{CO} -values of the parent, main-sequence population vary little (both across the main sequence with a given bin of stellar mass and between stellar mass bins); the boost-dependent α_{CO} -decrement alone hence determines the value of starburst conversion factors. As a consequence, lines of equal starburst- α_{CO} are nearly parallel to the main-sequence locus. At low stellar masses, lines of constant starburst- α_{CO} run nearly perpendicular to the iso-lines on the main-sequence locus. This is due to the rapid variation of α_{CO} for normal galaxies, which has the effect that ever higher boost-amplitudes are required in order for starbursts of successively lower stellar mass to reach equal absolute values of α_{CO} (e.g. the standard local ULIRG-value $0.8 M_\odot (\text{K km/s pc}^2)^{-1}$). Starting at an (s)SFR-excess of about $+3 \sigma_{\text{MS}}$, starbursts begin to dominate the main-sequence population by number. The transition between the main-sequence locus and the starburst-dominated part of M_* -SFR space is characterized by both a sudden drop of the average α_{CO} (see Fig. 14b) and an abrupt increase of the dispersion of α_{CO} , which is a result of the heterogeneous mixture of starbursting and high-sSFR main-sequence galaxies in this transition region. This is illustrated in the inset in the lower right corner of Figs. 15 to 17 where we plot the evolution of the interquartile range of α_{CO} -values measured in the total SFG population (i.e. including both starbursts and normal galaxies). On the main sequence ($\text{sSFR}/\langle \text{sSFR} \rangle_{\text{MS}} \lesssim 3$) the scatter in α_{CO} is caused by the metallicity dispersion of the of FMR at fixed M_* and

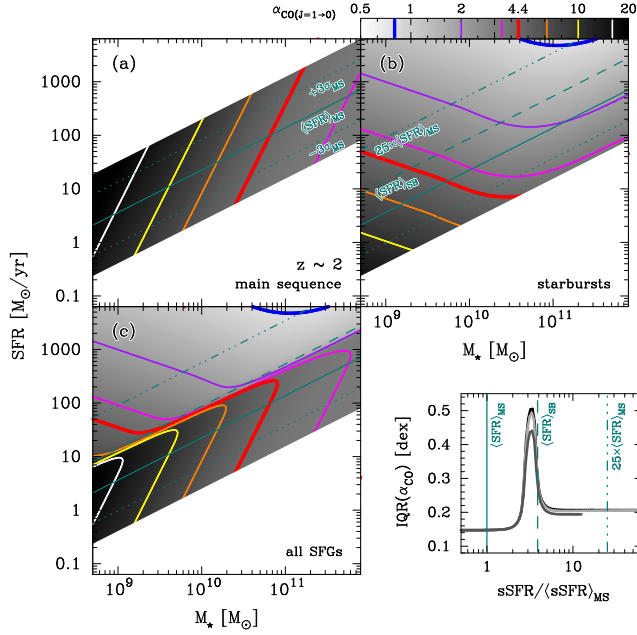


FIG. 17.— As in Fig. 15, but for $z = 2$.

SFR plus the dispersion of α_{CO} at fixed metallicity and is hence relatively small. The α_{CO} -scatter for starburst galaxies is larger than that on the main-sequence locus because it reflects both the dispersion of α_{CO} at fixed M_{\star} and SFR on the main sequence, and the fact that the shape of the boost-function implies that starbursts at a given $\text{sSFR}/\langle\text{sSFR}\rangle_{\text{MS}}$ have been boosted to higher (s)SFR starting from a range of positions on the main sequence.

6. DISCUSSION: TOWARD A SIMPLE DESCRIPTION OF MOLECULAR GAS IN STAR-FORMING GALAXIES

6.1. The boost-function: astrophysical context and limitations

6.1.1. Star formation enhancements in simulations and observations

Based on a suite of simulated interacting galaxies (with comparable masses and a representative range of both orbital configurations and morphologies) Di Matteo et al. (2007) and Di Matteo et al. (2008) derived the SFR-evolution of major mergers as compared to the evolution of identical, isolated galaxies. In Fig. 4 we plotted the maximal SFR-enhancements reported in Di Matteo et al. (2008), averaged between the Tree-SPH (smoothed particle hydrodynamics) simulations and grid-based N-body simulations carried out by these authors. Both the 2-SFM boost-function and the distribution of simulated SFR-enhancements have a clearly defined peak. The exact position of this peak (which corresponds to $\langle x \rangle_{\text{BK}}$ in the 2-SFM formalism) in the simulations depends on the gas content of the galaxies. In ‘local’ disk galaxies (simulated total gas fractions between 10 and 30%) the most frequently encountered maximal SFR-excess is approx. a factor of three, while for gas-rich simulated galaxies ($f_{\text{mol.}} \sim 50\%$) reminiscent of high- z disks it is twice as large, mainly because these tend to become Jeans-unstable and form dense gas clumps

when perturbed. The 2-SFM boost-function peaks at a roughly four-fold SFR-enhancement but it should not be directly compared to the simulation results because not all starbursts that contributed to the shape of the underlying (s)SFR-distribution in Rodighiero et al. (2011) can have been ‘caught’ at the peak of the starburst activity. With respect to the results of Di Matteo et al. (2007, 2008), observable distributions of SFR-booster for interacting galaxies will likely be modified if minor mergers and fly-bys, as well as the relative timing of starburst events, are accounted for. If SFR-enhancements in merger-driven starbursts depend on the mass ratio of the galaxies involved (e.g. Cox et al. 2008), then the boost distribution including minor mergers should be broader. Likewise, fly-bys and asynchronous burst-activity plausibly shift and skew the boost-distribution to lower SFR-enhancements.

Although the distribution of SFR-enhancements caused by interactions between galaxies is poorly constrained, observationally, there have been numerous studies aimed at quantifying the integrated contribution of excess star formation associated with mergers/interactions to the cosmic SFR density at redshifts $z < 2$ (e.g. Robaina et al. 2009, Kampczyk et al. 2011, Kaviraj et al. 2013). One attempt is the recent determination of the distribution of SFR-enhancements in SDSS galaxy pairs by Scudder et al. (2012) which we plot in blue in Fig. 4. Compared to the boost distribution in the simulations of major mergers in Di Matteo et al. (2008) it is indeed displaced to systematically lower SFR-enhancements. In addition to the expected shifting and skewing, the fact that the SDSS pair sample does not include mergers in which final coalescence has already taken place implies that their distribution of SFR-enhancements represents a lower observational limit to the total local SFR-excess distribution caused by interactions. The simulations of Di Matteo et al. (2007) and Di Matteo et al. (2008) encompass a broad variety of orbital configurations of merging galaxy pairs and have been statistically weighted to reflect the dependence of the collision rate on the relative velocities and impact parameters. However, they do not provide information on the contribution of minor interactions, nor are they carried out in a fully cosmological framework that accounts for, e.g., the preferential alignment of galaxies in different locations within the cosmic web (e.g. Hahn et al. 2010). This additional step was taken in simulations by Hopkins et al. (2010), such that their spectrum of merger-induced surplus SFR should be similar to the measurement of Scudder et al. (2012). Hopkins et al. (2010) incorporated the results of their own high-resolution merger simulations (Hopkins et al. 2009) in a cosmological (dark-matter) framework and were able to predict SFR-distributions of secularly evolving and starbursting galaxies (see Fig. 7 in Hopkins et al. 2010) that, in qualitative terms, resemble the split into main-sequence and starburst activity we proposed in S12 and which seem broadly consistent with the expected modifications to the boost-distributions of Di Matteo et al. (2008) discussed at the end of the last paragraph. For galaxies with a stellar mass of $10^{11} M_{\odot}$, where we can compare with our own double log-normal decomposition according to eq. 5, the approach of Hopkins et al. (2010) predicts (1) a SFR-boost distribution for starbursts that is broader and more

skewed to low boosts, and (2) typical SFR-enhancements that are smaller (for simulated $z \sim 0$ and 2 mergers) in comparison to both the outcome of the major merger simulations of Di Matteo et al. (2008) and also the 2-SFM boost-function.

To infer that galaxy-galaxy interactions cannot be the sole trigger of starburst activity, based only on the mismatch between the 2-SFM and measured or simulated boost distributions, would, however, be premature. The approach of decomposing an sSFR-distribution into two components – as done in Sect. 4.2 – leads to inherently poor constraints on the shape of the boost-function at low boosts (see cross-hatched area in Fig. 4) since galaxies with small sSFR-enhancements blend in entirely with the main-sequence population. This ‘maximization’ of the main-sequence contribution in eq. 5 will hence cause a truncation of the lower part of the boost-function. On the other hand, the distinction between secularly-evolving and only weakly starbursting systems itself is not clear-cut because minor merger events occur frequently. If all galaxies that have experienced minimal boosting are regarded as starbursts, then a boost-distribution that goes to zero at a (s)SFR-excess of zero (boost = 1) is unrealistic. The 2-SFM boost-function should thus best be viewed as the signature of strong boosting where a significant fraction of the ISM fuels starburst activity. Despite this limitation it is interesting that the peak position of the 2-SFM boost-function at an excess (s)SFR of a factor of four corresponds exactly to the average SFR-boost that was measured by Hwang et al. (2011) for FIR-selected galaxies at $z = 0$ and $z = 1$ undergoing an interaction with a late-type neighbor. In an alternative measurement of interaction-induced SFR-boosting in local late-type galaxy pairs, Park & Choi (2009) found an increase of the equivalent width of the H α -line by an identical factor four when the two galaxies were separated by less than 1% of the virial radius of the companion’s halo. This constancy of the average SFR-excess is reminiscent of the evidence for only mild evolution of the shape of the boost-function we presented in S12. Furthermore, it is worth noting that notwithstanding the uncertainties concerning the shape of the lower end of the 2-SFM boost-function, Béthermin et al. (2012) successfully used it as the basis for matching observed IR source counts. Their analysis was a good test of the viability of the 2-SFM description of starbursts since it employed different IR SEDs for main-sequence galaxies and starbursts.

6.1.2. Link to dark matter

Merging and star-formation activity – even in the “secular” mode – reflect the accretion of dark matter (DM) and the primordial gas bound to the DM haloes. It is thus interesting to check whether there are clear similarities between the distribution of SFRs of galaxies of a given mass and the accretion of DM onto the corresponding parent haloes. Dekel et al. (2009) determined the DM infall rates at the virial radius of >100 simulated DM haloes with mass $10^{12} M_{\odot}$ at $z \sim 2.5$ which typically host $\sim 10^{11} M_{\odot}$ galaxies. For these systems (which have masses comparable to the galaxies used by Rodighiero et al. 2011 to construct distributions of sSFR) the DM accretion spectrum shows an extended tail of high accretion rates which is dominated by “major”

merging activity where the mass ratio between accreted and parent DM halo is fairly high. It is obviously tempting to associate this feature of the DM accretion rate distributions in the simulations presented in Dekel et al. (2009) to the tail of excess SFRs contributed by starburst galaxies while the smooth accretion would then fuel the sustained secular mode of star formation that is characteristic of SFGs on the main sequence. This was already proposed by Dekel et al. (2009), who also point out that in this context the abbreviation “SFG” could legitimately stand for “stream-fed galaxy”. In analogy to our split of the sSFR-distribution in eq. 5, T. Goerdt et al. (in prep.) have decomposed the DM accretion rate distribution for such $z = 2.5$ DM haloes with virial mass $10^{12} M_{\odot}$ into two log-normal contributions and find that the one shifted to high accretion rates contributes approx. 10% to the infalling mass budget. This value is strikingly similar to the $14.2^{+1.7}_{-1.3}\%$ (68% confidence limits) we inferred in S12 for the contribution of burst-like star formation to the total SFRD at $z = 2$.

6.2. Universal star formation laws and the distribution of galaxies in the Schmidt-Kennicutt plane

The tightness of the star formation law (dispersion ~ 0.2 dex or less than a factor of two) which we found using our newly ‘homogenized’ literature data in Sect. 3.2 is remarkable and points to a very direct and apparently ubiquitous link between the global molecular content of galaxies and how much of it is being converted into stars. It is akin to stating that, for normal disk galaxies out to at least $z \simeq 2.5$, once the SFR has been measured the size of the associated molecular gas reservoir can be inferred with high accuracy, and vice-versa. In our calibration of the integrated S-K law in Sect. 3, we adopted a statistical (metallicity-dependent) estimate of the CO-to-H $_2$ conversion factor, α_{CO} , for 90% of the normal galaxies in our reference sample when we were translating the observed correlation between L_{IR} and L'_{CO} to a more physical relation between SFR and M_{mol} . While using an average α_{CO} and neglecting the associated scatter in principle artificially reduces the dispersion of the S-K law, it is not inconceivable that a dispersion in α_{CO} has produced the observed width of the L_{IR} vs. L'_{CO} relation and that the underlying star formation law might be intrinsically even tighter than the 0.2 dex we measured here. To truly test the universality of the ‘normal’-galaxy S-K law there are at least two complementary ways forward. On the one hand, it will be important to compile samples of galaxies for which star formation and gas estimates rely on strictly identical tracers (e.g. the ground-state transition of ^{12}CO). On the other hand, it may prove worthwhile to assess in detail (e.g. by means of a full sampling of the SLEDs of molecular gas tracers) how star-formation proceeds in different phases of the ISM. Having the capability of doing this in a resolved fashion, we also have the potential to reveal what causes the mild SFR-dependence of SFE, which manifests itself as a non-linear slope of the integrated S-K relation ($\text{SFR} \propto M_{\text{mol}}^{1.2}$). Saintonge et al. (2012) have proposed that the rise of SFE across the main sequence is due to morphological ‘stabilization’ of the ISM in bulged galaxies (see Martig et al. 2009), which are more abundant on the lower part of the main-sequence locus. Resolved

studies of the star formation law will also be able to reveal whether a similar mechanism is responsible for the SFE-increase with redshift in massive galaxies; while it could be due to the increasing absence of bulged galaxies at high redshift (e.g. Oesch et al. 2010), it seems just as plausible that star formation in an increasingly turbulent medium including massive star-forming clumps would proceed in a more efficient fashion.

The variations of SFE with SFR among normal galaxies are small compared to the strong SFE-enhancements that are observed in starbursting systems. In Sect. 5.1.2 we introduced an empirical, supra-linear scaling between the SFE- and (s)SFR-increase during starburst episodes. This relation can be understood very intuitively by the balance between the three quantities involved: SFR and M_* , which grow in the burst-phase and $M_{\text{mol.}}$ which decreases as gas is converted into stars. SFE, as the ratio between SFR and $M_{\text{mol.}}$, thus inevitably increases more strongly than sSFR. An immediate consequence of this is that we expect a more spread-out distribution of star formation efficiencies than is observed. In Fig. 9 we illustrate how, in the 2-SFM framework, the overlapping sSFR-distributions of normal galaxies and starbursts move apart into a more clearly double-peaked SFE-distribution. Discrete recipes for the assignment of CO-to-H₂ conversion factors to normal galaxies and starbursts are thus not the only way to obtain a bimodal distribution of galaxies in the S-K plane; this can also be achieved with a more physical, continuous description of star-formation in starbursts. Width and depth of the trough we predict between the ‘sequence of disks’ and ‘sequence of starbursts’ in the S-K plane depend on the shape of the lower end of the boost-function (see discussion in Sect. 6.1). Our model of an unbiased profile through the S-K plane at fixed gas mass does highlight, however, that observations of large cosmological volumes are necessary to fully sample the actual distribution of galaxies with respect to SFE: the relative amplitude of the SFE-distributions of starbursts and main-sequence galaxies in Fig. 9 is expected to be a factor of 30 and the contrast between the peak of the starburst distribution and the trough merely a factor two. A first attempt to construct a representative sampling of S-K space using the COLD-GASS survey was presented in Saintonge et al. (2012; see their Fig. 6b) and demonstrated just how insignificant starbursts are in determining the shape of the star formation law for the bulk of the population.

6.3. The consumption of gas reservoirs during starbursts

As a consequence of the high efficiency with which gas is converted to stars in starburst episodes, the gas reservoir in the host galaxy is used up more quickly than it can be replenished by accretion from the intergalactic medium. In Sect. 5.2.1 (see Figs. 10 and 11) we showed that the overall gas fractions (i.e. gas fractions taking into account the molecular and stellar mass content throughout the whole starbursting galaxy) of starbursts in our reference sample are indeed in general lower than the average gas fraction of galaxies which reside on the main sequence. We can use the 2-SFM description of starbursts to explicitly calculate how we expect the gas content of starbursting galaxies to change once it

has left its main-sequence state. Given that each of the starbursts in our calibration sample was observed in a different stage, this should be viewed as a comparison between the gas fraction prior to the onset of the burst and the gas fraction which would be measured approximately half-way through the starburst event. If we consider the gas-to-stellar mass ratio $\mu_{\text{mol.}} \equiv M_{\text{mol.}}/M_*$, the relation between pre-burst ($\mu_{\text{mol.}}^{\text{pre-burst}}$) and mid-burst gas content takes a simple and only boost-dependent form (see Fig. 18b):

$$\mu_{\text{mol.}}/\mu_{\text{mol.}}^{\text{pre-burst}} = (\text{boost}_{\text{sSFR}})^{1-\gamma_{\text{SFE}}}. \quad (29)$$

Here we have used that $\mu_{\text{mol.}} = \text{sSFR}/\text{SFE}$ and that the sSFR and SFE of the starburst are $\text{sSFR}/\text{sSFR}^{\text{pre-burst}} = \text{boost}_{\text{sSFR}}$ and $\text{SFE}/\text{SFE}^{\text{pre-burst}} = (\text{boost}_{\text{sSFR}})^{\gamma_{\text{SFE}}}$, respectively. In Fig. 18a we plot the variation of the typical ratio between mid-burst and pre-burst gas-to-stellar mass ratio as a function of sSFR-excess. This average trend is the result of pairing up each point on the dotted curve for the evolution of $\mu_{\text{mol.}}(\text{sSFR})$ for starbursts in Fig. 10b with a position on the corresponding relation for normal galaxies (dashed line in the same figure) by means of the boost-value $b_{\text{sSFR}}^{\text{max}}$ at the peak of the sSFR-dependent boost distribution (see Fig. 5 and Sect. 4.2.3). Note that this calculation assumes the stellar mass in the starbursting galaxy and its pre-burst, main-sequence state to be equal. By neglecting the fact that stellar mass has been added to the system during the first phase of the burst, our estimate of the ratio of mid-burst to pre-burst gas fraction effectively represents an upper limit. This simplification also makes the average trends in Fig. 18 independent of stellar mass and redshift, because all dependence of the absolute value of the pre-burst gas fraction on these two factors (see e.g. Fig. 13) is eliminated. The hatched/shaded regions straddling the median trend for $\mu_{\text{mol.}}/\mu_{\text{mol.}}^{\text{pre-burst}}$ reflect the 1σ uncertainty on the relation between average boost and sSFR (see also Fig. 8a).

Based on the theoretical understanding derived from the 2-SFM approach, we are for the first time also able to infer – in a statistical sense – the pre-burst gas fractions of the starburst galaxies in our reference sample, i.e. of eight local ULIRGs from Downes & Solomon (1998) and of three high-redshift starbursts studied by Magdis et al. (2012b). We do so under the same assumptions as already used to derive the theoretical curve discussed above and superimpose our estimates on the 2-SFM prediction in both panels of Fig. 18. Given that the typical sSFR-excess of our reference starbursts is about a factor ten, their median $\mu_{\text{mol.}}/\mu_{\text{mol.}}^{\text{pre-burst}}$ of ~ 0.35 is in quite good agreement with the 2-SFM prediction for the scenario of the ‘direct’ boost-function (black line in Fig. 18a). For the most common starbursts, which have a (s)SFR-boost equal to four, the molecular mass-to-stellar mass ratio half-way through the burst is expected to lie between 50% (30%) of its initial value for the direct (merger-corrected) boost-function.

It is interesting to explicitly compare our constraints on the gas fraction decrease during the starburst phase with that expected in the case that the starburst is triggered by a major merger. We approximate the SFR-evolution during the interaction-induced burst

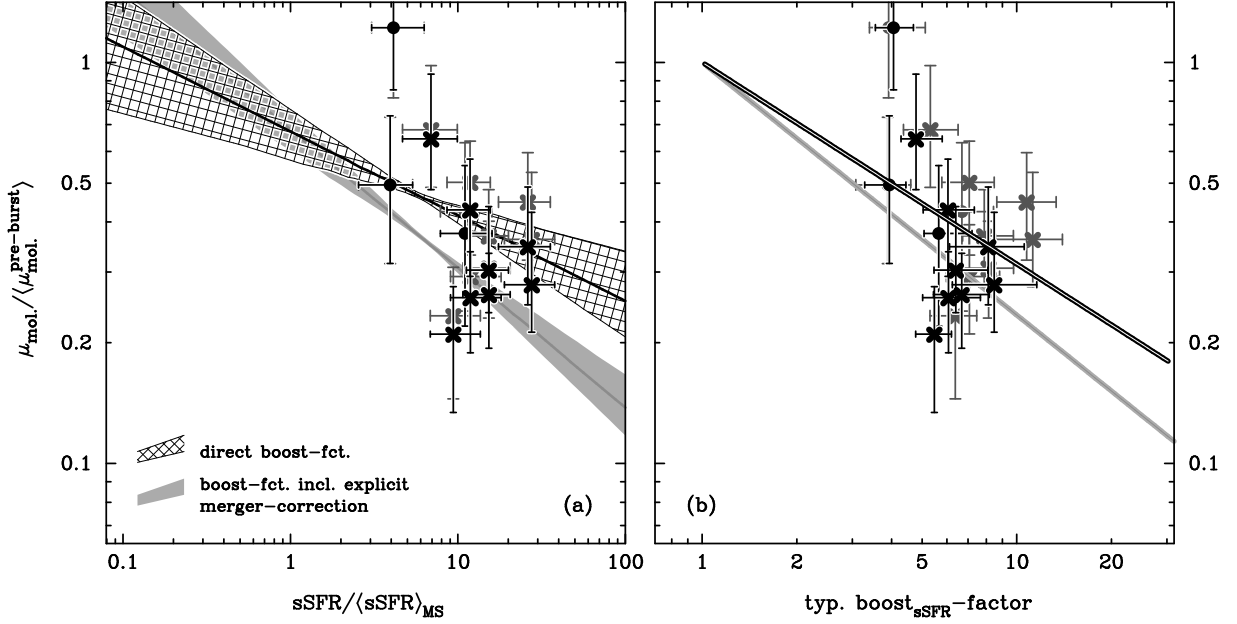


FIG. 18.— (a) Predicted ratio between the molecular gas-to-stellar mass ratio of starbursts, $\mu_{\text{mol.}} \equiv M_{\text{mol.}}/M_{\star}$, and the average expected mass ratio $\langle \mu_{\text{mol.}}^{\text{pre-burst}} \rangle$ prior to the onset of the burst (i.e. during a phase of secular growth on the main sequence). The variation with sSFR reflects the different sSFR-dependence, for normal galaxies and starbursts, of molecular gas-to-stellar mass ratios predicted by the 2-SFM description (see Fig. 10b; dashed and dotted lines, resp.). All symbols are as in Fig. 8. The pre-burst gas-to-stellar mass ratios of starburst galaxies from Downes & Solomon (1998) and Magdis et al. (2012b) were inferred assuming that these sources experienced the median (s)SFR-boost expected for sources with the same sSFR-excess (see Fig. 5).

(b) Dependence of the ratio $\mu_{\text{mol.}} / \langle \mu_{\text{mol.}}^{\text{pre-burst}} \rangle$ on the sSFR-boost of starburst galaxies (see eq. 29). The black (grey) line shows the 2-SFM prediction for the average trend for the direct (merger-corrected) boost-function.

by a top-hat function such that, at a time $t_{1/2}^{\text{merger}}$ after the beginning of the burst, stellar mass and gas mass become $M_{\star} = M_{\star}^{\text{pre-burst}} + \text{SFR} \times t_{1/2}^{\text{merger}}$ and $M_{\text{mol.}} = M_{\text{mol.}}^{\text{pre-burst}} - \text{SFR} \times t_{1/2}^{\text{merger}}$. We write the mid-burst gas fraction as

$$\begin{aligned} f_{\text{mol.}} &= \frac{M_{\text{mol.}}}{M_{\text{mol.}} + M_{\star}} = f_{\text{mol.}}^{\text{pre-burst}} - \frac{\text{SFR} \times t_{1/2}^{\text{merger}}}{M_{\text{mol.}} + M_{\star}} \\ &= f_{\text{mol.}}^{\text{pre-burst}} - f_{\text{mol.}} \frac{\text{SFR} \times t_{1/2}^{\text{merger}}}{M_{\text{mol.}}} \\ &= f_{\text{mol.}}^{\text{pre-burst}} - f_{\text{mol.}} \frac{\text{SFE}}{\text{SFE}^{\text{pre-burst}}} \frac{t_{1/2}^{\text{merger}}}{\tau^{\text{pre-burst}}}, \end{aligned}$$

and rearrange terms to obtain an expression for the ratio of the pre- and mid-burst gas fractions:

$$\frac{f_{\text{mol.}}}{f_{\text{mol.}}^{\text{pre-burst}}} = \left(1 + (\text{boost})^{\gamma_{\text{SFE}}} \frac{t_{1/2}^{\text{merger}}}{\tau^{\text{pre-burst}}} \right)^{-1}. \quad (30)$$

Here we used that the total mass ($M_{\text{mol.}} + M_{\star}$) stays constant and that the SFE before and during the starburst are related by the power-law in eq. 23. With a typical boost of approx. a factor six and $\gamma_{\text{SFE}} = 1.5$ (direct boost-function) we find $f_{\text{mol.}}/f_{\text{mol.}}^{\text{pre-burst}} \sim 0.6$ for $\tau^{\text{pre-burst}} \approx 1$ Gyr (the gas depletion time scale of main-sequence galaxies) and $t_{1/2}^{\text{merger}} \approx 50$ Myr (we take this number to be about half the time for which interaction-

induced star formation is sustained in numerical simulations of galaxy mergers, e.g. Di Matteo et al. 2008, Bournaud et al. 2011b). Accounting for the mass- and redshift-dependence of the conversion²⁰ between relative gas fractions and gas-to-stellar mass ratios, this corresponds to values of $\mu_{\text{mol.}} / \mu_{\text{mol.}}^{\text{pre-burst}}$ in the range of 0.4 to 0.5. Obviously, the simple calculation leading up to eq. 30 will in reality be complicated by, e.g., gas loss and heating in merging systems (e.g. Cox et al. 2004), the modified balance between the atomic and molecular hydrogen phase in dense, turbulent media, and IMF variations as have been proposed for starburst regions (e.g. Baugh et al. 2005, Papadopoulos et al. 2011, but see also Tacconi et al. 2008, Hayward et al. 2013). Taken at face value, the reasonable consistency of the estimates of the gas fraction decrease as per eqs. 29 and 30 may indicate that neither of these three factors plays a major role (or that these competing effects compensate each other). Systematic comparisons between the molecular gas fractions of normal and starbursting galaxies will reveal

²⁰ The relative gas fraction and gas-to-stellar mass ratio of the pre- and mid-burst state are related by

$$f_{\text{mol.}} / f_{\text{mol.}}^{\text{pre-burst}} = \mu_{\text{mol.}} / \mu_{\text{mol.}}^{\text{pre-burst}} \left(\frac{1 + \mu_{\text{mol.}}^{\text{pre-burst}}}{1 + \mu_{\text{mol.}}} \right).$$

For the massive SFGs discussed here, an initial gas-to-stellar mass ratio $\mu_{\text{mol.}}^{\text{pre-burst}}$ of ~ 5 -10% and 50-100% is expected at low and high-redshift, respectively. The term in brackets should thus vary between roughly 1.1 and < 2 .

whether the trends we proposed based on our small sample are robust. Further tests of the 2-SFM framework will now be discussed in Sect. 6.4.

6.4. *Observational validation of assumptions and predictions made by the 2-SFM approach*

The 2-SFM framework as we have developed it so far has produced a remarkably simple description of SFGs over the last 10 Gyr. One may legitimately wonder whether this simplicity is the true imprint of fundamental laws that govern galaxy formation in a cold dark matter Universe or the outcome of an incomplete or selective view of the star-forming population due to observational limitations. The answer to this question depends to some extent also on the scope of any investigation. The occurrence of extreme behaviour in rare outliers or small scale processes with little impact on global system properties – while relevant for a complete understanding of all complex aspects regulating star formation – does not imply a general inadequacy of a simpler approach, as we have been advocating here, which aims to provide a panoramic treatment. Further confirmation of the validity of the 2-SFM description will instead involve both (a) revisiting some of its key ingredients and (b) testing its predictions. Concerning point (a), the main focus should lie on verifying our hypothesis that galaxies with stellar mass significantly below $M_*/M_\odot = 10^{10}$ follow the same relations that were calibrated on galaxies which are more massive than this threshold. The universality of the S-K law, for example, will soon be routinely tested with ALMA down to low stellar masses and out to high redshift by targeted observations of lensed galaxies. With deeper follow-up of molecular transitions, it will also be possible to identify evolution in the normalization (e.g. Tacconi et al. 2013) and curvature of the star formation laws. A second assumption of the 2-SFM framework is that the double log-normal decomposition of the sSFR-distribution is applicable also at $z \neq 2$. To ascertain this, tracers of dust-obscured star-formation are indispensable as extinction-corrected SFR-measurements underestimate the true SFR of dusty starbursts (e.g. Hughes et al. 1998, Trentham et al. 1999, Buat et al. 2005, Chapman et al. 2005, Daddi et al. 2007a, Casey et al. 2013) and place these on the locus of the star-forming main sequence. Obtaining good statistics on the rare starbursting sources (comoving number densities are of order 10^{-5} Mpc^{-3}) at the high-end tail of the sSFR-distribution hence requires a combination of wide-area IR or radio surveys with complementary, deep optical or UV data. A non-universality of the double log-normal decomposition in eq. 5 would introduce more variation in the simple SFE vs. sSFR-excess relations, etc. than is currently suggested by the fairly limited data. Any evolution in the sSFR-decomposition into normal galaxies and starbursts would imply a more complex, redshift-dependent behaviour of average scaling relations in the space of normalized molecular gas properties than is shown in Fig. 10. A more fundamental question is whether the $z \sim 2$ sSFR-distribution of Rodighiero et al. (2011), on which we perform the decomposition to begin with, is accurate. Little is known about the lower tail of the sSFR-distribution, but it is unlikely that low-sSFR outliers to the main sequence should be responsible for a significant amount of star formation activity (see S12 and ref-

erences therein). In the absence of a single star formation tracer to map out the distribution of galaxies in the SFR- M_* plane, the two-pronged approach of Rodighiero et al. (2011) for reconstructing it with two different diagnostics (IR emission for dust-obscured galaxies and UV-emission for the bulk of the main-sequence population) relies on the consistency of the associated star formation estimates. Extinction-corrected UV-fluxes and IR measurements at $z \sim 2$ are known to agree in an average sense (e.g. Daddi et al. 2007a), but the dispersion about the mean extinction-correction could potentially contribute to the observed scatter of the main sequence of SFGs. The analysis of the main sequence at $0.5 < z < 1.3$ by Salmi et al. (2012) suggests that at least at these redshifts the dispersion of the sequence is mainly intrinsic. Since in Rodighiero et al. (2011) the sSFR-distributions of galaxies with $M_* \geq 10^{11} M_\odot$ are identical when computed with UV- or IR-emission, this seems to hold for the high-mass end of the $z \sim 2$ main sequence as well.

Concerning point (b), the analysis of this paper produced predictions that will be tested in future CO follow-up observations. With a good sampling of the transition region between main sequence and starburst galaxies in the SFR- M_* plane ($^{(s)}\text{SFR}/^{(s)}\text{SFR}_{\text{MS}} \in [3, 5]$), these observations will quantify the scatter of, e.g. SFE and determine whether it is indeed larger than elsewhere, as is expected for a heterogeneous mixture of normal galaxies and starbursts. While we predict such an increased dispersion to be measurable even using direct observables, e.g. L'_{CO} and L_{IR} , an estimate of the CO-to- H_2 conversion factor α_{CO} is necessary to calculate actual values of SFE and f_{gas} . Our predictions for the variation of α_{CO} in the SFR- M_* plane in Sect. 5.3.2 are in principle testable, but obtaining high-confidence measurements of α_{CO} will remain a challenging task that is best tackled using different, complementary strategies in parallel. The gas-to-dust ratio technique employed by Leroy et al. (2011), Magdis et al. (2011, 2012b), Magnelli et al. (2012) is powerful, in that it can provide constraints on the conversion factor for large data sets. However, the large scatter in measured gas-to-dust ratios in local, low-metallicity and low-mass galaxies (e.g. Draine & Li 2007, Galliano et al. 2008, Galametz et al. 2011; Rémy et al., in prep.) indicates that this method becomes highly inaccurate for $z > 3$ galaxies and galaxies with stellar mass $M_* \ll 10^{10} M_\odot$. An alternative approach is to interpret dynamical constraints from CO line profiles in the context of numerical simulations to infer α_{CO} as proposed by Daddi et al. (2010a). However, even barring the systematic uncertainties on model dark matter distributions, the application of this method to large data sets may be impracticable as it requires high signal-to-noise data and a fine spectral sampling of the emission feature.

Finally, we note that the (s)SFR-boost of starbursts, although much less easily determined than their (s)SFR-excess with respect to the average of the main-sequence population, is in principle measurable using high-fidelity and ideally also spatially resolved spectroscopy. When compared to the output of stellar evolution models, this kind of data would allow a detailed reconstruction of the SFH of boosted sources prior to the onset of burst activity. It would hence also reveal whether galaxies that show a strong sSFR-excess are truly experiencing

short-term boosting of their activity at all redshifts or whether they are merely a high-intensity tail of the ‘normal’ population. The episodic and merger-related nature of ULIRGs at low redshift is well-accepted (e.g. Sanders & Mirabel 1996; and references therein) but is harder to prove for starbursts in the distant Universe (e.g. Tacconi et al. 2006, Daddi et al. 2009, Ivison et al. 2013). The supporting evidence which has been accumulating in recent years, however (e.g. IR diagnostics, ISM temperatures, host galaxy structure and kinematics; see also our overview in the introduction and the discussion in Sect. 6.1), is at the basis of our proposed split into starburst and normal galaxy populations and the assumption that it provides a valid description of the star-forming population of much of the history of the Universe.

7. SUMMARY

The 2 Star Formation Mode (‘2-SFM’) framework provides a conceptually simple and self-consistent scheme for the prediction of basic properties of the star-forming galaxy (SFG) population. It relies on basic observables – e.g. the evolution of specific star formation rate (sSFR) in main-sequence galaxies or their stellar mass (M_*) distribution – and their mathematical description – e.g. the Schechter function parametrization of the stellar mass function or slope and normalization of the Schmidt-Kennicutt (S-K) law – to produce an analytic-empirical description of the statistical properties of SFGs which can be both predictive and help (re-)interpret existing measurements. A central ingredient of the 2-SFM framework is the distinction between ‘normal’ SFGs that reside on the star-forming main sequence and starbursts that are much rarer and regarded here as a ‘perturbation’ of the main-sequence state (see Sect. 4.1) that is probably dynamically induced or induced by interactions. We recently applied this approach successfully for the prediction of IR luminosity functions at $z \lesssim 2.5$ (Sargent et al. 2012) and of galaxy number counts between 24 and 1100 μm and at 1.4 GHz (B  thermin et al. 2012). In this article we have investigated the observational evidence that the molecular gas properties of massive ($M_* \gtrsim 10^{10} M_\odot$) SFGs are amenable to a similarly simplified description as their IR-emission.

We use a sample of approx. 90 normal SFGs (see Sects. 2.1.1 and 2.1.2) to derive scaling relations that describe the molecular gas content of secularly evolving SFGs at $z < 3$. When all involved quantities are normalized to the value a given observable takes for an average main-sequence galaxy, these scaling relations become strikingly simple (and in general also independent of redshift). In particular, we find that:

1. All literature measurements of SFR and M_{mol} in massive ($M_* > 10^{10} M_\odot$) main-sequence galaxies at $z < 3$ are compatible with the existence of a universal (i.e. redshift-invariant) star formation law for such systems. This integrated S-K relation is slightly supra-linear ($\text{SFR} \propto M_{\text{mol}}^{1.2}$) and tight (dispersion ~ 0.2 dex; see Fig. 1).
2. Star formation efficiency (SFE) varies very little across the main sequence (see Fig. 7) while the molecular gas mass fractions, $M_{\text{mol.}}/M_*$, increase

almost linearly with (s)SFR for main-sequence galaxies of a fixed stellar mass.

3. Changes in the sSFR of main-sequence galaxies are strongly correlated with changes of the molecular gas fraction, implying that both the dispersion of the main-sequence and the cosmic evolution of sSFR in general reflect variations of the gas content of normal galaxies (see Fig. 12).

Based on this characterization of gas in the main-sequence population, we are then able to predict the molecular gas properties of starburst galaxies which – in the 2-SFM approach – start out as normal galaxies that subsequently experience boosting to higher (s)SFRs. By considering the excess SFR and excess SFE of observed starburst galaxies with measured CO-to- H_2 conversion factors α_{CO} , we infer that SFE grows more strongly in the burst-phase than SFR (see Sect. 5.1.2). Taking into account the changing, sSFR-dependent mixture of starburst and normal galaxies that constitutes the total star-forming population, this leads to the following expectations:

4. Normal SFGs and starbursts are separated more strongly in the S-K plane than in the space of M_* and SFR (see Fig. 9). However, a separation that is as discrete as currently suggested by observations is not expected and is likely the outcome of the incomplete sampling of the S-K plane in surveys explicitly targeting strong starbursts and average main-sequence galaxies.
5. Even if starbursts are treated as a continuous extension of normal galaxies, with depletion times that decrease in proportion to their burst-related (s)SFR-enhancement, a nearly step-like, roughly ten-fold increase of the SFE is predicted at the sSFR where starbursting sources begin to outnumber the main-sequence population (see Fig. 10a).
6. A similar, albeit less pronounced step-like behaviour is predicted for molecular gas fractions (see Fig. 10b): while these continuously rise across the main sequence (see point 2 above), the higher SFE of starbursts causes their gas fractions to decrease to a value that is smaller than the average observed for a typical main-sequence galaxy. In Sect. 6.3 we provide recipes for how much gas fractions are expected to drop, depending on the intensity of the starburst, if – as is expected for, e.g., merger-induced starbursts – the time-scale for the exhaustion of the molecular fuel reservoir is much shorter than the time-scale for accretion of pristine gas from the cosmic web.

Based on the systematic difference between the $L'_{\text{CO}}/L_{\text{IR}}$ and $M_{\text{H}_2}/L_{\text{IR}}$ ratios of starbursts, we derive an empirical recipe for the CO-to- H_2 conversion factor, α_{CO} , of starburst galaxies (see Sect. 5.3.1). In combination with an assumed metallicity-dependence of α_{CO} for main-sequence galaxies, we are able to predict α_{CO} -variations for SFGs throughout the M_* vs. SFR plane (see Sect. 5.3.2). Due to the flatness of the mass-metallicity relation at high stellar masses, the conversion factor of Milky

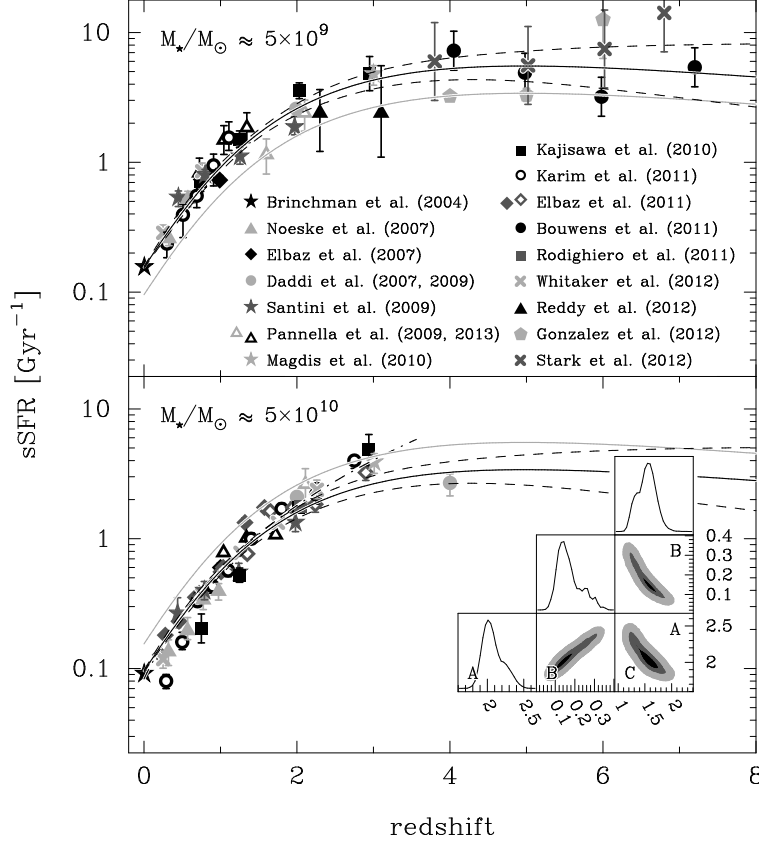


FIG. 19.—: Redshift-dependence of the sSFR of SFGs with stellar mass $M_*/M_\odot \approx 5 \times 10^9$ (top) and 5×10^{10} (bottom), as published in the recent literature (see legend; where necessary, literature values from adjacent mass bins were used to interpolate to the mass scales displayed here). Measurements derived based on image-stacking are indicated with open symbols and error bars denote the uncertainty on the sSFR-average rather than the sSFR-scatter in the population. Solid/dashed black lines – the best-fit evolution of the sSFR – parametrized as in eq. A1 (see inset panels on lower right for the covariance between the free parameters of the fit) – and associated 2σ -errors; light grey lines – sSFR-evolution in the other of the two stellar mass bins depicted in the figure, for comparison; dot-dashed line – evolution according to $(1+z)^{2.8}$ as used in S12 for the range $z \lesssim 2$.

Way-mass galaxies is expected to resemble the canonical Milky Way-value even at the cosmic epoch when the star-formation history of the Universe peaked. The simple, analytic-empirical description of molecu-

lar gas in star-forming galaxies developed in the present work will be used to infer the evolution of molecular gas mass functions and CO luminosity functions, as well as CO source counts in two forthcoming papers.

APPENDIX

LITERATURE MEASUREMENTS OF SPECIFIC STAR FORMATION RATE IN MAIN-SEQUENCE GALAXIES

The locus of the main sequence is known to depend on sample selection (e.g. Karim et al. 2011) and, in particular, on how actively star-forming the sample under consideration is. With the aim of deriving a representative, average evolution we gathered measurements from several recent studies of the distribution of SFGs in the (M_*, SFR) -plane that employed different selection criteria (e.g. different color cuts or selection by morphology, by near-IR flux/mass or by SFR), chose different star-formation tracers (e.g. UV, IR or radio emission) and/or adopted a variety of measurement techniques (e.g. individual detections vs. source stacking). By considering two separate mass scales at 5×10^9 and $5 \times 10^{10} M_\odot$ we obtain a constraint on the typical exponent ν of the M_* -dependence of sSFR, $\text{sSFR} \propto M_*^\nu$. We find that an exponent $\nu \simeq -0.2$ reproduces the systematic shift between the sSFR-evolution of galaxies in the two M_* -bins (see Fig. 19). This slope agrees closely with the value $\nu = -0.21 \pm 0.04$ we adopted (based on the $z \sim 2$ main sequence presented in Rodighiero et al. 2011) in our previous publications investigating the viability of the 2-SFM framework (see S12, Béthermin et al. 2012). Our literature compilation covers the redshift range $z < 7$, with a majority of the measurements tracing the steep rise of sSFR in main-sequence galaxies out to $z \sim 3$. At $z > 4$, drop-out samples constrain the sSFR-evolution at $M_* \sim 5 \times 10^9 M_\odot$, but they do not contain enough high-mass galaxies to probe the evolution in our second, more massive bin.

We parametrize the evolution of sSFR with a smoothly varying function of redshift with five free parameters which

we fit to the data in Fig. 19:

$$\text{sSFR}(M_*, z) = N(M_*) \exp\left(\frac{A \cdot z}{1 + B \cdot z^C}\right), \quad (\text{A1})$$

where

$$\begin{aligned} N(M_*) &= N(5 \times 10^{10} M_\odot) 10^{\nu \log(M_*/[5 \times 10^{10} M_\odot])} \\ A &= 2.05^{+0.33}_{-0.20} \\ B &= 0.16^{+0.15}_{-0.07} \\ C &= 1.54 \pm 0.32 \end{aligned}$$

Here ν is the slope of the $\log(\text{sSFR})$ vs. $\log(M_*)$ relation as above and the normalization at a stellar mass of $5 \times 10^{10} M_\odot$ is $N(5 \times 10^{10} M_\odot) = 0.095^{+0.002}_{-0.003} \text{ Gyr}^{-1}$. The quoted uncertainties are 68% confidence limits as determined by a Monte Carlo Markov Chain (MCMC; 10^6 realizations).

In Fig. 19 the 1σ -errors on the average sSFR-evolution according to eq. A1 are marked by dashed lines. Due to the abundant data (e.g., Noeske et al. 2007, Elbaz et al. 2007, Daddi et al. 2007b, 2009, Pannella et al. 2009, Karim et al. 2011, Rodighiero et al. 2011, Whitaker et al. 2012) and their generally high fidelity (error bars on the individual literature measurements span the statistical uncertainty on the mean rather than the population dispersion), formal uncertainties at $z < 2$ are small but increase steadily thereafter, reflecting the much sparser data at the highest redshifts. The growing formal errors do not include the systematic evolutionary uncertainties at $z > 3$, where the sSFRs of drop-out galaxies have been subject to frequent revision on an almost yearly basis. Initial measurements at $4 < z < 8$ by Stark et al. (2009) and González et al. (2010) – subsequently modified by Bouwens et al. (2012) to account for dust-extinction – suggested a much more gradual sSFR-evolution than expected by most theoretical models (see, e.g., Weinmann et al. 2011, and references therein). The most recent efforts have focused on quantifying the impact of nebular emission lines (e.g. Schaerer & de Barros 2010, de Barros et al. 2012, Gonzalez et al. 2012, Stark et al. 2012) on stellar mass measurements. It is presently unclear, however, whether corrections for nebular emission cause significant deviations from the nearly flat evolution that was found prior to their implementation: line-corrected sSFR-values scatter about the Bouwens et al. (2012) measurements²¹ at $z < 6$ and only then become consistently larger than non-corrected ones. Our analytical parametrization of the sSFR-evolution does not trace the apparent increase at $z \geq 6$ but these high redshifts are not the main focus of this article.

We thank F. Bournaud, A. Cibinel, P. Di Matteo, S. Ellison, G. Popping, A. Karim, K. Kraljic, S. Lilly, F. Walter and F. Renaud for helpful discussions/suggestions, as well as J. Scudder for providing the data shown in Fig. 4 and A. Leroy for kindly sharing new HERACLES measurements with us ahead of publication.

MTS, MB and ED acknowledge financial support from the EC through ERC-StG grant UPGAL 240039 and grant ANR-08-JCJC-0008. SJ was supported by ERC-grant ERC-StG-257720.

This article is partly based on observations with AKARI, a JAXA project with the participation of ESA. It has also made use of the NASA/IPAC Extragalactic Database (NED) which is operated by the Jet Propulsion Laboratory, California Institute of Technology, under contract with the National Aeronautics and Space Administration. Much of the analysis presented here was carried out in the Perl Data Language (PDL; Glazebrook & Economou, 1997) which can be obtained from <http://pdl.perl.org>.

REFERENCES

- Abdo, A. A., Ackermann, M., Ajello, M., et al. 2010, *ApJ*, 710, 133
- Agertz, O., Teyssier, R., & Moore, B. 2009, *MNRAS*, 397, L64
- Aravena, M., Carilli, C., Daddi, E., et al. 2010, *ApJ*, 718, 177
- Arnouts, S., Walcher, C. J., Le Fèvre, O., et al. 2007, *A&A*, 476, 137
- Asplund, M., Grevesse, N., Sauval, A. J., & Scott, P. 2009, *ARA&A*, 47, 481
- Baldry, I. K., & Glazebrook, K. 2003, *ApJ*, 593, 258
- Barton, E. J., Geller, M. J., & Kenyon, S. J. 2000, *ApJ*, 530, 660
- Baugh, C. M., Lacey, C. G., Frenk, C. S., et al. 2005, *MNRAS*, 356, 1191
- Behroozi, P. S., Wechsler, R. H., & Conroy, C. 2012, *arXiv:1207.6105*
- Belli, S., Jones, T., Ellis, R. S., & Richard, J. 2013, *arXiv:1302.3614*
- Bigiel, F., Leroy, A., Walter, F., et al. 2008, *AJ*, 136, 2846
- Bigiel, F., Leroy, A. K., Walter, F., et al. 2011, *ApJ*, 730, L13
- Béthermin, M., Daddi, E., Magdis, G., et al. 2012, *ApJ*, 757, L23
- Bolatto, A. D., Leroy, A. K., Rosolowsky, E., Walter, F., & Blitz, L. 2008, *ApJ*, 686, 948
- Boselli, A., Lequeux, J., & Gavazzi, G. 2002, *A&A*, 384, 33
- Bouché, N., Dekel, A., Genzel, R., et al. 2010, *ApJ*, 718, 1001
- Bouwens, R. J., Illingworth, G. D., Oesch, P. A., et al. 2012, *ApJ*, 754, 83
- Bournaud, F., Powell, L. C., Chapon, D., & Teyssier, R. 2011, *IAU Symposium*, 271, 160
- Bournaud, F., Chapon, D., Teyssier, R., et al. 2011, *ApJ*, 730, 4
- Brinchmann, J., Charlot, S., White, S. D. M., et al. 2004, *MNRAS*, 351, 1151
- Bryant, P. M., & Scoville, N. Z. 1996, *ApJ*, 457, 678
- Buat, V., Iglesias-Páramo, J., Seibert, M., et al. 2005, *ApJ*, 619, L51
- Buckley, J., & James, I. 1979, *Biometrika*, 66, 429
- Carilli, C. L., Daddi, E., Riechers, D., et al. 2010, *ApJ*, 714, 1407
- Casey, C. M., Chen, C.-C., Cowie, L., et al. 2013, *arXiv:1302.2619*
- Ceverino, D., Dekel, A., & Bournaud, F. 2010, *MNRAS*, 404, 2151
- Chabrier, G. 2003, *PASP*, 115, 763
- Chapman, S. C., Helou, G., Lewis, G. F., & Dale, D. A. 2003, *ApJ*, 588, 186
- Chapman, S. C., Blain, A. W., Smail, I., & Ivison, R. J. 2005, *ApJ*, 622, 772
- Chary, R., & Elbaz, D. 2001, *ApJ*, 556, 562

²¹ Independent, albeit tentative evidence for a flattening of the sSFR-evolution in the range $2 < z < 4$ is provided by the similar gas fractions in $z \sim 2$ BM/BX-selected galaxies and two $z \sim 3$ LBGs by Tacconi et al. (2010) and Magdis et al. (2012a), respectively. See Magdis et al. 2012a and our Sect. 5.2.2 for further discussion of the co-evolution of gas fractions and sSFR with cosmic time.

- Chenu, J. Y., Carter, M., Maier, D., Bortolotti, Y., Butin, G., Serres, P., Boucher, C., Mattiocco, F., & Lazareff, B. 2007, 'New SIS receivers for the IRAM Plateau de Bure interferometer', Joint 32nd International Conference on Infrared and Millimeter Waves, 2007 and the 2007 15th International Conference on Terahertz Electronics. IRMMW-THz., IEEE Conference Proceedings, 176-177
- Combes, F., García-Burillo, S., Braine, J., et al. 2011, *A&A*, 528, A124
- Combes, F., García-Burillo, S., Braine, J., et al. 2013, *A&A*, 550, A41
- Cowie, L. L., & Barger, A. J. 2008, *ApJ*, 686, 72
- Cox, T. J., Primack, J., Jonsson, P., & Somerville, R. S. 2004, *ApJ*, 607, L87
- Cox, T. J., Jonsson, P., Somerville, R. S., Primack, J. R., & Dekel, A. 2008, *MNRAS*, 384, 386
- da Cunha, E., Charmandaris, V., Díaz-Santos, T., et al. 2010, *A&A*, 523, A78
- Cresci, G., Mannucci, F., Sommariva, V., et al. 2012, *MNRAS*, 421, 262
- Cucciati, O., Tresse, L., Ilbert, O., et al. 2012, *A&A*, 539, A31
- Dabringhausen, J., Kroupa, P., & Baumgardt, H. 2009, *MNRAS*, 394, 1529
- Daddi, E., et al. 2007, *ApJ*, 670, 156
- Daddi, E., Alexander, D. M., Dickinson, M., et al. 2007, *ApJ*, 670, 173
- Daddi, E., Dannerbauer, H., Elbaz, D., et al. 2008, *ApJ*, 673, L21
- Daddi, E., Dannerbauer, H., Stern, D., et al. 2009, *ApJ*, 694, 1517
- Daddi, E., et al. 2010a, *ApJ*, 713, 686
- Daddi, E., et al. 2010b, *ApJ*, 714, L118
- Dale, D. A., Gil de Paz, A., Gordon, K. D., et al. 2007, *ApJ*, 655, 863
- Damen, M., Labbé, I., Franx, M., et al. 2009, *ApJ*, 690, 937
- Dannerbauer, H., Daddi, E., Riechers, D. A., et al. 2009, *ApJ*, 698, L178
- Davé, R., Finlator, K., & Oppenheimer, B. D. 2011, *MNRAS*, 415, de Barros, S., Schaerer, D., & Stark, D. P. 2012, *arXiv:1207.3663*
- Dekel, A., Birnboim, Y., Engel, G., et al. 2009, *Nature*, 457, 451
- Denicolò, G., Terlevich, R., & Terlevich, E. 2002, *MNRAS*, 330, 69
- Dessauges-Zavadsky, M., Christensen, L., D'Odorico, S., Schaerer, D., & Richard, J. 2011, *A&A*, 533, A15
- Di Matteo, P., Combes, F., Melchior, A.-L., & Semelin, B. 2007, *A&A*, 468, 61
- Di Matteo, P., Bournaud, F., Martig, M., et al. 2008, *A&A*, 492, 31
- Downes, D., & Solomon, P. M. 1998, *ApJ*, 507, 615
- Draine, B. T., & Li, A. 2007, *ApJ*, 657, 810
- Duffy, A. R., Kay, S. T., Battye, R. A., et al. 2012, *MNRAS*, 420, 2799
- Dunne, L., Ivison, R. J., Maddox, S., et al. 2009, *MNRAS*, 394, 3
- Elbaz, D., et al. 2007, *A&A*, 468, 33
- Elbaz, D., Hwang, H. S., Magnelli, B., et al. 2010, *A&A*, 518, L29
- Elbaz, D., Dickinson, M., Hwang, H. S., et al. 2011, *A&A*, 533, A119
- Erb, D. K., Shapley, A. E., Pettini, M., et al. 2006, *ApJ*, 644, 813
- Feldmann, R., Gnedin, N. Y., & Kravtsov, A. V. 2012, *ApJ*, 747, 124
- Förster Schreiber, N. M., Genzel, R., Bouché, N., et al. 2009, *ApJ*, 706, 1364
- Förster Schreiber, N. M., Shapley, A. E., Genzel, R., et al. 2011, *ApJ*, 739, 45
- Frayser, D. T., Ivison, R. J., Scoville, N. Z., et al. 1998, *ApJ*, 506, L7
- Fontanot, F., De Lucia, G., Monaco, P., Somerville, R. S., & Santini, P. 2009, *MNRAS*, 397, 1776
- Fu, J., Kauffmann, G., Li, C., & Guo, Q. 2012, *MNRAS*, 424, 2701
- Galametz, M., Madden, S. C., Galliano, F., et al. 2011, *A&A*, 532, A56
- Galliano, F., Dwek, E., & Chianal, P. 2008, *ApJ*, 672, 214
- Geach, J. E., Smail, I., Coppin, K., Moran, S. M., Edge, A. C., & Ellis, R. S. 2009, *MNRAS*, 395, L62
- Geach, J. E., Smail, I., Moran, S. M., MacArthur, L. A., Lagos, C. d. P., & Edge, A. C. 2011, *ApJ*, 730, L19
- Geach, J. E., Chapin, E. L., Coppin, K. E. K., et al. 2012, *arXiv:1211.6668*
- Genzel, R., et al. 2010, *MNRAS*, 407, 2091
- Genzel, R., Tacconi, L. J., Combes, F., et al. 2012, *ApJ*, 746, 69
- Gilbank, D. G., Bower, R. G., Glazebrook, K., et al. 2011, *MNRAS*, 414, 304
- Glover, S. C. O., & Mac Low, M.-M. 2011, *MNRAS*, 412, 337
- González, V., Labbé, I., Bouwens, R. J., et al. 2010, *ApJ*, 713, 115
- Gonzalez, V., Bouwens, R., Ilingworth, G., et al. 2012, *arXiv:1208.4362*
- Graciá-Carpio, J., Sturm, E., Hailey-Dunsheath, S., et al. 2011, *ApJ*, 728, L7
- Greve, T. R., Bertoldi, F., Smail, I., et al. 2005, *MNRAS*, 359, 1165
- Gruppioni, C., Pozzi, F., Rodighiero, G., et al. 2013, *arXiv:1302.5209*
- Hahn, O., Teyssier, R., & Carollo, C. M. 2010, *MNRAS*, 405, 274
- Hayward, C. C., Narayanan, D., Kereš, D., et al. 2013, *MNRAS*, 428, 2529
- Heisler, C. A., & Vader, J. P. 1994, *AJ*, 107, 35
- Hodge, J. A., Carilli, C. L., Walter, F., et al. 2012, *ApJ*, 760, 11
- Hopkins, P. F., Hernquist, L., Cox, T. J., et al. 2006, *ApJS*, 163, 1
- Hopkins, P. F., Cox, T. J., Younger, J. D., & Hernquist, L. 2009, *ApJ*, 691, 1168
- Hopkins, P. F., Younger, J. D., Hayward, C. C., Narayanan, D., & Hernquist, L. 2010, *MNRAS*, 402, 1693
- Howell, J. H., Armus, L., Mazzarella, J. M., et al. 2010, *ApJ*, 715, 572
- Hughes, D. H., Serjeant, S., Dunlop, J., et al. 1998, *Nature*, 394, 241
- Hwang, H. S., Elbaz, D., Magdis, G., et al. 2010, *MNRAS*, 409, 75
- Hwang, H. S., Elbaz, D., Dickinson, M., et al. 2011, *A&A*, 535, A60
- Ilbert, O., Salvato, M., Le Floc'h, E., et al. 2010, *ApJ*, 709, 644
- Isobe, T., Feigelson, E. D., & Nelson, P. I. 1986, *ApJ*, 306, 490
- Israel, F. P. 1997, *A&A*, 328, 471
- Ivison, R. J., Chapman, S. C., Faber, S. M., et al. 2007, *ApJ*, 660, L77
- Ivison, R. J., Swinbank, A. M., Swinyard, B., et al. 2010, *A&A*, 518, L35
- Ivison, R. J., Papadopoulos, P. P., Smail, I., et al. 2011, *MNRAS*, 412, 1913
- Ivison, R. J., Swinbank, A. M., Smail, I., et al. 2013, *arXiv:1302.4436*
- Juneau, S., Narayanan, D. T., Moustakas, J., et al. 2009, *ApJ*, 707, 1217
- Juneau, S., Dickinson, M., Alexander, D. M., & Salim, S. 2011, *ApJ*, 736, 104
- Kajisawa, M., Ichikawa, T., Yamada, T., et al. 2010, *ApJ*, 723, 129
- Kampczyk, P., Lilly, S. J., de Ravel, L., et al. 2011, *arXiv:1112.4842*
- Kaplan, E. L. & Meier, P. 1958, *J. Am. Statist. Assoc.*, 53, 457
- Karim, A., et al. 2011, *ApJ*, 730, 61
- Kartaltepe, J. S., Dickinson, M., Alexander, D. M., et al. 2012, *ApJ*, 757, 23
- Kaviraj, S., Cohen, S., Windhorst, R. A., et al. 2013, *MNRAS*, 429, L40
- Kawada, M., Baba, H., Barthel, P. D., et al. 2007, *PASJ*, 59, 389
- Kennicutt, R. C., Jr. 1998, *ApJ*, 498, 541
- Kennicutt, R. C., Jr. 1998, *ARA&A*, 36, 189
- Keres, D., Yun, M. S., & Young, J. S. 2003, *ApJ*, 582, 659
- Kewley, L. J., & Dopita, M. A. 2002, *ApJS*, 142, 35
- Kewley, L. J., & Ellison, S. L. 2008, *ApJ*, 681, 1183
- Kobulnicky, H. A., & Kewley, L. J. 2004, *ApJ*, 617, 240
- Kroupa, P. 2001, *MNRAS*, 322, 231
- Krumholz, M. R., Dekel, A., & McKee, C. F. 2012, *ApJ*, 745, 69
- Lara-López, M. A., Cepa, J., Bongiovanni, A., et al. 2010, *A&A*, 521, L53
- Lara-Lopez, M. A., Lopez-Sanchez, A. R., & Hopkins, A. M. 2012, *arXiv:1207.0950*
- Larson, D., Dunkley, J., Hinshaw, G., et al. 2011, *ApJS*, 192, 16
- Laskar, T., Berger, E., & Chary, R.-R. 2011, *ApJ*, 739, 1
- Lee, J. C., Gil de Paz, A., Kennicutt, R. C., Jr., et al. 2011, *ApJS*, 192, 6
- Leitner, S. N. 2012, *ApJ*, 745, 149
- Leroy, A. K., Walter, F., Brinks, E., Bigiel, F., de Blok, W. J. G., Madore, B., & Thornley, M. D. 2008, *AJ*, 136, 2782
- Leroy, A. K., et al. 2009, *AJ*, 137, 4670
- Leroy, A. K., et al. 2011, *ApJ*, 737, 12
- Leroy, A. K., Walter, F., Sandstrom, K., et al. 2013, *arXiv:1301.2328*
- Liu, X., Shapley, A. E., Coil, A. L., Brinchmann, J., & Ma, C.-P. 2008, *ApJ*, 678, 758
- Magdis, G. E., Rigopoulou, D., Huang, J.-S., & Fazio, G. G. 2010, *MNRAS*, 401, 1521
- Magdis, G. E., Daddi, E., Elbaz, D., et al. 2011, *ApJ*, 740, L15
- Magdis, G. E., Daddi, E., Sargent, M., et al. 2012a, *ApJ*, 758, L9
- Magdis, G. E., Daddi, E., Béthermin, M., et al. 2012b, *ApJ*, 760, 6
- Magnelli, B., Elbaz, D., Chary, R. R., Dickinson, M., Le Borgne, D., Frayer, D. T., & Willmer, C. N. A. 2009, *A&A*, 496, 57
- Magnelli, B., Elbaz, D., Chary, R. R., Dickinson, M., Le Borgne, D., Frayer, D. T., & Willmer, C. N. A. 2011, *A&A*, 528, A35
- Magnelli, B., Saintonge, A., Lutz, D., et al. 2012, *A&A*, 548, A22
- Magrini, L., Sommariva, V., Cresci, G., et al. 2012, *MNRAS*, 426, 1195
- Maiolino, R., Neri, R., Beelen, A., et al. 2007, *A&A*, 472, L33
- Mannucci, F., Cresci, G., Maiolino, R., Marconi, A., & Gnerucci, A. 2010, *MNRAS*, 408, 2115

- Martig, M., Bournaud, F., Teyssier, R., & Dekel, A. 2009, *ApJ*, 707, 250
- Mihos, J. C., & Hernquist, L. 1996, *ApJ*, 464, 641
- Monaco, P., Murante, G., Borgani, S., & Dolag, K. 2012, *MNRAS*, 421, 2485
- Moshir, M., Kopman, G., & Conrow, T. A. O. 1992, *IRAS Faint Source Survey*, Explanatory supplement version 2, JPL, Pasadena
- Moustakas, J., Kennicutt, R. C., Jr., Tremonti, C. A., et al. 2010, *ApJS*, 190, 233
- Mullaney, J. R., Daddi, E., Béthermin, M., et al. 2012, *ApJ*, 753, L30
- Narayanan, D., Cox, T. J., Shirley, Y., et al. 2008, *ApJ*, 684, 996
- Narayanan, D., Krumholz, M., Ostriker, E. C., & Hernquist, L. 2011, *MNRAS*, 418, 664
- Narayanan, D., Bothwell, M., & Davé, R. 2012, *MNRAS*, 426, 1178
- Noeske, K. G., Weiner, B. J., Faber, S. M., et al. 2007, *ApJ*, 660, L43
- Obreschkow, D., Heywood, I., & Rawlings, S. 2011, *arXiv:1109.2514*
- Oesch, P. A., Carollo, C. M., Feldmann, R., et al. 2010, *ApJ*, 714, L47
- Oliver, S., Frost, M., Farrah, D., et al. 2010, *MNRAS*, 405, 2279
- Omout, A., Petitjean, P., Guilloteau, S., et al. 1996, *Nature*, 382, 428
- Pannella, M., Carilli, C. L., Daddi, E., et al. 2009, *ApJ*, 698, L116
- Papadopoulos, P. P., Thi, W.-F., Miniati, F., & Viti, S. 2011, *MNRAS*, 414, 1705
- Papadopoulos, P. P., van der Werf, P., Xilouris, E., Isaak, K. G., & Gao, Y. 2012, *ApJ*, 751, 10
- Park, C., & Choi, Y.-Y. 2009, *ApJ*, 691, 1828
- Peng, Y.-J., Lilly, S. J., Kovač, K., et al. 2010, *ApJ*, 721, 193
- Perley, R. A., Chandler, C. J., Butler, B. J., & Wrobel, J. M. 2011, *ApJ*, 739, L1
- Pettini, M., & Pagel, B. E. J. 2004, *MNRAS*, 348, L59
- Pilyugin, L. S. 2001, *A&A*, 374, 412
- Popping, G., Caputi, K. I., Somerville, R. S., & Trager, S. C. 2012, *MNRAS*, 425, 2386
- Reddy, N. A., & Steidel, C. C. 2009, *ApJ*, 692, 778
- Reddy, N. A., Pettini, M., Steidel, C. C., et al. 2012, *ApJ*, 754, 25
- Renaud, F., Kraljic, K., & Bournaud, F. 2012, *ApJ*, 760, L16
- Richard, J., Jones, T., Ellis, R., et al. 2011, *MNRAS*, 413, 643
- Riechers, D. A., Walter, F., Carilli, C. L., et al. 2006, *ApJ*, 650, 604
- Riechers, D. A., Cooray, A., Omout, A., et al. 2011, *ApJ*, 733, L12
- Riechers, D. A., Hodge, J., Walter, F., Carilli, C. L., & Bertoldi, F. 2011, *ApJ*, 739, L31
- Robaina, A. R., Bell, E. F., Skelton, R. E., et al. 2009, *ApJ*, 704, 324
- Robertson, B. E., & Kravtsov, A. V. 2008, *ApJ*, 680, 1083
- Rodighiero, G., et al. 2010, *A&A*, 515, A8
- Rodighiero, G., Daddi, E., Baronchelli, I., et al. 2011, *ApJ*, 739, L40
- Rujopakarn, W., Rieke, G. H., Eisenstein, D. J., & Juneau, S. 2011, *ApJ*, 726, 93
- Saintonge, A., et al. 2011a, *MNRAS*, 415, 32
- Saintonge, A., Tacconi, L. J., Fabello, S., et al. 2012, *ApJ*, 758, 73
- Salim, S., Rich, R. M., Charlot, S., et al. 2007, *ApJS*, 173, 267
- Salmi, F., Daddi, E., Elbaz, D., et al. 2012, *ApJ*, 754, L14
- Salpeter, E. E. 1955, *ApJ*, 121, 161
- Sanders, D. B., Soifer, B. T., Elias, J. H., et al. 1988, *ApJ*, 325, 74
- Sanders, D. B., & Mirabel, I. F. 1996, *ARA&A*, 34, 749
- Sandstrom, K. M., Leroy, A. K., Walter, F., et al. 2012, *arXiv:1212.1208*
- Santini, P., Fontana, A., Grazian, A., et al. 2009, *A&A*, 504, 751
- Sargent, M. T., Béthermin, M., Daddi, E., & Elbaz, D. 2012, *ApJ*, 747, L31 (S12)
- Schaefer, D., & de Barros, S. 2010, *A&A*, 515, A73
- Schmidt, M. 1959, *ApJ*, 129, 243
- Schruba, A., Leroy, A. K., Walter, F., et al. 2012, *AJ*, 143, 138
- Scudder, J. M., Ellison, S. L., Torrey, P., Patton, D. R., & Mendel, J. T. 2012, *MNRAS*, 426, 549
- Skibba, R. A., Engelbracht, C. W., Dale, D., et al. 2011, *ApJ*, 738, 89
- Skrutskie, M. F., Cutri, R. M., Stiening, R., et al. 2006, *AJ*, 131, 1163
- Solomon, P. M., Downes, D., Radford, S. J. E., & Barrett, J. W. 1997, *ApJ*, 478, 144
- Solomon, P. M., & Vanden Bout, P. A. 2005, *ARA&A*, 43, 677
- Sommariva, V., Mannucci, F., Cresci, G., et al. 2012, *A&A*, 539, A136
- Stark, D. P., Ellis, R. S., Bunker, A., et al. 2009, *ApJ*, 697, 1493
- Stark, D. P., Schenker, M. A., Ellis, R. S., et al. 2012, *arXiv:1208.3529*
- Swinbank, A. M., Smail, I., Longmore, S., et al. 2010, *Nature*, 464, 733
- Swinbank, A. M., Papadopoulos, P. P., Cox, P., et al. 2011, *ApJ*, 742, 11
- Tacconi, L. J., Neri, R., Chapman, S. C., et al. 2006, *ApJ*, 640, 228
- Tacconi, L. J., Genzel, R., Smail, I., et al. 2008, *ApJ*, 680, 246
- Tacconi, L. J., et al. 2010, *Nature*, 463, 781
- Tacconi, L. J., Neri, R., Genzel, R., et al. 2012, *arXiv:1211.5743*
- Teyssier, R., Chapon, D., & Bournaud, F. 2010, *ApJ*, 720, L149
- Tremonti, C. A., Heckman, T. M., Kauffmann, G., et al. 2004, *ApJ*, 613, 898
- Trentham, N., Kormendy, J., & Sanders, D. B. 1999, *AJ*, 117, 2152
- U, V., Sanders, D. B., Mazzarella, J. M., et al. 2012, *arXiv:1209.1611*
- Walter, F., Bertoldi, F., Carilli, C., et al. 2003, *Nature*, 424, 406
- Walter, F., Brinks, E., de Blok, W. J. G., et al. 2008, *AJ*, 136, 2563
- Weinmann, S. M., Neistein, E., & Dekel, A. 2011, *MNRAS*, 417, 2737
- Weinmann, S. M., Pasquali, A., Oppenheimer, B. D., et al. 2012, *MNRAS*, 426, 2797
- Weiss, A., De Breuck, C., Marrone, D. P., et al. 2013, *arXiv:1303.2726*
- Whitaker, K. E., van Dokkum, P. G., Brammer, G., & Franx, M. 2012, *ApJ*, 754, L29
- Wilson, C. D. 1995, *ApJ*, 448, L97
- Wuyts, S., Förster Schreiber, N. M., van der Wel, A., et al. 2011, *ApJ*, 742, 96
- Wuyts, S., Förster Schreiber, N. M., Genzel, R., et al. 2012, *ApJ*, 753, 114
- Wyder, T. K., Martin, D. C., Schiminovich, D., et al. 2007, *ApJS*, 173, 293
- Yamamura, I., Makiuti, S., Ikeda, N., et al. 2010, *VizieR Online Data Catalog*, 2298, 0